Dissertation
Submitted to the
Combined Faculties for the Natural Sciences and for Mathematics
of the Ruperto-Carola University of Heidelberg, Germany
for the degree of
Doctor of Natural Sciences

presented by

Laura Panavaite
Born in Vilnius, Lithuania
Oral examination: May 26, 2017

Emergence of cellular heterogeneity and body plan in early mammalian development

Referees: Dr. Alexander Aulehla

Prof. Dr. Nicholas S. Foulkes

This work was carried out at the European Molecular Biology Laboratory in Heidelberg from September 2013 to March 2017 under supervision of Dr. Takashi Hiiragi.

To

Milda and Arūnas

SUMMARY

In mammalian development, cell-to-cell gene expression heterogeneity first emerges in early embryo when segregation of embryonic and extraembryonic lineages is initiated. Lineage-specific gene expression is especially enhanced within the inner cells of the early blastocyst. I studied this initial phase of cellular heterogeneity to mechanistically understand how the first cell fate decisions are made in the mammalian embryo. To this end, we have performed a gene trap screen and generated mouse lines with Venus reporter expression in one of the two first lineages – inner cell mass and trophectoderm. To quantitatively describe gene expression dynamics at a single-cell resolution in living embryos, we have performed lineage tracking, quantitative gene expression and cell position analyses that allowed us to build a comprehensive lineage map of mouse pre-implantation development. We identified lineage-specific gene regulation that paves the way to embryonic cell fate decisions and determined that first embryonic lineages of the blastocyst – trophectoderm and the inner cell mass – are formed at different timing and by separate mechanisms.

The first phase of lineage-specific gene expression heterogeneity is resolved by segregation of first embryonic lineages and formation of the first embryonic axis within the late blastocyst. Within the inner cell mass of the blastocyst, new cellular heterogeneity arises that will dictate the body axis formation. During subsequent body-patterning phases, an inner cell mass-derived layer of cells called the visceral endoderm provides crucial signals for establishment of anterior-posterior axis. However, due to the difficulty of crossing the implantation barrier *in vitro*, the mechanism of generating a signaling center within the visceral endoderm remains elusive. In this work, I have presented a 3D peri-implantation culture method that supports continuous mouse embryo development *in vitro* from pre- to post-implantation stages while preserving its in-vivo-like geometry. Such embryos retain the expression of lineage-specific markers, are minimally delayed in their development, preserve in-vivo-like proportions, and correctly specify anterior-posterior axis in the absence of maternal cues. Observing and manipulating embryos

in this culture, we were able to explore the hidden heterogeneity within inner cell mass population that predicts future body patterning. By combining 3D culture, time-lapse light sheet fluorescence microscopy, and single-cell RNA-Seq, we explored the lineage and character of cells that play a crucial role in setting up the anterior-posterior axis, and investigated the role of communication between the epiblast and the visceral endoderm in the development of the peri-implantation embryo and the establishment of the embryonic body plan.

ZUZAMMENFASSUNG

In der Entwicklung von Säugetieren entsteht eine Genexpressionsheterogenität zwischen Zellen erstmals im frühen Embryo, wenn die Segregation von embryonalen und extraembryonalen Zellabstammung beginnt. Die abstammungsspezifische Genexpression ist bei den inneren Zellen der frühen Blastozyste besonders ausgeprägt. Ich habe die Anfangsphase dieser zellulären Heterogenität untersucht, um die ersten Entscheidungen über das Zellschicksal mechanistisch zu verstehen. Zu diesem Zweck haben wir einen ‚Gene-Trap Screen' durchgeführt und dadurch Mauslinien generiert, die Venusreporterexpression in einer der beiden ersten Zellabstammungslinien – der inneren Zellmasse und dem Trophektoderm – zeigen. Diese haben uns befähigt die Zellabstammungslinien zu verfolgen und deren quantitative Genexpression und Position im Embryo zu analysieren, um die Dynamik der Genexpression in Einzelzellauflösung im lebenden Embryo zu beschreiben und so eine umfassende Kartierung der Zellabstammungslinien in der Präimplantationsentwicklung der Maus zu erstellen. Wir konnten abstammungsspezifische Genregulation erkennen, die den Weg für embryonale Zellschicksalsentscheidungen bereitet. Weiterhin konnten wir feststellen, dass die beiden ersten embryonalen Abstammungslinien der Blastozyste zu unterschiedlichen Zeiten und durch gesonderte Mechanismen entstehen.

Die erste Phase von abstammungsspezifischer Heterogenität der Genexpression wird durch die Abspaltung der ersten embryonalen Zelllinien und der Formation der ersten embryonalen Achse im späten Blastozystenstadium aufgelöst. Innerhalb der inneren Zellmasse in der Blastozyste entsteht eine weitere, neue zelluläre Heterogenität, die die Bildung weiterer Körperachsen festlegen wird. Während der folgenden Musterbildungsphasen produziert das viszerale Endoderm, eine Zellschicht der inneren Zellmasse, entscheidende Signale für die Entwicklung der anteroposterioren Achse. Jedoch ist der Mechanismus der Bildung des Signalzentrums im viszeralem Endoderm weithin unbekannt, da es bis dato nicht möglich war Embryonen zu diesem Zeitpunkt -während der Implantation- *in vitro* zu kultivieren. In dieser Arbeit präsentiere ich eine Methode der 3D-Embryokultivierung bis über den Zeitpunkt der Implantation hinaus (Peri-

Implantation) die eine kontinuierliche Embryoentwicklung *in vitro* ermöglicht. Die so kultivierten Embryonen bewahren die Expression von linien-spezifischen Markern, sind nur minimal verzögert in ihrer Entwicklung, behalten ihre natürlichen Proportionen und entwickeln die korrekte anteroposteriore Achse ohne maternale Einflüsse. Wir konnten durch Beobachtung und Manipulation der kultivierten Embryonen die Heterogenität der inneren Zellmasse untersuchen, die die zukünftigen Bildung der Körperschemata festlegen wird. Durch die Kombination von 3D Kultur, Zeitrafferlichtblatt-fluoreszenzmikroskopie und RNA-Sequenzierung von einzelnen Zellen konnten wir die Abstammung und Art der Zellen, die für die Bildung der anteroposterioren Achse notwendig sind, bestimmen. Weiterhin haben wir die Bedeutung der Kommunikation zwischen Epiblast und viszeralen Endoderm in der Entwicklung der Embryos und die Bauplanetablierung des embryonalen Körpers zu diesem Zeitpunkt untersucht.

TABLE OF CONTENTS

ABBREVIATIONS

2D – 2-dimentional

3D – 3-dimentional

3D-geec – 3D gel embedded embryo culture

A-P – anterior-posterior

a.u. – arbitrary units

AVE – anterior visceral endoderm

BAC – bacterial artificial chromosome

bp – base pairs

BSA – bovine serum albumin

cDNA – complementary DNA

Cdx2 – Caudal type homeobox 2

CerI – cerberus 1

CRISPR – clustered regulatory interspaced short palindromic repeat

D-V – dorsal-ventral

DAPI – 4,6-diamidino-2-phenylindole

DLS – digital light sheet

DMEM – Dulbecco'sModified Eagle's Medium

DMSO – dimethyl sulfoxide

DNA – deoxyribonucleic acid

DPBS – Dulbecco's phosphate-buffered saline

dpc – day post conception

DVE – distal visceral endoderm

e.g. – *exempli gratia*, for example

ECM – extracellular matrix

EDTA – ethylenediaminetetraacetic acid

EGFP – enhanced green fluorescent protein

Epi - epiblast

ES – embryonic stem

ExE – Extraembryonic ectoderm

Fgf4 – fibroblast growth factor 4

Gata4 – GATA binding protein 4

Gata6 – GATA binding protein 6

gDNA – genomic DNA

H2B – histone 2B

hCG – human chorionic gonadotropin

HEPES – 4-(2-hydroxyethyl)-1-piperazineethanesulfonic acid

Hex – homeobox protein

i.e. – *id est*, that is

ICM – inner cell mass

IRES – internal ribosomal entry site

IU – international unit

IVC – *in vitro* culture

KSOM – potassium simplex optimization medium

KSOM-H – KSOM with HEPES

L-R – left-right

LB – Luria broth

M - molar

MEF – mouse embryonic fibroblast

mRNA – messenger RNA

Myr – myristoylation signal

mz – maternal-zygotic

Oct4 – Octamer-binding transcription factor 4

Palm – palmitoylation signal

PBS – phosphate buffered saline

PCR – polymerase chain reaction

PMSG – pregnant mare's serum gonadotropin

Pou5f1 – POU domain, class 5, transcription factor 1

PrE – primitive endoderm

qRT-PCR – quantitative real time PCR

RNA – ribonucleic acid

rpm – rounds per minute

RT – room temperature

s.d. – standard deviation

Sox – SRY-box containing gene 2

SPIM – single plane illumination microscopy

T-PMT – total reflected light channel

T7 – sequence of T7 promoter

TE – trophectoderm

TF – transcription factor

U – units

v/v – volume per volume

w/v – weight per volume

WT – wild type

ZP – zona pellucida

1. INTRODUCTION

Early development of the mammalian embryo

Mammalian development commences with fertilization of an oocyte within the female oviduct (Fig 1.1). In the following days, the zygote, surrounded by a protective glycoprotein envelope called the zona pellucida (ZP), undergoes multiple rounds of cleavage to produce a ball of cells called the morula that travels along the oviduct. At this time, a cavity appears between the cells and the embryo develops vesicular morphology: a single-layer epithelium surrounding a fluid-filled cavity and a clump of cells positioned on one side (Fig 1.1 b). This structure, called the blastocyst, is made up of two distinct cell lineages. The trophectoderm lineage (TE; Fig 1.2) is made of the first cells that loose pluripotency - the ability to give rise to the whole organism. These cells contribute exclusively to the extraembryonic tissues (Rossant and Tam 2009). The second lineage, positioned on the inside of the blastocyst, and called the inner cell mass (ICM; Fig 1.1), retains its pluripotent characteristics and gives rise to the embryo proper and thus all the embryonic tissues (Fig 1.2, reviewed in Johnson 2009).

As the blastocyst matures, it enters the uterus and becomes ready for implantation (reviewed in Wang and Dey 2006). Soon after, it makes connection to the uterine wall, and the placenta – a joint organ between the embryo and the mother – starts developing in all eutherian mammals (reviewed in Behringer et al. 2006). Most mammalian embryos are characterized by common pre-implantation morphogenesis, and undergo a shared sequence of developmental events, such as cleavage, compaction and blastocyst formation. Blastocysts of human, rabbit, mouse, rat, bat, hamster, pig, cow and guinea pig are difficult to distinguish except for the difference in their size and developmental timing (1.3 a), though they are set apart by distinct expression patterns of lineage-specific transcription factors (Berg et al. 2011, Kuijk et al. 2008, Rossant 2011, Niakan and Eggan 2013). Curiously, at the time of implantation remarkable morphological differences appear between rodent and non-rodent mammalian embryos (Fig 1.3 b, c). The shared gastrula morphology of the order *Rodentia* is different to that of other mammalian orders. Most eutherians and metatherians produce gastrulating embryos that are disc-shaped and closely resemble the avian gastrula, while rodent embryos are cup-shaped and elongated

(Fig 1.3 c). While the difference between rodent and other mammal early post-implantation embryo morphology is an interesting biological problem in itself (Nakamura et al. 2016, Sasaki et al. 2016), the key developmental structures and patterns are preserved in such embryos. As has been previously noted, if unfolded, the cup-shaped rodent gastrula would differ very little, if at all, from the gastrulas of other mammals in its proportions and basic plan (Beddington and Robertson, 1999). Thus rodent embryos remain a convenient model system to study both pre- and post-implantation mammalian development.

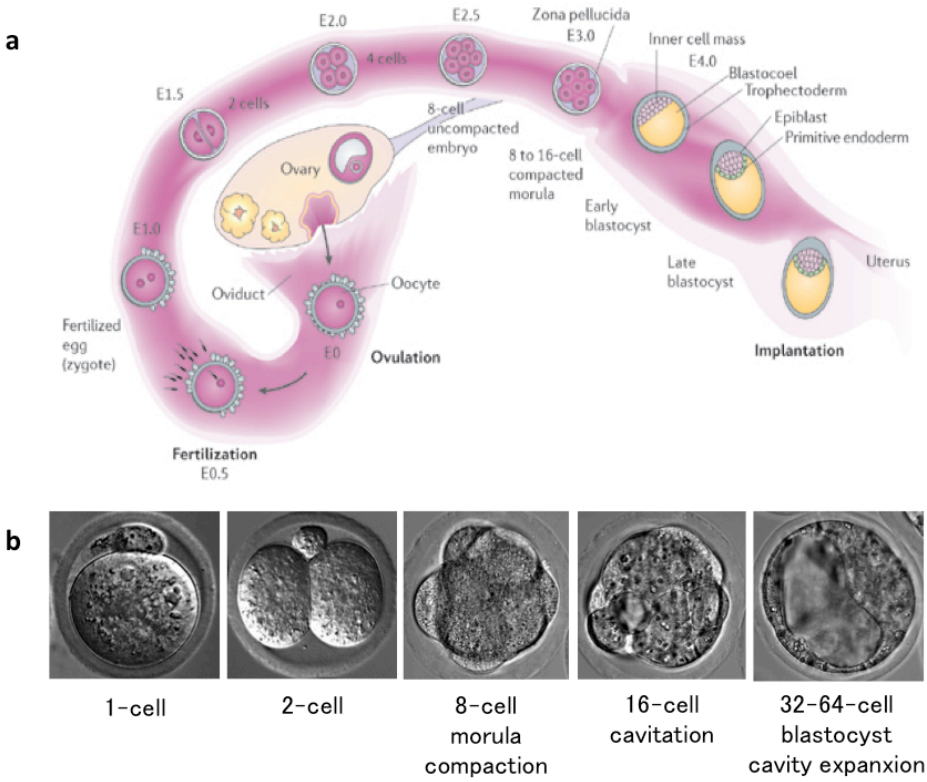

Figure 1.1. Early mouse embryonic development.

a, Mouse pre-implantation development from fertilization to implantation (adapted from Wang and Dey 2006). E, embryonic day. **b,** Wide field microscopic images of key stages in pre-implantation mouse embryo development.

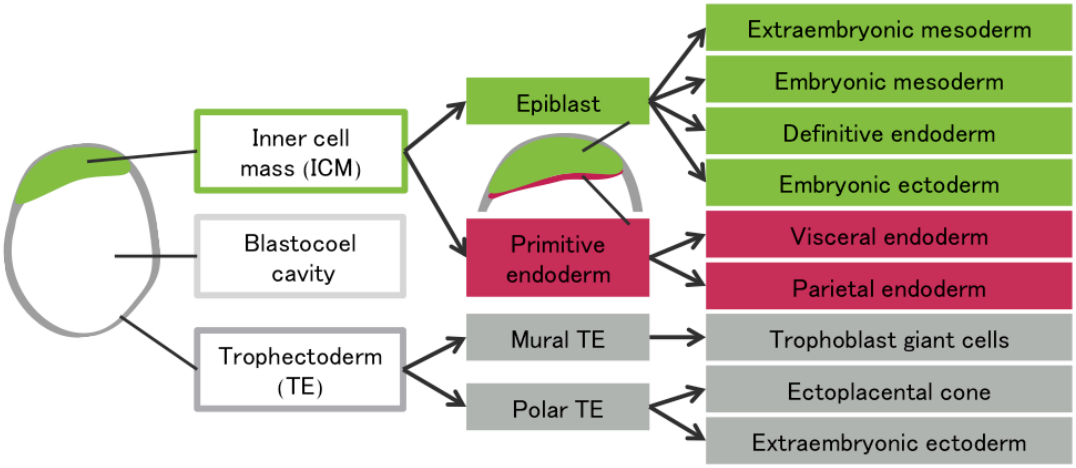

Figure 1.2. Mouse embryonic lineages.

First embryonic lineages of the blastocyst give rise to distinct developmental structures. TE gives rise to extraembryonic tissues, while ICM gives rise to primitive endoderm and the epiblast, that in turn give rise to other extraembryonic tissues and embryo proper, respectively. Adapted from Lu et al. 2001. Green: ICM and its lineage, grey: TE and its lineage, red: PrE and its lineage.

First lineage segregation

The question of the first lineage differentiation, crucial for our understanding of development and for biomedical applications, has been addressed extensively throughout the last decades. Yet the molecular mechanism by which the first two mammalian cell lineages, TE and ICM, are specified is not fully understood. Two different models stipulate a mechanism by which a cell makes the decision for one of these two lineages. The inside-outside model (Fig 1.4 a) proposes that cell fate is determined depending on cell position within the 16-cell stage morula (Tarkowski and Wroblewska 1967). The cells positioned on the inside of the embryo and surrounded by cell-cell contacts will develop into ICM, while the cells retaining contact to the outside will develop into TE. On the other hand, the cell polarity model (Fig 1.4 b) suggests that TE vs. ICM decision is driven by cleavage plane orientation during 8- to 16-cell division (Johnson and Ziomek 1981). The cells that divide symmetrically produce two polar daughters that will become TE; the cells that divide asymmetrically produce one polar daughter that will become TE, and one apolar

daughter that will become ICM. It is noteworthy that both the inside-outside model and the cell polarity model work on the assumption that the first cell fate decision is binary: after 8- to 16-cell division, every cell becomes either TE or ICM (Niwa et al. 2005).

Recent discoveries have revealed unprecedented complexity within the early embryo, such as dynamic cellular rearrangements (Motosugi et al. 2005, Kurotaki et al. 2007) and stochastic cell-to-cell molecular heterogeneity (Dietrich and Hiiragi 2007, Plusa et al. 2008, Ralston and Rossant 2008, Onishi et al. 2014). Together, these findings are not reconciled with those available models of first lineage segregation. Consequently, the link between molecular identity of cells in the early embryo and the mechanism of first lineage segregation remains to be investigated further.

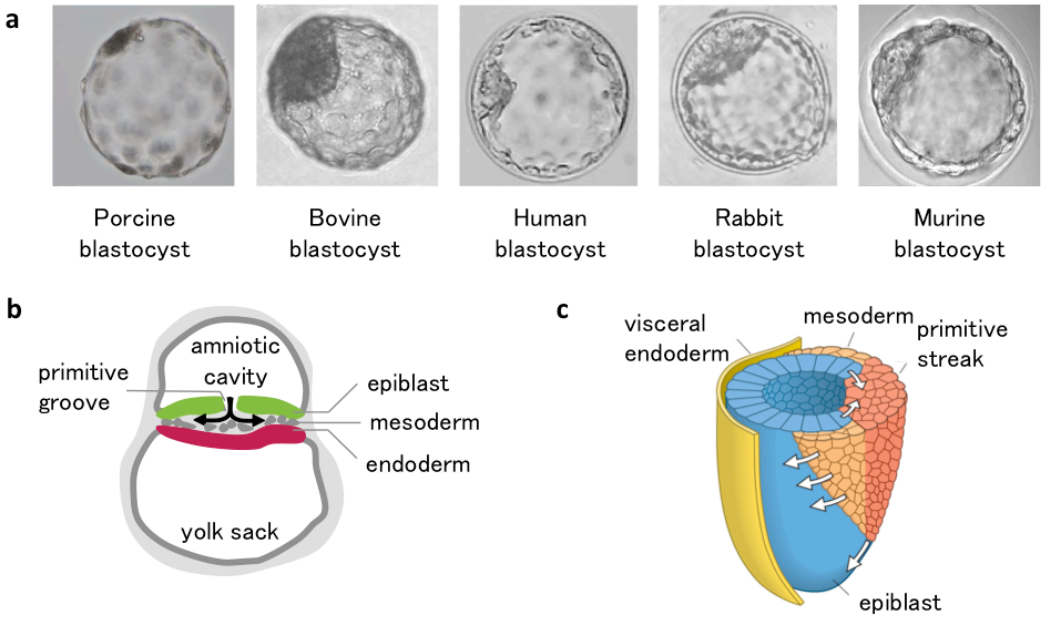

Figure 1.3. Different mammalian pre-implantation embryos.

a, Blastocysts of pig, cow, rabbit, mouse and human. Adapted from Beier et al. 1983, Zhang et al. 2009, Xue et al. 2016, Golding et al. 2015. **b,** Human gastrula. **c,** mouse gastrula. Adapted from Wolpert et al. 2014). Arrows mark movement of cells during gastrulation.

Heterogeneity in the ICM and second lineage segregation

After trophectoderm lineage has been set aside, the inner cell mass is further segregated into the epiblast (Epi) and the primitive endoderm (PrE) lineages (Fig 1.2 and 1.8). While TE is mostly important for interaction between the uterus and the embryo (Rossant and Tam 2009), part of PrE lineage-derived visceral endoderm (VE) remains in close contact with the epiblast during immediate post-implantation development and provides signals that are crucial for its patterning and for induction of key morphogenetic events (reviewed in Arnold and Robertson 2009, Rossant and Tam 2009, Srinivas 2006, Beddington and Robertson 1999).

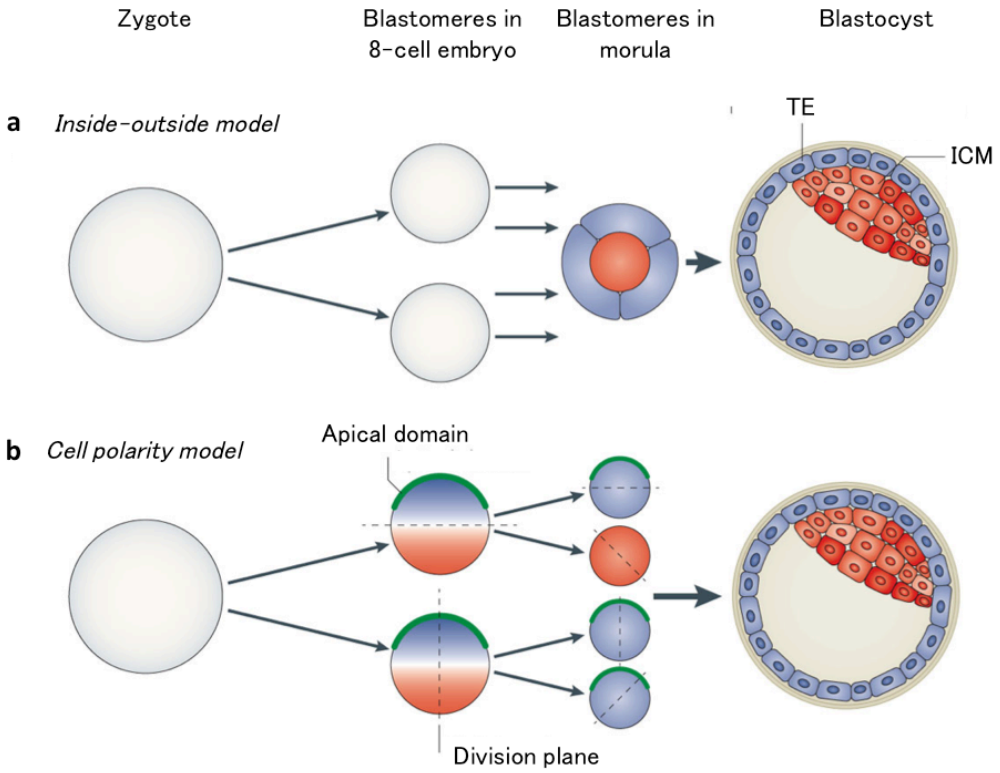

Figure 1.4. Classical models of first cell lineage segregation in the mouse embryo.

a, The inside-outside model proposes that cells make decision between TE and ICM depending on their inside or outside position within the embryo. **b,** The cell polarity model states that cells that inherit apical domain during division become TE, and the cells that do not become apolar ICM. Adapted from Wennekamp et al. 2013.

The first PrE-specific gene expression can be detected as early as 2.5 days post conception (dpc). At this point, transcription factor Gata6 that is later restricted to PrE, as well as Nanog that is epiblast-specific, will start to be expressed by all ICM

cells (Chazaud et al. 2006, Plusa et al. 2008). At 3.5 dpc, two distinct populations emerge from this overlapping pattern: expression of Gata6, Gata4, Sox7, Sox17 define PrE precursors, while Nanog, Sox2 and other pluripotency factors define EPI precursors (reviewed in Schrode et al. 2013). Each of the transcription factor groups initially displays salt-and-pepper expression within the ICM (Chazaud et al. 2006, Plusa et al. 2008). Importantly, while the cells within the ICM show bias to EPI or PrE at this point, they retain certain level of plasticity until the blastocyst maturation is completed at 4.5 dpc (Gabarek et al. 2012). A comprehensive study on single cell gene expression dynamics in ICM during second lineage segregation revealed initial gene expression heterogeneity within the ICM, that is progressively resolved into lineage-specific gene expression patterns as the blastocyst matures (Fig 1.5, Ohnishi et al. 2014).

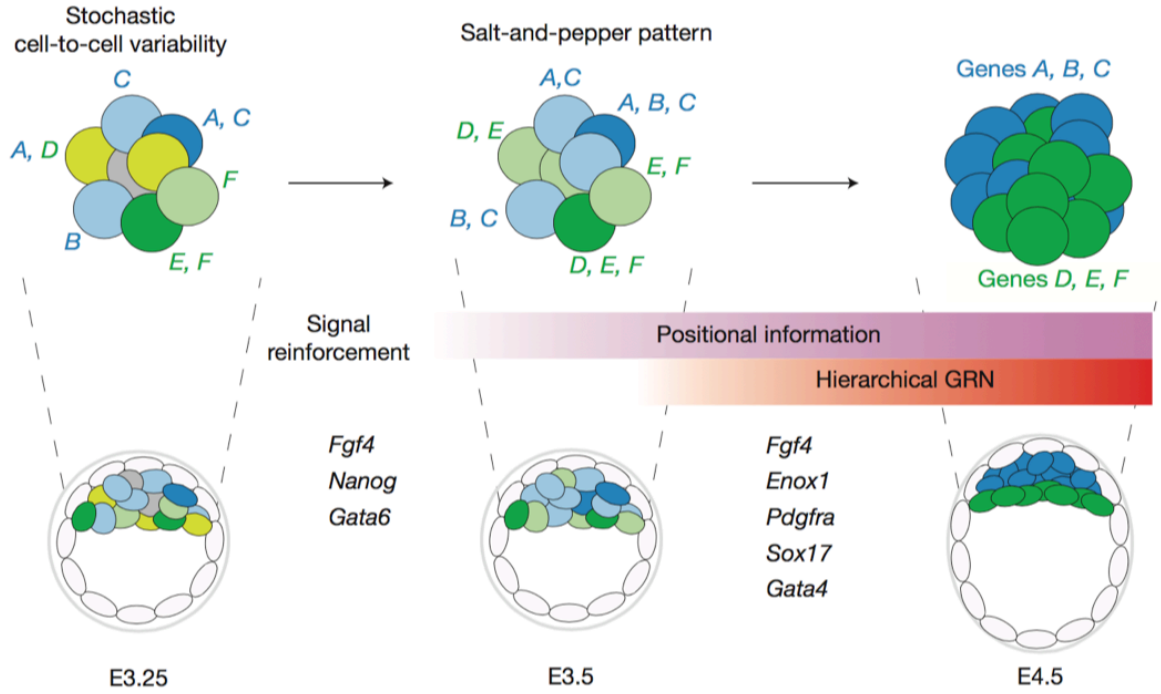

Figure 1.5. Progressive EPI versus PrE lineage segregation in the early mouse embryo.

Stochastic onset of gene expression generates cellular heterogeneity of gene expression within the ICM(genes A, B, C represent the lineage marker for blue cells, and D, E, F for green cells). This variability is further enhanced by signaling and feedback loops and cell interactions to produce salt-and-pepper distribution of two emerging cell populations. Eventually integrating gene regulatory network (GRN) activity and cell positional information, two transcriptionally distinct and spatially segregated lineages (represented by blue and green cells) are established in the late blastocyst. Adapted from et al. Ohnishi et al. 2014.

While the precursors for the second lineage segregation are harbored by the ICM, it is apparent that ICM itself if not prepatterned, but rather displays a stochastic cell-to-

cell gene expression variability that may be relevant to developmental plasticity and regulative capacity of the early mouse embryo (Ohnishi et al. 2014, Yamanaka et al. 2010, reviewed in Wennekamp et al. 2013).

Heterogeneity and stochastic lineage choice in various biological systems

Cell fate decisions are tightly controlled to yield cell populations, tissues, and organs of reproducible quality, size and form. However, many biological systems display transcriptional state heterogeneities that are resolved in a manner with both deterministic and stochastic features.

Developmental and homeostatic programs make use of stochastic mechanisms to generate differences in an apparently homogeneous cell population. For example, transient heterogeneity and stochastic cell fate induction within bacterial populations allow them to survive adverse environmental conditions, a mechanism called stochastic switching (Fig 1.6 a, reviewed in Veening et al. 2008, Gefen et al. 2009). In multicellular organisms, variation is often integrated into developmental programs. In worms, insects, and vertebrates alike, stochastic fate choices are utilized to increase diversity of sensory receptors by random selection (reviewed in Johnston and Desplan 2010). For instance, in mouse embryos, vast transcriptional heterogeneity within retinal progenitor population underlies cell fate and proliferation decisions (Trimarchi et al. 2008). Finally, importance of stochastic stem cell fate regulation in adult tissue homeostasis has been recently described (reviewed in Simons and Clevers 2011). Further studies will be needed to shed light on how gene expression heterogeneity is generated in deterministic or stochastic manner and the what is its biological role.

Stochastic decisions are an effective way to generate heterogeneity within a cell population leading to a variety of fates. Yet, when a reproducible and robust outcome is required, these decisions can be directed, or compensated for. For example, in the neural cells within developing vertebrate spinal cord, transcription factors are turned on in a stochastic manner, but the motor neuron pool is ultimately subdivided into further populations by a bi-stable double negative regulatory loop (Helmbacher

et al. 2003, Dasen et al. 2003). Furthermore, once this heterogeneous mosaic of fates is generated within a pool, the newly specified neurons need to spatially cluster according to their type in order to form a functional neural network (Fig 1.6 b). This sorting and clustering mechanism has been demonstrated to be Cadherin-dependent (Price et al. 2002, Livet et al. 2002). Alternative non-cell autonomous mechanism to coordinate resolution of stochastic heterogeneity into two stable cell fates is lateral inhibition, as exemplified by Delta-Notch signaling (reviewed in Bray 2006, Voas and Rebay 2004, Greenwald 1998).

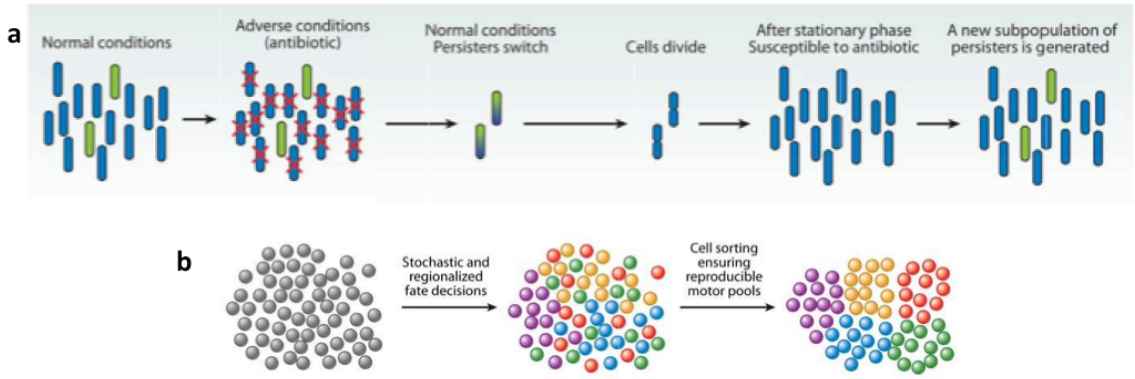

Figure 1.6. Stochastic cell fates in different biological systems.

a, Stochastically arising subpopulation of dormant perister bacteria survive adverse conditions to repopulate the colony, after which new persisters are stochastically generated within the population. **b,** Stochastic fate decisions within a pool of motor neuron progenitors is compensated by cell sorting and migration to establish coherent motor pools. Adapted from Johnston and Desplan 2010.

Taken together, these examples illustrate how stochastic gene expression heterogeneity can be used in diverse biological systems as a mechanism for survival, a way to initiate cell fate differentiation during development, and to maintain robust stem cell populations for adult tissue renewal. Resolving the heterogeneity in a functional way in a multicellular organism by regulatory loops and cell sorting aids in successfully achieving developmental goals. Most importantly, in order to study cellular heterogeneity and stochastic cell fate determinations it is important to use tools that allow continuous collection of dynamic information over time.

Self-organization of the blastocyst

Self-organization refers to the emergence of complex patterns from units of lower complexity in the absence of external instructions. The force driving self-organization is the intrinsic properties of these units, and their local interactions. Self-organizing systems are defined by dynamic, contextual and interdependent relations among their parts (Saetzler et al. 2011). Typically, the self-organizing systems gain robustness from positive and negative feedback loops, and display an emergence of coherent patterns and functions from initial noise (reviewed in Karsenti 2008, Sasai 2013).

In all these respects, an early mouse embryo is a self-organizing system. The embryonic ability to form a blastocyst containing two cell lineages is inherent to each lower complexity unit of an early embryo, referring specifically to the cells of an 8-cell morula (Dietrich and Hiiragi 2007, Korotkevich et al. 2017). While the morula embryo is highly heterogeneous in its gene expression, cell position and gene expression adjustments during subsequent pre-implantation development lead to emergence of consistency between cell developmental potential and its lineage and spatial assignment. In this way, before moving on to the post-implantation axis-establishment stage, initial heterogeneity of lineage-specific gene expression is resolved, leading to the formation of a pattern of higher complexity – a blastocyst of a defined morphology and comprising first cell lineages.

Establishment of body axes in mammalian development

Correct and timely establishment of body axes is crucial for successful embryonic development. The vertebrate body plan is defined by dorsal-ventral (D-V), anterior-posterior (A-P) and left-right (L-R) axes (Fig 1.7 a). Studies in various model organisms have provided knowledge of the mechanisms by which these axes are generated, but the exact origins of, for example, anterior-posterior axis of the mammalian embryo remain a controversial topic.

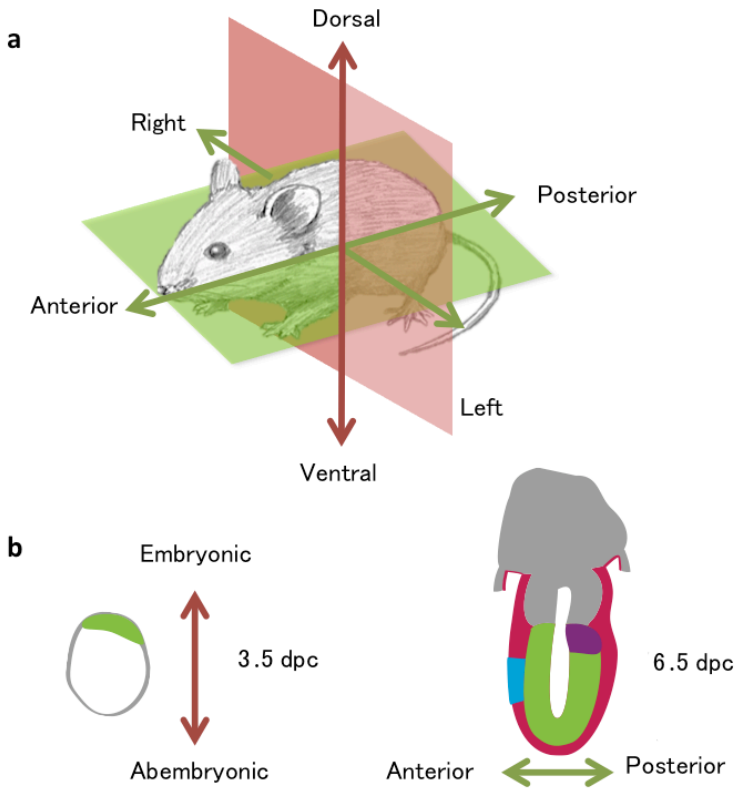

Figure 1.7. Mammalian body plan.

a, The mammalian body plan is made up of three main axes: dorsal-ventral, anterior-posterior, and left-right. **b,** First axes that emerge during development. Left: Blastocyst has embryonic-abembryonic axis that will be converted into dorsal-ventral axis. Right: Primitive streak-stage embryo acquires anterior-posterior axis, where anterior is defined by the position of anterior visceral endoderm (blue), and posterior by the position of primitive streak (purple).

In the mammalian embryo, first pivotal events in the establishment of body plan take place during pre- and peri-implantation development. Blastocyst stage lays down the groundwork for the first major axis to be established during development. During cavitation, the ICM is pushed towards one side of the embryo, generating embryonic-abembryonic axis (Fig 1.7 b). The embryonic-abembryonic axis corresponds to the proximal-distal axis of the mouse embryo at egg cylinder stage, and the proximal-distal axis in turn corresponds to D-V axis of the later stages and the adult animal (Rossant and Tam, 2009).

The second axis to be established during mouse development is the A-P axis. The A-P axis becomes apparent at around 6.5 dpc, when the primitive streak forms in the future posterior end of the embryo (Fig 1.7 b, Fig 1.8). More detailed investigation

revealed that the primitive streak is formed on the side of the epiblast that is furthest from the anterior visceral endoderm (AVE), a set of visceral endoderm cells that secrete signals conferring anterior identity to the adjacent epiblast (Beddington and Robertson 1998, Thomas and Beddington 1996). Thus understanding the origin of AVE holds the key to deciphering the mechanism of A-P axis establishment.

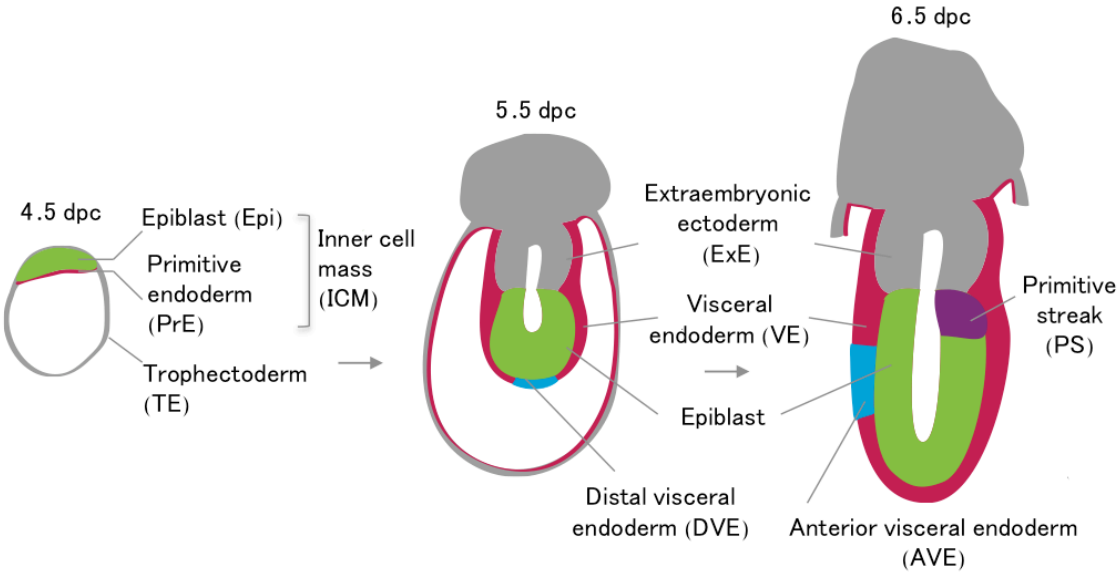

Figure 1.8. Mouse peri- and early post-implantation development

TE (grey) outgrows to give rise to extraembryonic ectoderm after implantation. Epi (green) develops an amniotic cavity and becomes cup-shaped. PrE (red) gives rise to VE that proliferates to cover epiblast and ExE, as well as to line the inner side of mural TE. At 5.5 dpc, DVE (blue) can be seen at the distal part of VE. At 6.5 dpc AVE (blue) is located on anterior side of VE, and the PS (purple) forms on the posterior part of Epi.

Third and last, the L-R axis is established at around 8.5 dpc. To establish L-R axis, pre-existing spatial cues are required – D-V and A-P axes pave the way for L-R axis determination (Okada et al. 2005, Nonaka et al. 2005). L-R symmetry is broken by leftward fluid flow generated by clockwise-rotating, posteriorly tilted primary cilia of the node (Nonaka et al. 1998, Shinohara et al. 2012). What determines the tilt or the primary cilia is the topic of ongoing studies (reviewed in Takaoka et al. 2007, Takaoka and Hamada 2012).

Origin and characteristics of DVE/AVE

Distal visceral endoderm (DVE) is key to establishing anterior visceral endoderm (AVE), a signaling center that specifies the future anterior side of the embryo (Fig 1.8). At 5.5 dpc, the cells positioned at the distal tip of the visceral endoderm acquire columnar shape, leading to tissue thickening at this point (Rivera-Pérez et al. 2003). These cells are collectively referred to as DVE. In addition to their morphology, DVE cells are set apart from the remaining VE cells by their different gene expression. One of genes marking DVE/AVE cells is Lefty1 (Yamamoto et al. 2004), a Nodal target gene that is also encoding a Nodal antagonist (reviewed in Papanayotou and Collignon 2014). Another well-characterized gene that faithfully marks DVE/AVE is a homeobox gene Hex (Thomas et al. 1988, Barbera et al. 2000, Rivera-Pérez et al. 2003). Finally, a cytokine Cerl1 marks early DVE cells in post-implantation embryo, and can inhibit canonical Wnt signaling and regulate Nodal signaling during gastrulation as well as the formation and patterning of the primitive streak (Mesnard et al. 2006).

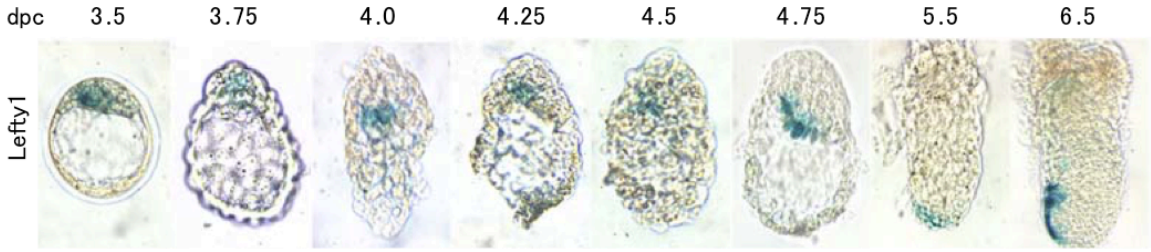

Figure 1.9. Lefty1 expression pattern in peri-implantation mouse embryo.

Lefty1-9.5 lacZ transgene in mouse embryos 3.5-6.5 dpc (adapted from Takaoka et al. 2006). Lefty1 transcript is first seen in 3.5 dpc embryo, shows restriction to PrE in 4.5 dpc embryo, and is located on one side of VE in 6.5 dpc embryo.

Several studies have tried to identify DVE/AVE precursor cells. Lefty1 and Hex transcripts have been detected in the epiblast as early as E3.5 (Fig 1.9, Takaoka et al., 2006). Hamada and colleagues found that Lefty1-positive cells in the PrE at E4.75 contribute to the DVE, bot not to AVE (Takaoka et al. 2011). On the other hand another study reported that Lefty1 expression is lost between E4.75 and E5.25 and that DVE cells arise anew during early post-implantation development (Hoshino et al. 2015). Direct lineage tracing experiments remain to be performed to

unequivocally identify the origin of DVE and AVE precursors and to characterize the lineage of DVE cells and the pattern of anterior marker expression during peri-implantation development.

AVE, a specialized subset of VE that provides signaling crucial for setting up the A-P axis, is also marked by Lefty1, Hex and CerI (Belo et al. 1997, Thomas et al. 1998, Yamamoto et al. 2004). AVE cells migrate to one side of the VE (Srinivas et al. 2004), and confer anterior identity to the adjacent Epi cells. Several studies have demonstrated that mutants of Nodal and Nodal signaling pathway are capable of inducing DVE formation but lack AVE due to inability for DVE cells to migrate to anterior (Norris et al. 2002, Ding et al. 1998). Such embryos do not develop further due to severe gastrulation defects.

At the time of the onset of DVE movement to the anterior side to form AVE, restricted localization pattern of Wnt activity may be the first apparent epiblast symmetry break (Fig 1.10, reviewed in Arnold and Robertson 2009). At the same time, DVE and later AVE antagonize Nodal signaling in the epiblast. Ultimately, the Epi furthest away from AVE is where the primitive streak emerges.

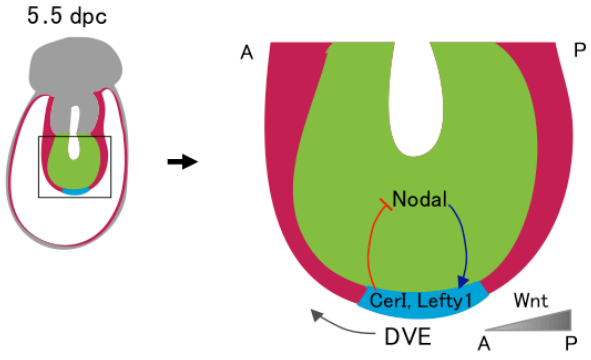

Figure 1.10. Signaling in early post-implantation embryo.

As DVE cells move forward, Wnt antagonists Lefty1 and CerI act to attenuate Wnt signaling along the future A-P axis. At the same time, signals from DVE antagonize Nodal signalling in the adjacent epiblast. Adapted from Arnold and Robertson, 2009.

To address the origin of AVE, Takaoka et al. (2011) have genetically ablated DVE cells in 5.5 dpc embryo and asked whether AVE can still be formed. While Lefty1-positive cells reappeared in such embryos, these cells now failed to migrate to one side of the embryo and eventually AVE did not form. Another study showed that clonal

descendants of single ICM cells contributed to only a portion of anterior marker-expressing visceral endoderm cells (Torres-Padilla et al. 2007), suggesting a polyclonal origin of AVE.

Embryo implantation

During first days of mammalian development, a population of cells that will be important for making mother-to-fetus connections is set aside as the blastocyst prepares for implantation. In order to interact with the mother's uterus, the blastocyst frees itself from the ZP by partially digesting it using a small trypsin-like protease (O'Sullivan et al. 2001, Perona and Wassarman 1986). The first reported contact to the uterine wall is made by the trophectoderm, by L-selectin binding to the uterine wall's sulphated polysaccharides (Genbacev et al. 2003).

At the same time, the mother's uterus is also undergoing changes, preparing to receive the fertilized embryo. Under the direction of oesterogen and progesterone produced by the mammalian ovaries, specific uterine cell types proliferate and differentiate to make the uterus receptive for embryo implantation (Carson et al. 2000, Paria et al. 2002, Dey et al. 2004). The structure of uterine epithelium and the mode of interactions between embryo and uterus at the earliest stages of implantation vary between different mammalian species (reviewed in Wang and Dey 2006). In the guinea pig, the trophoblast penetrates between the uterine epithelium cells, followed by entire embryo embedding itself in the uterine stroma (Fig 1.11 a). In the rabbit, the trophoblast fuses with a few uterine epithelial cells. In the primates, the trophoblast on the side of ICM first penetrates between uterine epithelium cells, and then through the basal lamina (Fig 1.11 a). In most rodents, the after hatching from ZP, the embryos enter the uterine crypts, and the closure of these crypts brings the embryonic trophectoderm in close proximity to the luminal epithelium. At this time, the trophoblast cells penetrate the uterine epithelium (Fig 1.11 a), and after death of uterine cells the basal lamina is penetrated by the underlying decidual cells (reviewed in Wang and Dey 2006, Carson et al, 2000). Blastocyst enclosed within a uterine crypt can bee seen in Fig 1.11 b.

While a mature blastocyst should interact with the uterine wall *in vivo*, electron micrographs of embryos in utero at peri-implantation stage did not show direct cell-cell junctions between uterine epithelium and trophoblast cells (Parr et al. 1987). *In vitro*, peri-implantation stage embryos have been reported to displace stromal cells from a monolayer grown on cell culture dish (Salomon and Sherman, 1975). It has been extensively demonstrated that uterine epithelial cells undergo apoptosis upon contact with the trophoblast (Welsh et al. 1993, Parr et al. 1987). In contradiction to the classical apoptosis model of epithelial luminal barrier model, it has also been proposed that the uterine epithelium cells are entosed by trophoblast early during implantation (Li et al. 2015). It is important to note that in both models of implantation, uterine luminal epithelium is likely partially eliminated by the implanting blastocyst.

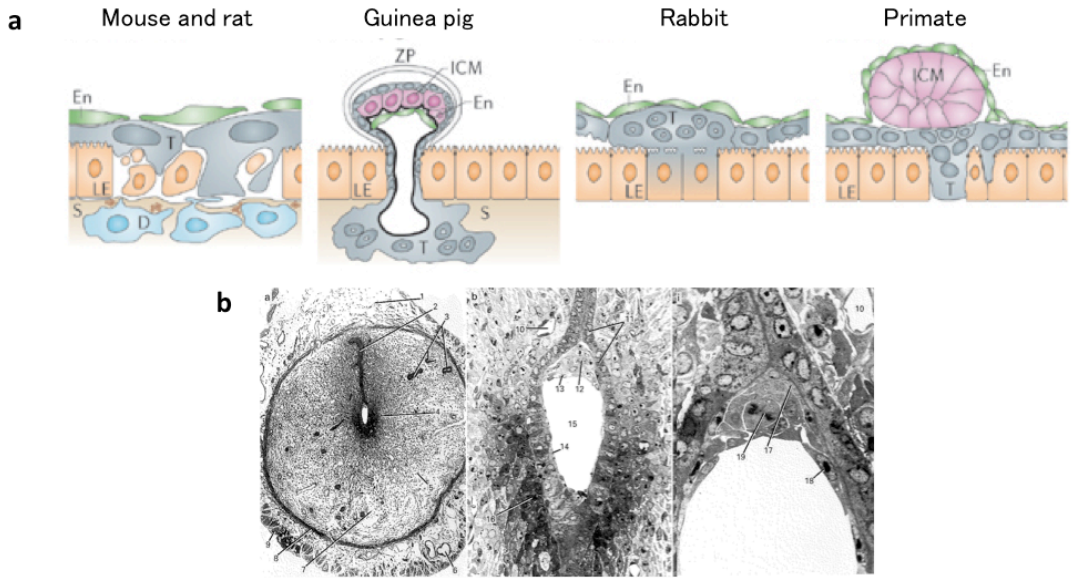

Figure 1.11. Mammalian embryos during implantation.

a, implantation in different mammals. D, decidual cells; En, embryonic endoderm; LE, uterine epithelium; S, stroma; T, trophoblast (adapted from Wang and Dey, 2006); **b,** mouse embryo in utero late on 4.5 dpc. Left, full view of decidua with embryo in a uterine crypt. Middle, close-up view of embryo surrounded by endometrium. Right, close-up view of ICM, polar TE and parietal endoderm. Adapted from Kaufman, 1999).

Taken together it remains to be shown whether the uterine cues are required for the development of the embryo proper before establishment of vascular connections to the mother. Therefore a question remains whether at the earliest stages such interaction is at all necessary to allow developmental progress.

Peri-implantation embryo culture

Due to the difficulty of crossing the implantation barrier *in vitro*, so far it was not possible to directly demonstrate the connection between anterior marker-expressing cells in the blastocyst and those in the post-implantation embryo. It has been suggested that Lefty1 expression is lost during implantation, and thus DVE forms de novo at E5.0 (Hoshino et al. 2015). As direct tracking data has so far not been available, it remains unclear whether the progenitors of DVE/AVE are set aside early on during blastocyst development, or whether they form de novo by an inductive/inhibitory signaling activity of the epiblast and the TE-derived extra-embryonic ectoderm (ExE).

The first available long-term embryo culture protocols (Hsu 1972, Hsu 1973) report that blastocysts can be cultured to post-implantation stage, attaching to the culture dish to form egg cylinders and in rare cases even proceed to early somitogenesis stage (Fig 1.12 a, Hsu 1972, Hsu 1973, Wu et al. 1981). While certain characteristics of these embryos resemble normal development, it is important to note that the general morphology is drastically altered, and development stops at the time of organogenesis (Hsu 1973). Another practical drawback to this culture method is the need for high concentration of serum, in particular human cord serum. Varying quality of different batches of sera renders the high performance of this culturing method difficult to maintain

In a recent report (Bedzhov et al. 2014), more defined culture media conditions have been proposed. This method uses minimal amount of serum in the medium, and only relies on serum for a short time. Embryos cultured in this medium attach to the bottom of the dish, and are capable of producing an elongating egg cylinder with a proamniotic cavity (Fig 1.12 b). Such embryos have been reported to establish anterior-posterior axis, as marked by asymmetric expression of anterior and posterior markers (Morris et al. 2012, Bedzhov et al. 2015). Furthermore, this culturing method has been used for culturing human embryos *in vitro* for the longest period to date (Shahbazi et al. 2016, Deglincerti et al. 2016).

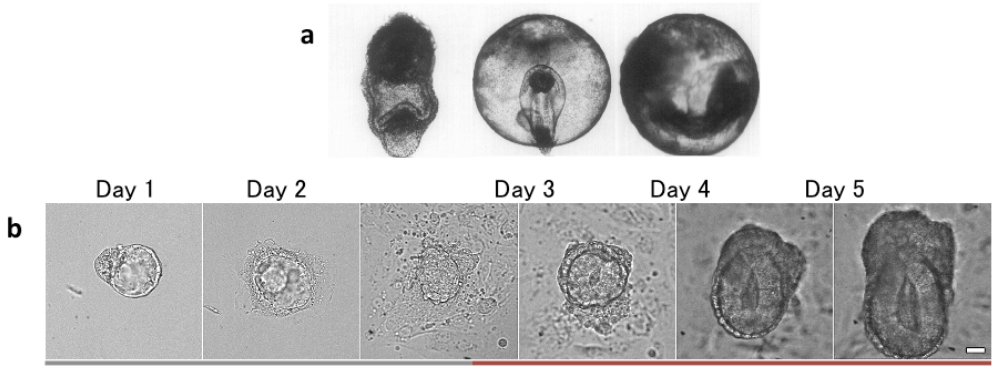

Figure 1.12. Mouse embryo peri-implantation culture.

a, Embryo cultures in a prolonged *in vitro* culture from blastocyst to somite stage (adapted from Hsu 1973).From left to right: embryo cultured 7 days from 3.5 dpc; embryo cultured for 8 days from 3.5 dpc with somites visible; embryo cultured for 9 days from 3.5 dpc. **b,** embryo cultured through peri-implantation stages in chemically defined medium. Embryo attaches to the bottom of culture dish, and after 4-5 days of culture, egg cylinder emerges (adapted from Bedzhov et al. 2014).

The abovementioned culture system has shed light on behavior or DVE, and on the self-sufficiency of the embryo when establishing anterior-posterior axis in the absence of maternal cues. However, Hiramatsu et al. (2013) have demonstrated the requirement of unidirectional spatial constriction for DVE/AVE migration. This claim was further challenged by Bedzhov et al. (2015), who have demonstrated AVE migration in the absence of spatial constrictions. It therefore remains unclear whether maternal tissues contribute to AVE migration. Interestingly, unidirectional constriction by uterine tissues was proposed to contribute to the establishment of the elongated shape of the rodent embryo, as opposed to disk-shaped avian and non-rodent mammalian embryo (Hiramatsu et al. 2013). Indeed mouse embryos grown *in vitro* beyond implantation stage and thus not impacted by unidirectional constriction are rounder than their *in vivo* counterparts (Hsu 1973, Fig 1.12 a).

Ultimately, the currently available culturing methods demonstrate the capacity of the mammalian embryo for self-organization in the absence of maternal cues, though whether mechanics of embryo constriction guide development of A-P axis remains controversial. The culture efficiency and the resulting morphology of peri-implantation embryos suggest that further method improvements will be needed to truly recapitulate peri-implantation development *in vitro*.

2. AIMS AND STRATEGY

The overarching goal of my PhD study is to characterize the emergence and resolution of cellular heterogeneity and to investigate its possible role in lineage progression and body patterning during early mouse development.

Cell-to-cell gene expression heterogeneity first emerges in the morula embryo when symmetry between cells, both in differentiation potency and geometry, is broken during the transition from 8-cell to 16-cell stage. This gene expression heterogeneity is enhanced within the inner cell mass (ICM) cells of the early blastocyst, before their progressive segregation into epiblast (Epi) or primitive endoderm (PrE) lineages. I studied this first phase of cellular heterogeneity to understand how the first cell fate decisions are made in the mammalian embryo. It is well established that a lineage tree of early mouse development is variable between embryos, therefore it is not possible to predict future lineage only from the division pattern or to identify progenitors for the first lineages. Thus I aimed to integrate the dynamics of lineage-specific gene expression and the information of cell position within the embryo into a classic lineage tree. To this end, we performed a gene trap screen and generated mouse lines with ICM or TE-specific Venus reporter expression. With such lines we were able to produce an enhanced lineage map that would allow us to identify lineage-specific gene regulation that paves the way to embryonic cell fate decisions. This helped us to understand how initial gene expression heterogeneity in the morula is resolved into first two lineages in the early blastocyst.

The first-phase gene expression heterogeneity is eventually resolved by forming three distinct lineages in the late blastocyst. During subsequent body-patterning phases, new lineage-specific gene expression heterogeneity should emerge within the blastocyst that will dictate the embryonic body axis formation. However, the mechanism and dynamic changes associated with this second-phase cellular heterogeneity emergence are poorly understood. Therefore, I have expanded my study to peri-and post-implantation stages of embryonic development to examine the exit from pluripotency and emergence of a rare cell population that directs embryo body patterning. I asked whether the heterogeneity within the ICM of the blastocyst predicts future patterning, and specifically, whether the ICM harbors progenitors for distal visceral endoderm and anterior visceral endoderm, primitive endoderm-derived cell populations that are responsible for establishing anterior-

posterior axis in the embryo. To answer these questions, I aimed to develop embryo culture method that would allow me to monitor embryonic development during peri-implantation stages. By combining this culture method with light-sheet microscopy live imaging, we investigated the progenitors of distal visceral endoderm and anterior visceral endoderm within the pre-implantation embryo, and followed their lineage and development throughout the peri-implantation stage.

3. MATERIALS AND METHODS

Molecular work

Extraction of genomic DNA

Genomic DNA (gDNA) was extracted from mouse tail biopsies. The biopsies were digested overnight using 0.5 mg/ml Proteinase K (Sigma, P2308) in buffer containing 50 mM Tris-HCl pH 8.0 (Sigma, T2663), 100 mM NaCl (Sigma, S5150), 100 mM EDTA pH 8.0 (Fluka, 03690) and 1% SDS (sodium dodecyl sulphate, Serva, Cat. No. 39575.02). Equal volume of 2-propanol was added to the supernatant to precipitate gDNA, followed by air-drying the pellet overnight at room temperature. Finally, the pellet was dissolved in Tris-EDTA (Qiagen) at 65°C for 15 min, while shaking at 450 rpm in a thermo mixer (Thermomixer comfort, Eppendorf).

Extraction of gDNA for genotyping in this study was done by Ramona Bloehs, Stefanie Friese, Ivica Lehotska, Katja Langenfeld and Wibke Schwarzer.

DNA production

To amplify DNA for RNA production, 1 µg plasmid DNA was added to 50 µl competent Escherichia coli (E.coli) DH5α bacteria (Life Technologies, 18265-017). The mixture was incubated for 15-30 min on ice, then heat-shocked in 42°C water bath for 30 sec and transferred back on ice for 2 min. Next, 500 µl SOC medium (Sigma, S1797) was added and the mixture was incubated 30 more min at 37°C in a shaker set to 500 rpm. 1 µl and 100 µl of the mixture were used to plate on LB-agar plates with a required antibiotic, and the plates incubated overnight at 37°C.

Single colonies were picked for inoculating Miniprep cultures, for which 5 ml LB medium supplemented by a required antibiotic was used. 150 µl of Miniprep cultures were used to inoculate 150 ml of Maxiprep cultures that were prepared as above. Miniprep and Maxiprep cultures were incubated overnight at 37°C and agitated at 230 rpm. QIAprep Spin Miniprep Kit (Qiagen) and HiSpeed Plasmid Maxi Kit (Qiagen) were used to extract plasmid DNA as described in the manufacturer's protocol.

RNA isolation from trophectoderm cells and reverse transcription

20% v/v of trichloromethane was added to TE samples in TRI reagent (see section on bisection), and the samples were centrifuged at 4°C at 12,000 rpm for 15 min. The supernatant was transferred into a fresh tube, and 50% v/v 2-propanol and 3 µl glycogen (Ambion, AM9510) were added. After 15 min incubation on ice, the samples were once again centrifuged for 30 min at 4°C at 12,000 rpm, after which the supernatant was discarded, and the pellet washed with 80% ethanol. For reverse transcription, SuperScript III First- Strand Synthesis System for RT–PCR (Life Technologies, 18080- 051) was used, following the manufacturer's instructions and using oligo (dT)20 priming method. The cDNA synthesis was carried out for 1 h. RNA isolation was done together with Stefanie Friese.

qRT–PCR

Single-cell cDNA samples were prepared by Yusuke Onishi as described in Ohnishi et al 2014. qRT–PCR was performed using SYBR" Green PCR Master Mix (Life Technologies, 4309155) on ABI StepOne devices (Life Technologies, 4376357, Ser. No. 272006386) according to the manufacturer's instruction with 5 µM primer concentration in 10 µl final sample volume, run for 40 cycles. Each reaction was run in duplicates. qRT-PCR was done together with Stefanie Friese. The primers sequences are listed in Table 1.

Gapdh was used as a housekeeping gene control, and a negative control lacking cDNA was included in all runs. ES cell cDNA samples were added to each experiment in two dilutions to ensure normalized amplification between experiments. The primers sequences can be found in Table. StepOne Software (Life Technologies, version 2.3) was used to process raw data and setting a threshold for determining Ct values in the linear phase of amplification, at an equal value for the same gene in different experiments. The baseline was selected automatically and controlled manually for any software algorithm-induced mistakes. Quality of each experiment was confirmed by evaluating negative control, ES cell cDNA amplification and melt curves. A threshold for determining Ct values was set in the linear phase of amplification, at an

equal value for the same gene in different experiments. The baseline was selected automatically using StepOne Software. All replicates were included in the calculation.

Table 1. DNA primers used for qRT-PCR.

Mouse line	Primer sequence
Cripto-tdTomato	ATGTACGGCTCCAAGGCGTAC
	TGAACTCCACCAGGTAGTGGC
Hex-membVenus	ATCTGAAGCCAGCGCCATTGGCC
	TCCTTGAAGAAGATGGTGCG
	CTAGGCCACAGAATTGAAAGATCT
	GTAGGTGGAAATTCTAGCATCATCC
Lefty1-membVenus	CAGGCA TCCAGCAGAGAACG
	TCCTTGAAGAAGATGGTGCG
	CTAGGCCACAGAATTGAAAGATCT
	GTAGGTGGAAATTCTAGCATCATCC
Lifeact-GFP	TCAAGAAATTCGAAAGCATCTCAAAGG
	GACCATGTGATCGCGCTTCTCGTT
mTmG, mG	CTCTGCTGCCTCCTGGCTTCT
	CGAGGCGGATCACAAGCAATA
	TCAATGGGCGGGGGTCGTT
Nanog-GFP	TGAACCGCATCGAGCTGAAG
	GCAATGCCCCAACCAGT
Nanog-mCherry	CCTGTCCCCTCAGTTCATGT
	TTGACCTCAGCGTCGTAGTG
Pdgfra-GFP	CCCTTGTGGTCATGCCAAAC
	GCTTTTGCCTCCATTACACTG
	ACGAAGTTATTAGGTCCCTCGAC
R26-H2B-mCherry	TCCCTCGTGATCTGCAACTCCAGTC
	AACCCCAGATGACTACCTATCCTCC
	GCTGCAGGTCGAGGGACC
SEC lines	CCTAACGTTACTGGCCGAAG
	CCTAGGAATGCTCGTCAAGAAG
Sox2-GFP	AAGTTCATCTGCACCACCG
	TCCTTGAAGAAGATGGTGCG
	ACCAGCTCGCAGACCTACAT
VET lines	TGAACCGCATCGAGCTGAAG
	GCAATGCCCCAACCAGT

mRNA production

To produce myr-PALM-tdiRFP mRNA for injection into embryos, 3 µg of DNA plasmid (Fig 2.1) was digested for 16 h at 37°C using 5 u PacI restriction enzyme (New England Biolabs, R0547L) in total volume of 50 µl. To separate fragments after enzyme restriction reaction, DNA mixed with loading dye (Life Technologies, R0611)was loaded onto 1% (w/v) agarose (Lonza, 50004) gel made in TAE buffer (Life Technologies, B49) with 0.03 µl/ml DNA stain (Serva, 39804.01). 1 kb Plus ladder (Thermo Fisher, 10787018) was used to determine the size of resulting fragment. The band corresponding to the size of a linearized plasmid was identified and cut out from the gel, and DNA was extracted using gel extraction kit (Qiagen, 28704).

In vitro transcription of mRNA was done using mMESSAGE mMACHINE® T7 ULTRA Transcription Kit (Thermo Fisher, AM1345). Polyadenylatoin was performed using Poly(A) Tailing Kit (Thermo Fisher, AM1350).

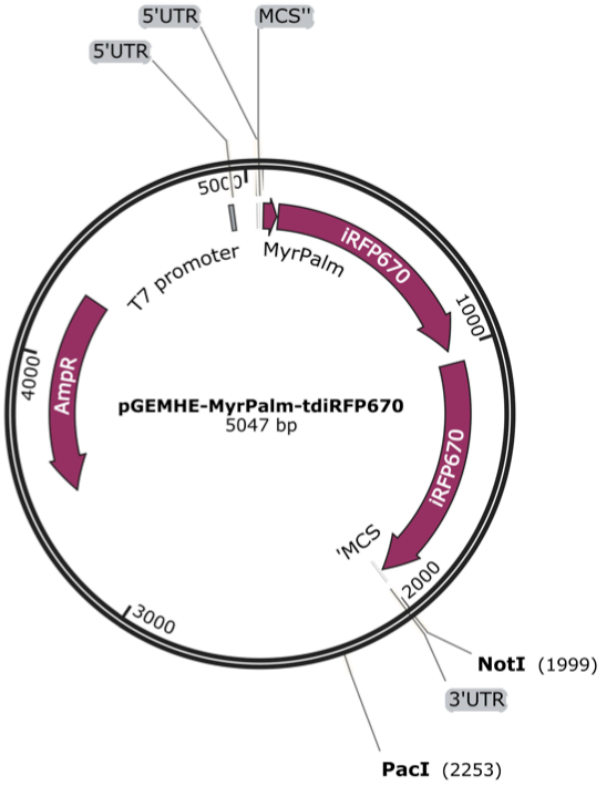

Figure 2.1. Construct used to produce Myr-PALM-tdiRFP mRNA for microinjections.

Animal work

Mouse keeping

All animal works were performed in the animal facility at the European Molecular Biology Laboratory, according to the permission by the institutional veterinarian overseeing the operation (ARC number TH11 00 11). The animal facilities are operating according to international animal welfare rules. Mouse colonies were maintained in pathogen-free conditions on 12h light – 12 h dark cycle.

Mouse strains

Wild-type embryos were obtained by breeding F1 (C57Bl/6xC3H) males with F1 (C57Bl/6xC3H) females.

The following transgenic mouse lines were used in this study: Cdx2-EGFP knock-in (McDole and Zheng, 2012), R26-H2B-mCherry (Abe et al, 2011), mTmG and mG (Muzumdar et al, 2007), Lefty-membVenus, Hex-membVenus, GATA4-membTomato (Takaoka et al. 2006, Takaoka et al. 2014), Lefty-mCherry (gifts from Hamada lab, Osaka university, unpublished), Pdgfrα-EGFP (Plusa et al. 2008), Cripto-tdTomato (see generation of transgenic lines), Sox2-GFP (Arnold et al. 2011), Nanog-GFP (generated in Hiiragi lab from cells described in Filipczyk et al. 2013), Nanog-mCherry (see generation of transgenic lines), Lifeact-GFP (Riedl et al. 2010).

Genotyping

The genotype of transgenic animals was determined by PCR or RT-qPCR on genomic DNA. The primers used are listed in Table 2 Genotyping in this study was done by Ramona Bloehs, Stefanie Friese, Ivica Lehotska, Katja Langenfeld and Wibke Schwarzer.

Transgenic mouse line generation

Gene trap lines

First generation gene trap screen resulting in VET lines was performed by Jens Dietrich as described in Dietrich et al. 2015. Second generation gene trap resulting in SEC lines was performed by Sebastian Wennekamp (Wennekamp, PhD thesis, 2013).

Table 2. DNA primers used for determining genotype of transgenic mice.

Target gene	Primer sequence
2610305D13Rik	TGAATGTTTGCTCCTCACCA
	TGAGACATTCCCATTCCTCTG
Cdx2	ATTGTTTGCTGCTGTTCGAGTC
	CGACTTCCCTTCACCATACAAC
Gapdh	ATGAATACGGCTACAGCAACAGG
	CTCTTGCTCAGTGTCCTTGCTG
Gm13145	TGGACTTCTCATCGGAGGAA
	TGTTCCACGACCTTCTCCTT
Gm13152	TAATCCGGGCAACAAGAATG
	GCACAATGACCTCTGAGCAA
Gm13242	CTGCCAGATCAGAGGTCTCC
	TGGTGAGGAGCAAACATTCA
Oct4	GGCTCCTGATCAACAGCATCAC
	GATGCTGTGAGCCAAGGCAAG
Rex2	TGCTCAGTCAACTCTCCGTAA
	TGGTGAGGAGCAAACATTCA
Sox2	CATGAGAGCAAGTACTGGCAAG
	CCAACGATATCAACCTGCATGG
Tmem50b	GCGGTGGCTTCTCTATTCAT
	AGAGAACCGTGTGCATTTT
Zfp600	CATGGATGTGATGTTGGAGAA
	TGTGCTGTGTTTCTTGTTCCA

Embryonic stem cell culture

Embryonic stem cells (ESCs) used for culture were Nanog-mCherry (knock-in, gift from Konstantinos Anastassiadis, TU-Dresden). Inactivated mouse embryonic fibroblasts (MEFs) were plated one day before the start of ESC culture (day 0) and cultured overnight in MEF medium (Dulbecco's Modified Eagle's Medium (DMEM) 4,500 mg/ml glucose, without sodium pyruvate (Gibco, 41965) supplemented by 10% Fetal Calf Serum (brand), 2 mM glutamine (Sigma, G-7513 or Gibco, 25030), and 50 U/ml penicillin/50 mg/ml streptomycin (Sigma, P-0906 or Gibco, 15070).

On day 1, ESCs were unfrozen and plated on top of MEFs in ESC medium (Dulbecco's Modified Eagle's Medium (DMEM) 4,500 mg/ml glucose, without sodium pyruvate (Gibco, 41965) supplemented by 20% Fetal Calf Serum, 2 mM glutamine, and 50 U/ml penicillin/50 mg/ml streptomycin, 1X non-essential amino acids (Gibco, 11140), 100 µM b-mercaptoethanol (brand), 1 X nucleosides (Millipore, Embryomax ES-008-D), 10 U/l LIF (Murine Leukemia Inhibitory Factor ESGRO™ (Gibco, 3275SB), 25mM Hepes pH7.3 (Sigma H-0887). The initial plating density was 1 -3 x 10^6 ES cells per 60 mm dish, the cells were replated at 2 - 5 x 10^6 ES cells per 100 mm dish.

ES cell injection into blastocysts

ES cells were split in the morning one day before injection into blastocysts. The colonies were detached by incubating in 0.05% Trypsin (Sigma, D-6552) with 0.02% EDTA (Gibco, 45300) in 1x D-PBS (Gibco, 14190) for 5 min, and dissociated by pipetting up and down with a 200 µl pipette tip. Cells were counted using Neubauer Chamber, and plated on at following densities: $1x10^5$, $3x10^5$, $6x10^5$ cells/60 mm dish. ES cell clones were picked and injected into blastocysts by Yvonne Petersen at EMBL Transgenic Service.

Preparation and injection of BAC construct

Cripto-tdTomato bacterial artificial chromosome (BAC) construct was a gift from Hiroshi Hamada, Osaka University. Prior to injection, 0.5 µg of the construct was digested for 4 h with PI-SceI enzyme (New England Biolabs, R0696) at 10 U/mL concentration in total volume of 50 µl. Next, dialysis was performed in a 10 cm cell culture dish containing 15 ml dialysis buffer (10 µM EDTA and 0.1 M NaCl in water, filter sterilized). A nitrocellulose dialysis membrane (Millipore, VSWP01300, 0.025 µm) was floated in the dish, and digested BAC was added on top. After 1 h BAC was collected and stored until injection the next day. BAC injection into embryos was done by Yvonne Petersen at EMBL Transgenic Service.

Embryo work

Recovery and culture of pre-implantation embryos

Superovulation in female mice was induced by intraperitoneal injection of 5 international units (IU) of pregnant mare's serum gonadotropin (PMSG, Intervet Intergonan) and intraperitoneal injection of 5 IU human chorionic gonadotropin (hCG), Intervet Ovogest 1500) 48 h later. On the day of embryo recovery, the females were sacrificed by cervical dislocation and either the oviduct or the oviduct and the uterus were removed.

Embryos at 1.5 dpc were collected from the oviduct by flushing with a KSOM-Hepes (Millipore, MR-024-D) by inserting a fine canule (Acufirm, 1400 LL 23) into the infundibulum. Embryos at 2.5-3.5 dpc were collected the same way, but both the oviduct and the uterus were flushed. Embryos were washed by transferring them through several microdrops of KSOM-Hepes, and cultured in 10 µl drops of KSOM (Millipore, MR- 121-D) covered with mineral oil (Sigma, M8410 or Acros Organics) in 5% CO2 atmosphere at 37°C. Embryos were transferred using an aspirator tube (Sigma, A5177-5EA) and a pipette pulled from glass capillaries (Blaubrand intraMARK 100 µl, Brand, 7087-44).

Recovery of post-implantation embryos

To recover post-implantation embryos at 5.0 – 6.5 dpc, the mice were sacrificed and whole uteri were removed. The dissection embryos from the deciduae was performed as described in Nagy et al. 3rd edition. The embryos were dissected and stored shortly in Phenol Red-free DMEM-F12 (Gibco, 21041-025), before being fixed or otherwise treated as described in respective sections below.

Recovery and culture of embryos prior to peri-implantation culture

Pre-implantation embryos for 3D-geec were recovered at 2.5 or 3.5 dpc and incubated in KSOM as explained above. Starting with 4.5 dpc, naturally hatched embryos were selected and moved to 2D peri-implantation culture or 3D-geec. Embryos that took longer to hatch (latest on the morning of 5 dpc) were transferred later. If required, the embryos were screened for fluorescence or time-lapse imaged prior to 3D-geec as explained below.

Immunofluorescent staining of pre-, peri-, post-implantation embryos

Embryos were fixed in 4% paraformaldehyde (Sigma, P6148) in PBS for 15 min (pre-implantation) or 25 min (post-implantation or 3D-geec embryos). When staining transgenic embryos, they were screened for fluorescence and sorted into positive and negative groups prior to fixation, and remained separated throughout the procedure. Fixed embryos were washed with 0.1% Tween-20 (Sigma, P7949) in PBS (PBS-T) and permeabilized 0.5% Triton X-100 (Sigma, T8787) in PBS for 30 min (pre-implantation) or 45 min (post-implantation or 3D-geec embryos), followed by washing in PBS-T and blocking with 3% BSA in PBS-T (blocking solution) for 4 h up to 48 h. Incubation with primary antibodies in blocking solution at 4°C was performed overnight, and after washing in blocking solution, incubation with secondary antibodies and Phalloidin was performed for 2 h. Next, the samples were washed with PBS containing DAPI and imaged in the same solution. All incubation,

washing and imaging steps were carried out at room temperature unless stated otherwise. The antibodies and dyes used are described in Table 3.

Table 3. Antibodies and dyes used for immunofluorescent staining.

	Target	Name	Source	Dilution	Producer	Serial No.
Primary antibodies	GFP	anti-GFP pAb	rabbit polyclonal IgG	1:500	MBL	Code No. 598
	Cdx2	anti-CDX-2 [CDX2-88]	mouse monoclonal IgG	1:200	Biogenex	MU392-UC
	Sox2	anti-Sox2 Y-17	goat polyclonal	1:100	Santa Cruz Biotechnology	sc-17320
	Lefty1	Human/Mouse Lefty	goat polyclonal IgG	1:100	R&D Systems	AF746
	GATA4	GATA-4 (H-112)	rabbit polyclonal IgG	1:100	Santa Cruz Biotechnology	sc-9053
	GATA6	Human GATA-6	goat polyclonal IgG	1:100	R&D Systems	AF1700
	Oct3/4	Oct3/4 (C-10)	mouse monoclonal	1:100	Santa Cruz Biotechnology	sc-5279
Secondary antibodies	anti-rabbit	Alexa Fluor 546	donkey	1:200	Life Technologies	A10040
	anti-goat	Alexa Fluor 488	donkey	1:200	Life Technologies	A11055
	anti-mouse	Cy5	donkey	1:400	Jackson ImmunoResearch	715-175-150
	anti-mouse	Alexa Fluor 488	donkey	1:200	Life Technologies	A21202
Dyes	(DNA)	DAPI	-	1:2000	Life Technologies	D3571
	(Actin)	Rhodamine Phalloidin	-	1:100	Invirogen	R415
	(Actin)	Phalloidin 633	-	1:50	Life technologies	A22284

Microinjection

Microinjection of myr-PALM-tdiRFP mRNA was performed with a microinjector (Eppendorf, FemtoJet) connected to a micromanipulator (Narishige, MON202-D) using Zeiss Observer.Z1 epifluorescence microscope (Zeiss) at 32°C. Embryos were transferred into a 10 µl drops of KSOM-H on a glass bottom dish (MatTek, P506-1.5-14-F) covered in mineral oil. The mRNA was injected into the cytoplasm of each of the two blastomeres of 2-cell stage embryos (1.5 dpc, 42-44 h after hCG injection into the female). For injection, microinjection needles were used that were pulled from

filament-containing capillaries (Warner Instruments, G100TF-6). For holding, holding pipettes were used that were pulled from capillaries without filament (Warner Instruments, GC100T-15). Both types of needles were pulled with micropipette puller (Sutter Instruments, P-97), and further prepared using a microforge (Narishige, MF-900).

Isolation of single blastomeres from morula

To isolate single cells, zona pellucida was removed from 8-cell stage embryos (2.5 dpc) by incubating embryos in 0.5 % (w/v) Proteinase K (Sigma, P8811, in KSOM-H with 0.5% PVP-40) for 3 min. After washing, the zona pellucida-free embryos were transferred to Ca^{2+} and Mg^{2+}-free KSOM medium (custom made as described in Biggers et al. 2000) for 10 min. Single cells were dissociated by pipetting up and down using an embryo-transfer capillary that has been flame-polished to achieve a narrow diameter. Embryos without zona and single cells were cultured in Petri dishes (Falcon, 351008) to avoid attachment to the dish surface.

Isolation of mural trophectoderm cells by manual bisection

4.5 dpc embryos were left to hatch naturally from zona pellucida. The embryos were manually bisected by cutting at the ICM-blastocoel boundary with 30Gx1/2 needle (BD, 305771). ICM and polar TE cells were separated from mural TE cells , and each sample was transferred to 100 µl TRI reagent (Ambion, AM9738) on ice and stored at -20°C until RNA extraction.

Isolation of single cells from 4.5 dpc embryos

Single cells were isolated from blastocysts based on previously described protocol (Ohnishi et al. 2014). Naturally hatched 4.5 dpc embryos were selected for single cell isolation and screened for required marker expression using LSM 780 (Zeiss). Embryos were moved to KSOM containing anti-mouse lymphocyte serum (Cedarlane,

CL2301, 1:5 dilution) for 30 min at 37°C, followed by washing in KSOM-H. Embryos were then transferred to KSOM containing Guinea pig complement serum (Cedarlane, CL5000F, 1:2 dilution) for 30 min at 37°C, followed by another wash in KSOM-H. The lysed TE was removed by pipetting up and now using narrow flame-polished capillary. The isolated ICM was transferred to 1 mM EDTA/HBS (Sigma, 55037C) for 8 min at RT, followed by incubation in 0.1% Trypsin in 1 mM EDTA/HBS for 7 min at 37°C. The ICM was then moved to KSOM-H and pipetted up and down using various diameter glass pipettes pulled from glass capillaries and flame polished (as described in section "Recovery and culture of pre-implantation embryos"), or pulled using micropipette puller (as described in section "Microinjection"). Single isolated cells were transferred into 1 µl KSOM drops in an imaging dish (MatTek, P356-1.5-20-C) and screened for required fluorescent singal using LSM 780 (Zeiss). Single cells of interest were then moved to 3.4 µl of Single-cell RNA-seq lysis mixture in 200 µl tube (Axygen, PCR-02-C) and placed on dry ice or at -80°C. The Single-cell RNA-seq lysis mixture contained 4 U Recombinant Ribonuclease Inhibitor (Takara, 2313B), 2.9 mM dNTP (Thermo Fisher, R0193), 0.56% Triton X-100 (Sigma, T8787) in nuclease-free water (Thermo Fisher, AM9932) in total volume of 3.4 µl.

2D peri-implantation culture

Hatched embryos were moved to 8 Well slide (µ-Slide 8 Well ibiTreat, Ibidi, 80826), 3-6 embryos/well, containing 250 µl warm IVC1 medium (as described in Bedzhov et al. 2014: advanced DMEM/F12 (Life Technologies, 12634-010) supplemented with 20% (v/v) heat-inactivated FCS (Fetal Bovine Serum (South America), Embryonic Stem Cells tested, Biosera, FB1001S), 2 mM GlutaMAX (Life Technologies, 35050-061), penicillin (25 units/ml)/streptomycin (25 µg/ml, Life Technologies, cat. no. 15070-063), 1× ITS-X (10 mg per liter insulin, 5.5 mg per liter transferrin, 0.0067 mg per liter sodium selenite and 2 mg per liter ethanolamine, Life Technologies, 51500-056), 8 nM β-estradiol (Sigma-Aldrich, E8875), 200 ng/ml progesterone (Sigma-Aldrich, P0130) and 25 µM *N*-acetyl-l-cysteine (Sigma-Aldrich, A7250).

After the embryos have attached to the bottom of the dish (1-2 days), IVC1 medium was replaced by pre-warmed IVC2 medium (advanced DMEM/F12 supplemented

with 30% (vol/vol) KSR (Life Technologies, 10828010), 2 mM GlutaMAX, penicillin (25 units/ml)/streptomycin (25 μg/ml), 1× ITS-X (10 mg per liter insulin, 5.5 mg per liter transferrin, 0.0067 mg per liter sodium selenite and 2 mg per liter ethanolamine,) 8 nM β-estradiol, 200 ng/ml progesterone and 25 μM *N*-acetyl-l-cysteine). IVC2 medium was refreshed every day for the duration of the experiment. Alternatively, hatched embryos were transferred into 8 Well slide containing 250 μl warm FBS only. FBS was refreshed daily for the duration of the experiment.

The 8-well slides were placed inside Humidifying Chamber (Olaf Humidifying Chamber with μ-Slide Click Rack, Ibidi, 80009), and incubated as described for pre-implantation embryos.

Isolation of primary endometrial cells

Protocol for endometrial cell isolation was adapted from Salomon and Sherman, 1975. Whole uteri were isolated from 1-4 dpc pregnant females and embryos were removed as described in section "Pre-implantation embryo recovery". Uteri were cleaned off of fat and mesentery, cut along the long axis, and minced into small pieces using dissection scissors and a disposable scalpel. The pieces were digested in solution containing 1.5% Trypsin, 0.2% EDTA, 0.5 mg/ml Clostridium collagenase (Sigma, C0130, in 0.05 M Trizma pH7.4 buffer) and 200 units/ml bovine pancreatic DNase (Sigma, D4527, in 0.15 M NaCl and 5 mM $CaCl_2$ buffer) for 10 min at 37°C, shaking at 1400 rpm. The solution with the tissues was forcefully resuspended using 1 ml pipette tip and incubated for another 10 min. The large pieces in the solution were allowed to settle, and the supernatant was transferred into MEF medium (see section "ESC culture"). Incubation and re-pipetting steps were repeated two more times with the undigested pieces. The three resulting supernatant fractions were then pooled, spun at 1200 rpm for 5 min, resuspended in MEF medium and plated on a cell culture dish. The medium was changed every second day.

Embryo culture on uterine endometrial monolayers

MEF medium was aspirated from the uterine monolayers, and the cells were washed with warm D-PBS. IVC1 medium was added to the dish, and the cells were allowed to adjust for 5 h. As in 2D peri-implantation culture, naturally hatched embryos were transferred into the dish containing endometrial monolayer and allowed to attach for at least 1 day. After attachment, IVC1 medium was replaced with IVC2 medium, which was further refreshed once per day.

3D-geec: Matrigel-Collagen I embedding

Mixture for embedding was prepared on ice using pre-chilled PBS and micropipette tips for pipetting, first adding PBS, then Collagen I (Corning® Collagen I, Rat tail, Cat. No. 354236), followed by Matrigel (Corning® Matrigel® Basement Membrane Matrix Growth Factor Reduced, Cat. no. 356230; or Corning® Matrigel® Basement Membrane Matrix Growth Factor Reduced, Phenol Red Free, Cat. no. 356231), at proportions 2:1:3. 2-4 hatched embryos were moved to an empty dish in around 1 µl of KSOM, and 30 µl of the above mixture was added on top, following by immediate mixing by pipetting up and down, and transfer to the center of 8-well slide. Care was taken to place the embryos at the top of the drop and away from the slide bottom. The drops were allowed to rest for 20 min at 37°C (see methods for embryo culturing), and 350 µl of pre-warmed IVC1 medium was added on top. In the evening on the next day, the medium was exchanged to pre-warmed IVC2 medium. IVC2 medium was refreshed every day for the duration of the experiment, and incubation conditions were as described above.

3D-geec: Hydrogel embedding

The technique of mounting of embryos in Hydrogel corresponds to mounting in Matrigel mixture. Hydrogel mixtures were prepared at room temperature as described by the manufacturer (3-D Life Dextran-PEG Hydrogel Kit, Cellendes, Cat. No. G90-1). The final concentrations or maleimide and thiol groups used were 2.0

mmol/l, 2.5 mmol/l and 3.0 mmol/l, the final volume 30 µl/well. The dishes were allowed to rest for 2 min at room temperature, and 350 µl of pre-warmed IVC1 medium was added on top. The medium was exchanged and the incubation was carried out as described above.

Custom-made PEG gel components were received from Matthias Lutolf (EPFL Lausanne). For 1.5% PEG-V (degradable hydrogel), the mixture contained 1x hydrogel buffer, 1.5% (w/v) PEG-V polymer, 1x FXIII and Advanced DMEM/F12 added to a final amount of 25 µl. For 1.5% PEG-A (non-degradable hydrogel), the mixture contained 1x hydrogel buffer, 1.5% (w/v) PEG polymer, 1x FXIII and Advanced DMEM/F12 added to a final amount of 25 µl. For 0.8% PEG-V, the mixture contained 1x hydrogel buffer, 0.8% (w/v) PEG-V polymer, 1x FXIII and Advanced DMEM/F12 added to a final amount of 25 µl. For 0.8% PEG-A, the mixture contained 1x hydrogel buffer, 0.8% (w/v) PEG-A polymer, 1x FXIII and Advanced DMEM/F12 added to a final amount of 25 µl.

The custom-made hydrogel mixtures were prepared in the following way. Buffer and respective PEG were mixed, vortexed and shortly spun down. The corresponding amount of medium containing 2-4 embryos was cast as a drop on the surface of an embryo culture dish, the PEG-buffer mixture was added and the resulting drop was mixed by pipetting up and down. FXIII was thawed on ice, and the required amount was added to the drop with embryos, mixing immediately by pipetting up and down for up to 1 min to achieve a homogenous gel. After mixing, the gel was cast onto 8-well Ibidi dish, and care was taken to place embryos at the top of the drop and away from the bottom of the dish. The dish was transferred to 37°C for 20 min, and finally the polymerized gel drop was covered with 350 µl of pre-warmed IVC1 medium. From this step on, culturing was done as described for Matrigel-Collagen I embedded embryos.

MuVi-SPIM mounting

For MuVi-SPIM, Ultra-low melt agarose (StarLab GmbH, Germany) was used to mount 6.5 dpc embryos inside a glass micropipette and 1-2 mm of agarose with the

embedded embryo was pushed out before moving the sample to the microscope, as described in de Medeiros et al. 2015).

Leica SP8 DLS mounting

A special embedding groove was prepared from 1% agarose in 3.5 cm glass-bottom dishes (Greiner bio-one, 627860) as shown in results. Embryos were suspended in Matrigel-Collagen I mixture and transferred to the groove, followed by 20 min incubation at 37°C. The agarose groove and the embryos were then covered with 2 ml of pre-warmed IVC1 medium and kept in 37°C incubator until transfer to the microscope.

Zeiss Lightsheet Z.1 mounting

Embryos were prepared as described in section 'Matrigel-Collagen I mixture embedding'. Instead of casting onto 8-well dish surface, the embryos and the ECM mixture were immediately aspirated into an Fluorinated ethylene propylene (FEP) tube (Karl Schupp, FSFEP01050106, 01.05x1.06 mm/ WS 0.05 mm) by pulling a plunger (Brand, 701932) up by 1-1.5 cm. The FEP tube with embryos and gel was air-dried for up to 5 min, then submerged in pre-warmed IVC1 medium in a 2 ml screw-cap tube until transfer to the imaging chamber.

Microscopy

Zeiss LSM 780

Embryos were imaged on LSM780 (Zeiss) with 40x water-immersion C-Apochromat 1.2 NA objective lens (Zeiss), using Zen 2014 software (Zeiss). Live imaging was done at 37°C and 5% CO_2 humidified atmosphere using an in-house made LSM780-compatible incubator.

Lightsheet imaging

Prior to imaging on Lightsheet Z.1 (Zeiss), the imaging chamber and all mounting materials were cleaned by submerging in 70% EtOH in an ultrasound bath for 30 min, followed by rinsing with sterile water and air-drying. 15 ml of IVC1 or IVC2 medium was equilibrated in a cell culture incubator in 10 cm cell culture dish for at least 30 min before start of imaging. 50 ml Luer Lock syringes (Braun, 4617509F) and Luer Lock extension lines (Braun, 4097262) were used to transfer medium into the imaging chamber. Embryos were imaged with 20x W-Plan Apochromat objective lens UV-VIS, NA 1.0, using Zen software (Zeiss). The filters used were BP 505-545 and LP 585, lasers used were 514 nm (50 mW, 2%) and 561 nm (20 mW, 1%). Imaging was done at 0.8x zoom factor. The imaging was done at 37°C (heating plate set at 37.5°C) and 5% CO_2 humidified atmosphere. Medium was replaced every 4-6 hours, and the chamber was replaced every 12-18 hours.

Imaging on Leica DLS SP8 (Leica) was done using LAS X software lightsheet mode, with Leica HC PL Fluotar 2.5x/0.07 illumination objective equipped with TwinFlect mirror device, and Leica HC FLUOTAR L 25x/0.95 W detection objective. Imaging was done in custom-made incubator at 37°C in a humidified atmosphere.

Imaging on MuVi-SPIM was done as detailed in de Medeiros et al. 2015), with two Nikon 10X NA 0.3 objectives for illumination and two Nikon 25X NA 1.1 objective lenses for detection, all water-immersion, 50:50 laser beam splitter (non-polarized), and two tube lenses (Nikon 200 and 300 mm). The cameras used were Hamamatsu Flash 4 V1 cameras enabling confocal slit detection.

Laser ablation

Laser ablation on MuVi-SPIM was done using Mikan laser (1030 nm wavelength, pulse duration 200 fs, average power 800 mW, repetition rate 54 MHz). 25x immersion objective of NA 1.0 was used to focus the infrared laser. Laser ablation on MuVi-SPIM was performed with the help of G. de Medeiros.

Laser ablation on LSM 780 NLO (Zeiss) was done using tunable pulsed infra-red laser (Chameleon Vision). The two-photon laser was used at 800 nm and 100% power, and ablation was done for 20 iterations with 1.58 µs pixel dwell. The objective used was 40x water-immersion C-Apochromat 1.2 NA objective lens (Zeiss), using Zen 2014 software (Zeiss).

Image analysis

Image processing

The raw images were processed using Fiji running ImageJ (NIH, USA) and Zen 2014 software (Zeiss). Multiview fusion deconvolution of MuVi-SPIM image was done as described in de Medeiros et al. 2015,.

Image data quantification

The intensity measurements for VET lines were performed by J.E. Dietrich as described in Dietrich et al. 2015).

Sox2-GFP fluorescence intensity was measured using Fiji. For each measurement, a center slice for the cell being measured was selected. For full embryos, the average signal intensity in Sox2-GFP channel was measured in the nuclear area and normalized to the signal intensity in the H2B-mCherry channel. The maximum Sox2-GFP to H2B-mCherry ratio was set to 1. For reduced system, the average signal intensity in Sox2-GFP channel was measured in the largest circular area fitting within a cell. No normalization was performed since reduced system does not display the same non-linear loss of fluorescent signal with increase of distance from the imaging objective as intact embryos due to their small size.

Cells were counted using Fiji cell counter on a respective channel. Embryo long axis and Epi short axis were determined by Fiji measurements.

Unfolding of PrE into 2-dimensional sheet

Segmentation of blastocysts for PrE unfolding was done using Ilastik 1.2.0 pixel classification and object classification pipeline. 3D mesh was created using Fiji and Meshlab 1.3.3. Unfolding of cavity-facing cell layer was done using existing Matlab package as described in Heemskerk and Streichan 2015. Matlab (R2016b) was used for all intermediate steps and for all visualization with the exception of first 3D mesh resulting from processing with Meshlab as described above. The center of cavity-facing cell layer was done manually, and the region of interest was set at a radius of 60 pixels along the 3D mesh. Computational unfolding of PrE was done by Balint Balazs.

4. RESULTS

Emergence and resolution of cellular heterogeneity during blastocyst formation

ICM-specific reporter lines display an unexpected stochastic ICM gene upregulation in cells that do not form ICM. It is thrilling to ask how, throughout the time the first lineages arise, is this stochastic heterogeneity of lineage marker expression generated and resolved, and whether it has any biological role.

The work described in first result chapters of this thesis has been initiated by Jens Erik Dietrich. Together with my contributions, it is part of a publication (Dietrich, Panavaite et al. 2015). Here, I describe the core findings of this project, and provide detailed description of gene-trap line characterization, which was my experimental contribution to the publication.

Venus trap in the mouse embryo

We wished to establish an experimental system for monitoring expression dynamics of lineage – specific genes during early mouse embryogenesis at single-cell resolution. Fluorescent reporter mice for each of the cell lineages in the blastocyst were established by the means of a lentiviral transgenesis-driven gene trap, performed prior to this thesis by J.E. Dietrich (Dietrich et al. 2015). A promoter-less Venus reporter sequence tagged with a nuclear localization sequence (NLS) was used in the design of a lentiviral gene-trap vector, giving the screen a name 'Venus trap' (VET).

From many random integrations obtained, we have selected those lines that show expression restricted to one of the first embryonic lineages, TE or ICM. The lines selected for further characterization, Tmem50b$^{Gt(Venus)fVET17B}$ (hereafter written as Tmem50b^{Gt}) and 2610305D13Rik$^{Gt(Venus)VET53A}$ (hereafter written as 2610305D13Rik^{Gt}) are shown in Fig 4.1.

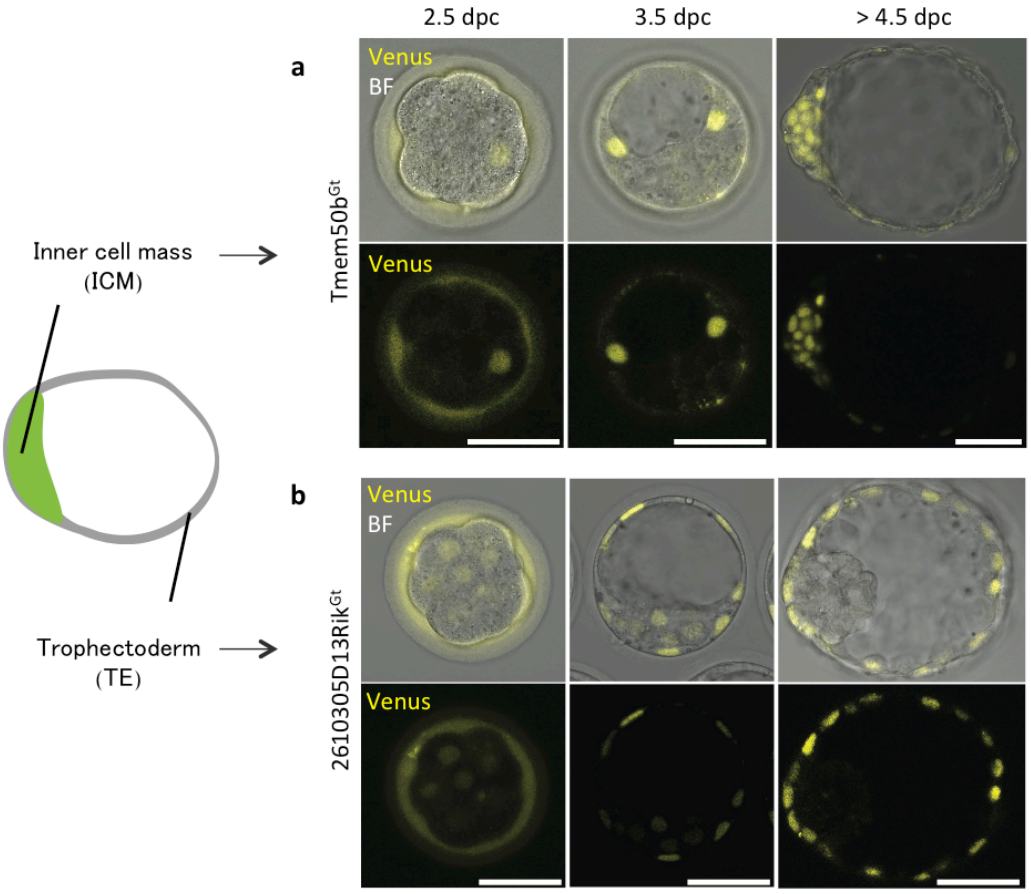

Figure 4.1. TE and ICM reporter lines generated by Venus trap in the mouse embryo.

Brightfield and confocal live images of developing embryos at 2.5 dpc, 3.5 dpc and beyond 4.5 dpc. **a,** TE-specific line Tmem50b^{Gt} and **b,** ICM-specific line 2610305D13Rik^{Gt}. Scale bars, 50 µm. All fluorescent images are single confocal sections, representative for n≥3 independent experiments (adapted from Dietrich et al. 2015).

Characterizing Venus-trap mouse lines

To confirm the lineage-specific expression of two of the resulting lines, Tmem50b^{Gt} specific to TE and 2610305D13Rik^{Gt} specific to ICM, we performed immunofluorescent staining against Venus together with other established lineage markers, Cdx2 (TE) and Sox2 (ICM, Epi). We observed that at 4.5 dpc, in Tmem50b^{Gt} embryos nuclear Venus staining overlapped with trophectoderm-specific Cdx2 staining (Fig 4.2 a). The ICM cells that are positioned on the inside of the embryo were Cdx2 and Venus-negative. Meanwhile, in 2610305D13Rik^{Gt} nuclear Venus

staining was restricted to the ICM, while TE cells had extra-nuclear background staining only (Fig 4.2b). At this stage, Sox2 is marking only the epiblast, but not the primitive endoderm. Notably, Venus staining was present in all ICM, including Sox2-positive and negative cells.

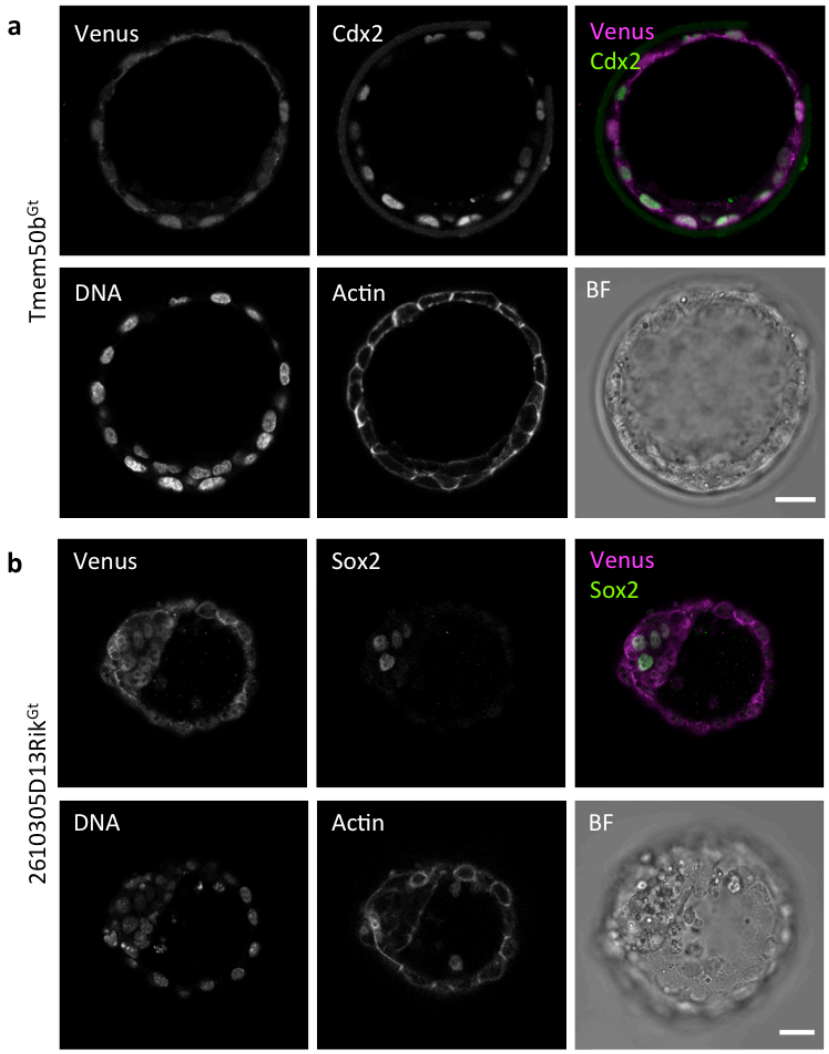

Figure 4.2. Lineage-specific expression of Venus reporters.

A single-section immunofluorescence image of E4.5 blastocysts simultaneously stained with actin dye, DNA dye, and antibodies against Venus and and lineage-specific markers**.** **a,** Tmem50b^{Gt} embryo co-stained for Cdx2 (n=7 embryos in n=2 experiments) and **b,** 2610305D13Rik^{Gt} embryo co-stained for Sox2 (n=6 embryos in n=3 experiments). In the merged images Venus is shown in magenta, Cdx2 and Sox2 in green. BF, brighfield. Scale bars, 20 µm. From Dietrich et al. 2015.

In addition, we confirmed lineage-specific expression of the trapped genes, Tmem50bGt and 2610305D13RikGt by qRT–PCR using single-cell cDNA samples of Epi and PrE cells, and pooled samples of TE cells. Single-cell cDNA samples for qRT–

PCR were prepared by Y. Ohnishi, and cell position (inside, outside, TE, Epi or PrE) was determined as described in Ohnishi et al. 2014. Mural TE samples were prepared by manual bisection of mural TE from polar TE and ICM. Gapdh was used as a housekeeping gene control, and ES cell cDNA samples were run with each experiment in to ensure normalized amplification between sequential experiments.

The normalized Ct values were calculated as follows:
ΔCt = Ct(sample) - Ct(control),

where Ct(sample) is the average cycle number at which amplification curve for the gene of interest reached the gene-specific threshold, Ct(control) is the average cycle number at which amplification curve for the house-keeping gene reached the gene-specific threshold, and ΔCt is the normalized Ct value for the given sample. The normalization sample was always run within the same experiment as the gene of interest sample.

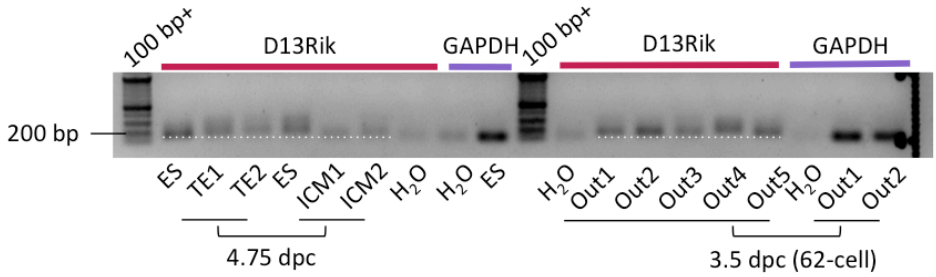

Figure 4.3. Confirming size of RT-qPCR products.

Reactions run on agarose gel post-RT-qPCR to determine presence of secondary products. Marker points to 200 bp.. Dashed line marks the expected 2610305D13Rik (D13Rik) amplicon size (139 bp). Samples: ES: embryonic stem cells, TE1 and TE2: mural trophectoderm, Out1-4: cells in outer position in 62-cell embryo, ICM1 and ICM2: ICM and polar trophectoderm of 4.75 dpc embryo, H_2O: water control.

ΔCt value could not be calculated according to this formula for negative controls where no cDNA was used, and for samples where cDNA for the gene in question was not present. As no product was amplified in these samples, the Ct value could not be determined by the StepOne Software algorithm. To allow inclusion of these samples, their Ct values were manually set to the maximum experiment cycle number. No statistical analysis of data distribution could be performed for these experiments, because several cells do not have a numerical value assigned as explained above.

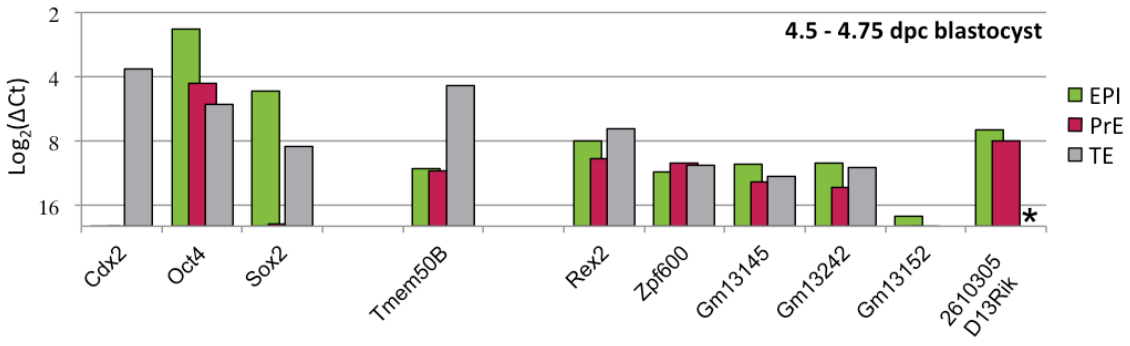

Figure 4.4. Lineage-specific expression of genes trapped in VET mouse lines.

Gene expression levels in single cells (EPI, PrE) or a collection of TE cells derived from E4.5 – 4.75 blastocysts, depicted as RT-PCR threshold cycle (Ct) normalized to the Gapdh level (ΔCt). Each bar represents an average ΔCt value for a given gene. For values see text. EPI n=18 cells, PrE n=14 cells, TE =2 pooled samples containing n=37 TE each). From Dietrich et al. 2015.

The normalized ΔCt values were used to calculate average single gene ΔCt values and standard deviations within EPI, PrE or TE category. The number of cells or pooled cell samples were: EPI n=18 cells, PrE n=14 cells, TE n=2 pooled samples containing n=37 mural TE each. Average ΔCt values for a given gene were as follows (EPI; PrE; TE, average ± standard deviation (s.d.)): Cdx2 (24.7 ± 0.4; 24,47 ± 0.45; 3.68 ±0.27), Oct4 (2.3 ±0.44; 4.33 ± 0.9; 5.37 ± 0.05), Sox2 (4.82 ±1.19; 19.19 ± 7.64; 8.49 ±0.25), Tmem50b (11.14 ± 6.26; 9.43 ± 5.4; 4.38 ± 0.03), 2610305D13Rik (6.41 ± 0.99; 8.55 ± 2.12; N/A), Gm13145 (10.56 ± 4.53; 11.73 ± 3.64; 11.59 ± 0.43), Gm13152 (18.29 ± 2.38; 17.35 ± 3.3; N/A), Gm13242 (12.34 ± 3.55; 11.97 ± 5.64; 10.61 ± 0.35), Rex2 (5.38 ± 4.75; 9.92 ± 6.47; 7.02 ± 0.17); Zfp600 (10.48 ± 4.89; 9.55 ± 4.09; 10.41 ± 0.1). In several single cell samples, Ct value could be calculated, but the melting curve analysis has shown that the product melting temperature (Tm) was shifted and did not correspond to that of other samples. In such cases, after completion of RT-qPCR amplification, the samples in question were run on an agarose gel in order to identify the size of the resulting product. In all such cases, the product size did not correspond to the expected size (Fig 4.3). These samples were marked by an asterisk in Fig 4.4 and Fig 4.5 and their Ct values were not used to calculate average and standard deviation.

All single cell Epi and PrE samples as well as pooled TE samples were evaluated for expression of lineage-specific genes Cdx2 (TE), Oct4 (TE, Epi, PrE, later restricted to Epi and PrE), and Sox2 (Epi). Log2(ΔCt) values for these genes in each type of sample are shown in Fig 4.4. Lower Log2(ΔCt) value corresponds to higher number of transcripts for the corresponding gene in the given sample. The expected gene expression pattern was observed in each sample category, with the exception of some Sox2 transcripts detected in TE sample. Due to the fact that TE samples were acquired in a different manner and contain many cells obtained from the blastocyst, a possibility remains that some Sox2-expressing cells were included in these samples.

Having established that our samples show lineage-specific gene expression profiles, we next asked if Tmem50B, a gene trapped by line Tmem50b^{Gt}, is restricted to TE. Indeed we were able to detect high number of Tmem50B transcript in the trophectoderm, compared to Epi and PrE samples (Fig 4.4).

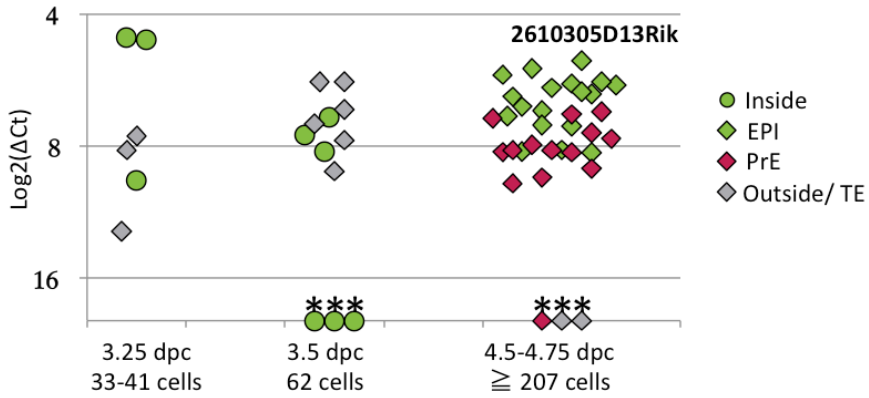

Figure 2.5. Change of expression of 2610305D13Rik during blastocyst maturation.

2610305D13Rik expression in single cells (inside, outside, EPI and PrE) and a collection of TE cells derived from 3.25, 3.5 and 4.5-4.75 dpc blastocysts, depicted as RT-PCR threshold cycle (C_t) normalized to the Gapdh level (ΔC_t). Each dot represents one cell, except for the collective TE samples at E4.5-E4.75 that contain n=37 TE each. Asterisk (*) indicates samples for which only secondary PCR products could be detected. From Dietrich et al. 2015.

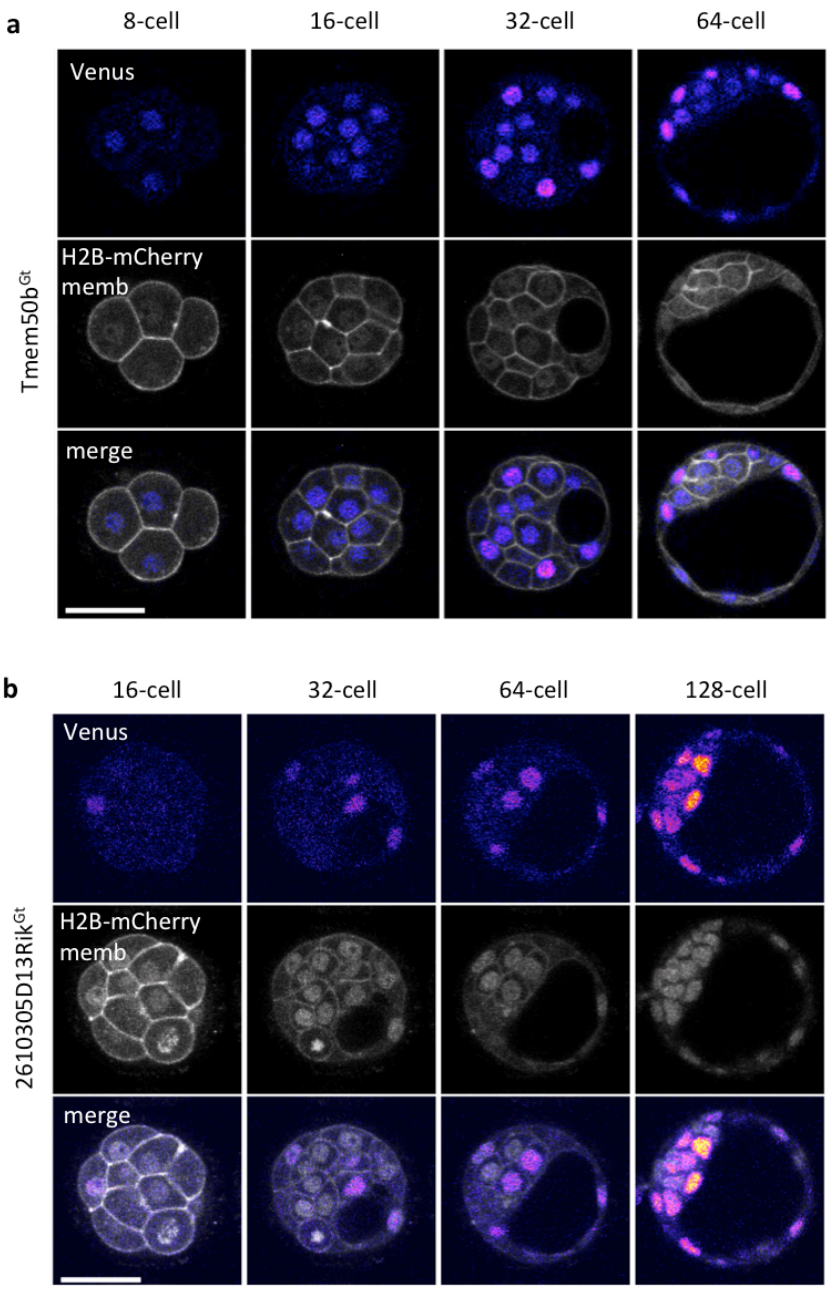

Figure 4.6. Expression of TE and ICM reporters from 8- to 128-cell stage imaged live in 4D.

a, Tmem50b^{Gt}(Venus),-H2B-mCherry, mT embryo developing from 8- to 64-cell stage (n=27 embryos in n=3 experiments). **b,** Representative images of a 2610305D13Rik^{Gt}(Venus), H2B-mCherry, mT embryo developing from 16- to 128-cell stage (n=27 embryos in n=3 experiments). Scale bars, 50 μm. Venus expression images are shown in fire LUT, membrane and mCherry are shown in grey scale LUT. From Dietrich et al. 2015.

It is important to note that due to the presence of highly repetitive sequences in the integration site for line VET53A, several candidates for the gene trapped were plausible. The repetitive sequences in question had an equally high homology with

genes 2610305D13Rik, Gm13145, Gm13242, Gm13152, Rex2 and Zfp600. We thus wanted to examine gene expression profiles for each of these candidate genes. Consistent with our time-lapse imaging and immunofluorescent staining results, we were looking for a gene that is expressed in both Epi and PrE at late blastocyst stage, but was not found in TE. Indeed, the only gene showing this expression profile was 2610305D13Rik (Fig 4.4). We thus tentatively assigned the trapped gene as 2610305D13Rik^{Gt}.

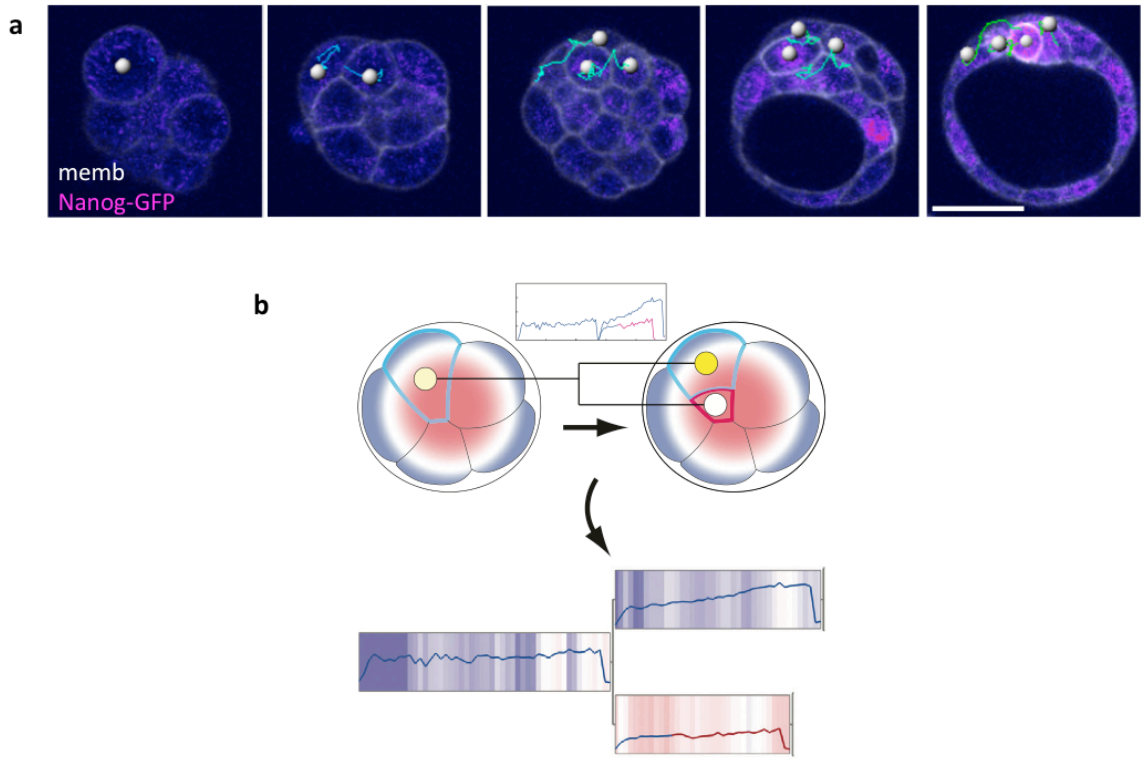

Figure 4.7. Method of establishing gene maps of pre-implantation development.

a, lineage tracking in Nanog-GFP, mT embryo. The white dots mark single nuclei from which fluorescence intensity is measured. GFP expression is shown in fire LUT, membranes are shown in grey scale LUT. Image produced by J.E. Dietrich. **b,** Binary cellular position - inside (red) or outside (blue), determined by membrane contacts, and relative nuclear position, scaled by blue-white-red-gradient, were combined with fluorescence intensity of the reporter measured as in (a) and incorporated into the lineage map. Scale bar, 50 µm. Adapted from Dietrich et al. 2015, and unpublished data by J. E. Dietrich.

Next, in order to confirm that 2610305D13Rik is restricted to ICM in a progressive manner, we looked for 2610305D13Rik transcripts in the inside or outside cells of 3.25 dpc or 3.5 dpc embryo, as well as in Epi, PrE or TE cells in 4.5-4.75 dpc embryo. We observed that at early blastocyst stage, 2610305D13Rik transcripts were detected in the inside as well as the outside cells, while at late blastocyst stage, only

Epi and PrE, but not TE cells had 2610305D13Rik transcript (Fig 4.5). These findings were consistent with our time-lapse imaging (in 2610305D13Rik^{Gt} line, Venus-positive cells are progressively restricted to ICM, Fig 4.6), and with immunofluorescent staining (at E4.5 in 2610305D13Rik^{Gt} line, Venus expression is restricted to PrE and Epi, Fig 4.2 b).

Together, these experiments verified that the fluorescent reporters and the trapped genes were restricted to their respective lineages at late blastocyst stage.

Lineage segregation map of mouse pre-implantation development

Tmem50b^{Gt} and 2610305D13Rik^{Gt} gene trap lines were further selected for in-depth analysis, live imaging and cell tracking, and the collected data used to establish a map of TE and ICM lineage segregation.

An example of time-lapse imaging of embryos expressing one of the gene trap reporters, nuclear marker H2B-mCherry and membrane marker mT is shown in Fig 4.6. In line Tmem50b^{Gt}, Venus reporter can be first seen in 8-cell stage embryo. Throughout development to 32-cell stage, the cells in the outside positions upregulate this reporter (Fig 4.6 a). In line 2610305D13Rik^{Gt}, Venus reporter is not visible until 16-cell stage (Fig 4.6 b). Heterogeneous Venus expression pattern in this line persists to blastocyst stage, and is only finally restricted to ICM at 128-cell stage or later (Fig 4.6 b, Fig 4.2 b).

Each nucleus of 8-cell stage embryo was tracked to establish the lineage tree as shown in Fig 4.7 a, and the fluorescence intensity signal was quantified over time. Measurements collected from time-lapse images of Tmem50b^{Gt} and 2610305D13Rik^{Gt} lines were used for establishing lineage maps. In the lineage map (Fig 4.7 b), every box represents one cell cycle, connected by lines to indicate lineage. Within the box, the color indicates relative position of the cell to the center of the embryo: red hues indicate that the cell is positioned more centrally (inside), blue hues indicate that the cell is positioned closes to the periphery (outermost position).

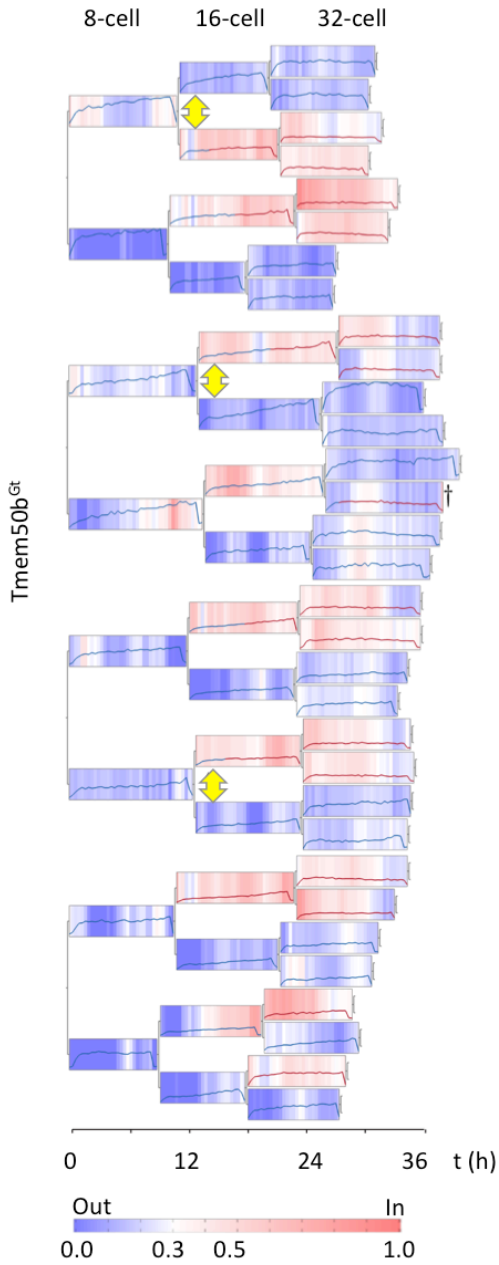

Figure 4.8. Lineage map for all cells in one Tmem50b^{Gt}-reporter embryo.

A lineage map integrating reporter expression dynamics with cell position in Tmem50bGt, H2B-mCherry, mT embryo at 8- to 32-cell stage. Blue and red lines indicate outside and inside cells, respectively. Blue-white-red scale indicates relative distance of nuclei to the surface of the embryo. Dagger marks cells undergoing apoptosis and cell lineages lost during imaging are labelled with an "L". Yellow arrows highlight representative descendant pairs as a result of asymmetric divisions with clear difference in the expression level.

The line graph inside the box shows the marker expression level over time. Venus expression intensity is normalized first to H2B-mCherry, and subsequently to the

maximum expression intensity of all cells in the same cell-cycle stage of an embryo. Each box in the lineage tree ranges from 0 to 1 in normalized expression. Lineage maps were generated by S. Gunther.

The lineage maps allowed us to analyze quantitative gene expression dynamics during the first lineage segregation in mouse blastocyst development. In order to compare with existing models of lineage segregation, we looked for a link between cell division pattern or cell position, and upregulation of lineage-specific gene exprssion. We observe that while both TE and ICM markers show initial expression heterogeneity, asymmetric division drives the upregulation of TE-specific gene expression, and this allows a prediction of TE lineage, to some extent, at the 16-cell stage (Fig 4.8). However, if the same analysis for the ICM markers revealed that ICM marker expression does not demonstrate this clear correlation with the division pattern (Fig 4.9). Importantly, ICM-specific markers are restricted to ICM (ICM-specific gene network established) only at 64-cell stage, and the initiation of a single ICM marker expression does not allow predicting the future cell fate. Our analyses suggest that the expression of TE and ICM lineage markers is not initiated in a reciprocal manner, but rather with different timings and through distinct mechanisms. The upregulation of a TE lineage marker begins earlier and may be largely driven by asymmetric division, while that for the ICM marker may not be following the same mechanism, and remains to be further elucidated (summarized in discussion Fig 5.1). Ultimately, the existence of distinct mechanisms for specification of the TE and ICM cell fate raises a question if stochastic cell-to-cell heterogeneity plays an important role in establishing pluripotency.

Towards enrichment of the lineage map

The lineage map of a single lineage reporter was not sufficient to predict inner cell mass fate, possibly due to the stochastic onset of gene expression. We thus aimed to test the hypothesis that a combination of stochastic heterogeneities of gene expression would provide us with the ability to predict ICM fate. We stipulated that if

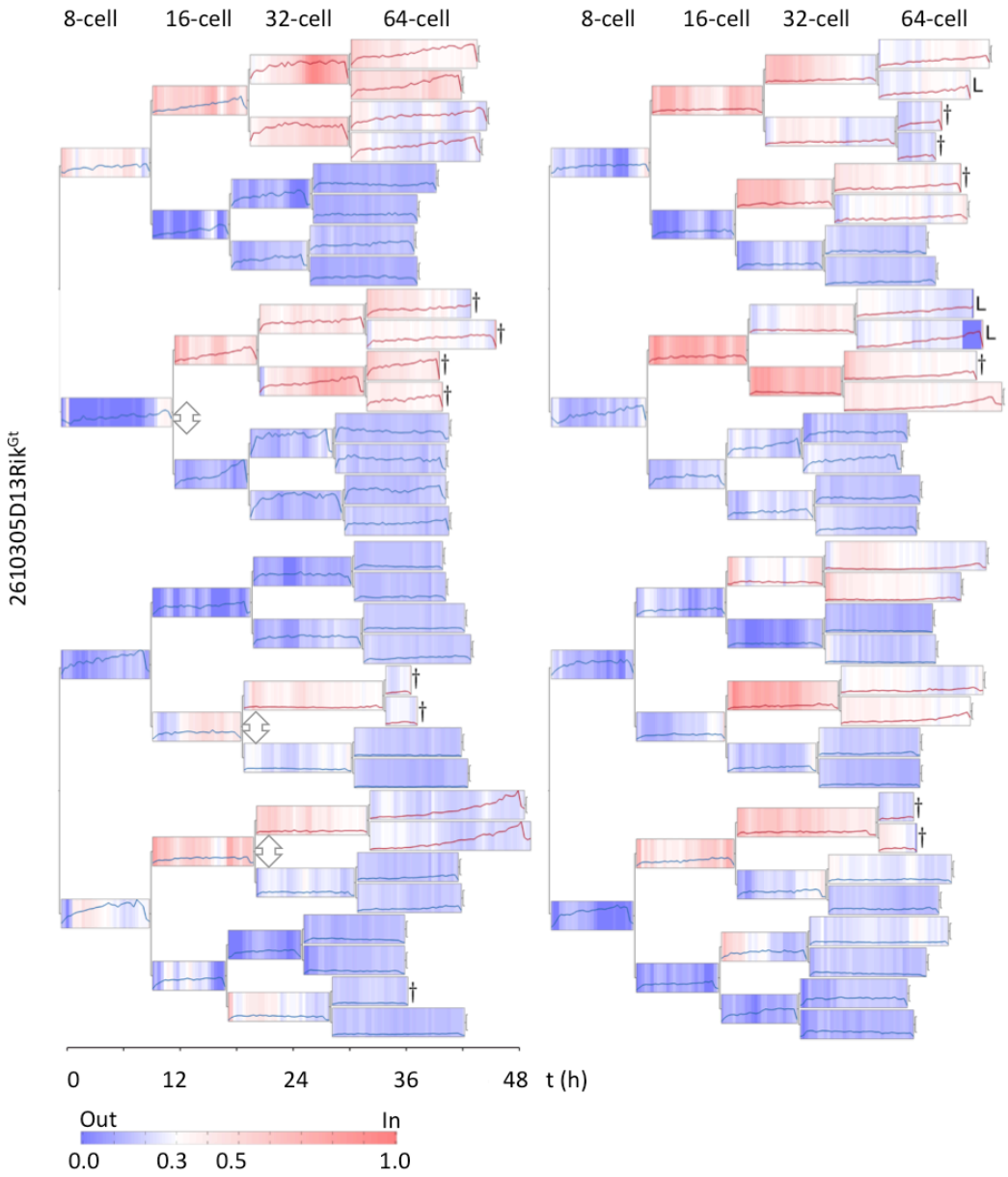

Figure 4.9. Lineage map for all cells in one 2610305D13Rik^{Gt}-reporter embryo.

A lineage map integrating reporter expression dynamics with cell position in 2610305D13Rik^{Gt}, H2B-mCherry, mT embryo at 8- to 64-cell stage. Blue and red lines indicate outside and inside cells, respectively. Blue-white-red scale indicates relative distance of nuclei to the surface of the embryo. Dagger marks cells undergoing apoptosis and cell lineages lost during imaging are labelled with an "L". White arrows highlight representative descendant pairs as a result of asymmetric divisions with essentially no difference in the expression level.

gene expression heterogeneity amongst different pluripotency genes is indeed stereotypic, a pattern of lineage segregation will be visible in the ICM-lineage map

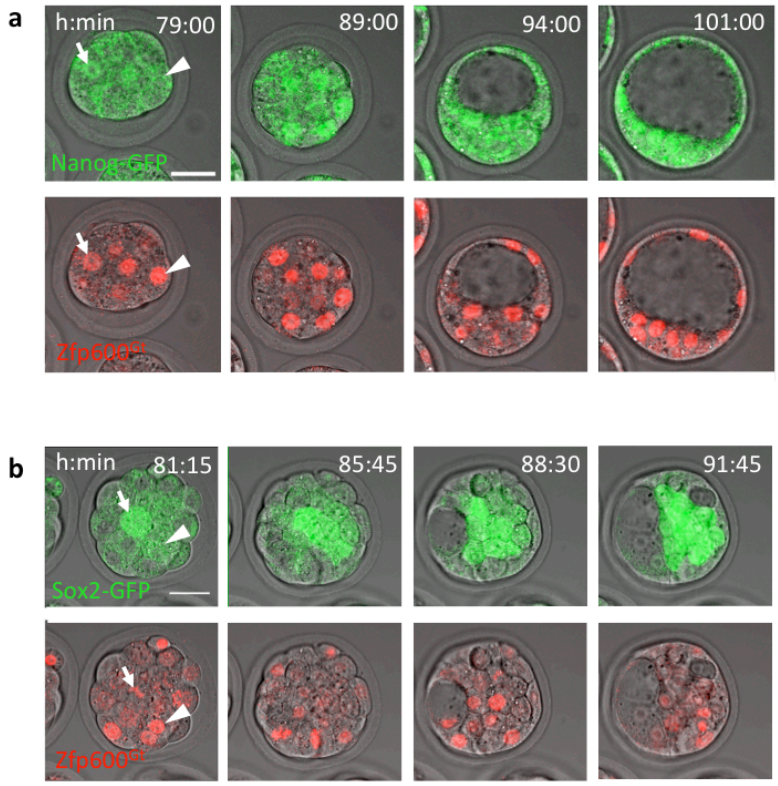

Figure 4.10. Heterogeneities in early mouse embryo revealed by simultaneous two reporter imaging.

a, Live imaging of developing Nanog-GFP x Zfp600-H2B-mCherry embryo from 79 to 125 h after hCG injection. **b,** Live imaging of developing Sox2-GFP x Zfp600-H2B-mCherry embryo from 81 to 91 h after hCG injection. Arrows point to double-positive nuclei, arrowheads point to nuclei positive for Zfp600-H2B-mCherry only. Scale bars, 30 µm.

that will help us identify a mechanism by which pluripotent cell lineage is established.

Wanting to combine two different fluorescent reporters in the same embryo, we employed a second-generation gene trap line Zfp600$^{Gt(mCherry)SEC14}$ (from here on referred to as Zfp600^{Gt}; PhD thesis by S. Wennekamp) that is largely restricted to ICM at late blastocyst stage. First, we used this mCherry reporter line in combination with lines expressing canonical pluripotency markers Sox2-GFP or Nanog-GFP. The expression patterns of these GFP-expressing reporters are compared to Zfp600^{Gt} expression in the same embryo in Fig 4.10. Similar to 2610305D13Rik^{Gt}, expression of Zfp600^{Gt} starts on 2.5 dpc. Two-channel live imaging of Nanog-GFP x Zfp600^{Gt} embryo developing from 16- to 128-cell stage has revealed cell-to-cell expression

heterogeneity of both of these lineage markers (Fig 4.10 a). Initially, several blastomeres are expressing either or both of the markers at varying levels, with no apparent correlation between the expression levels of the two markers at the early stage. Later in blastocyst development, both markers are mostly restricted to the ICM and the variability between them in the same cell starts to be resolved (Fig 4.10 a).

Next, we examined the reporter combination of Sox2-GFP with Zfp600^{Gt}(Fig 4.10 b). We observed that the in-out differential expression of Sox2-GFP precedes that of Zfp600^{Gt}, which at the same stage is expressed in a heterogeneous manner as

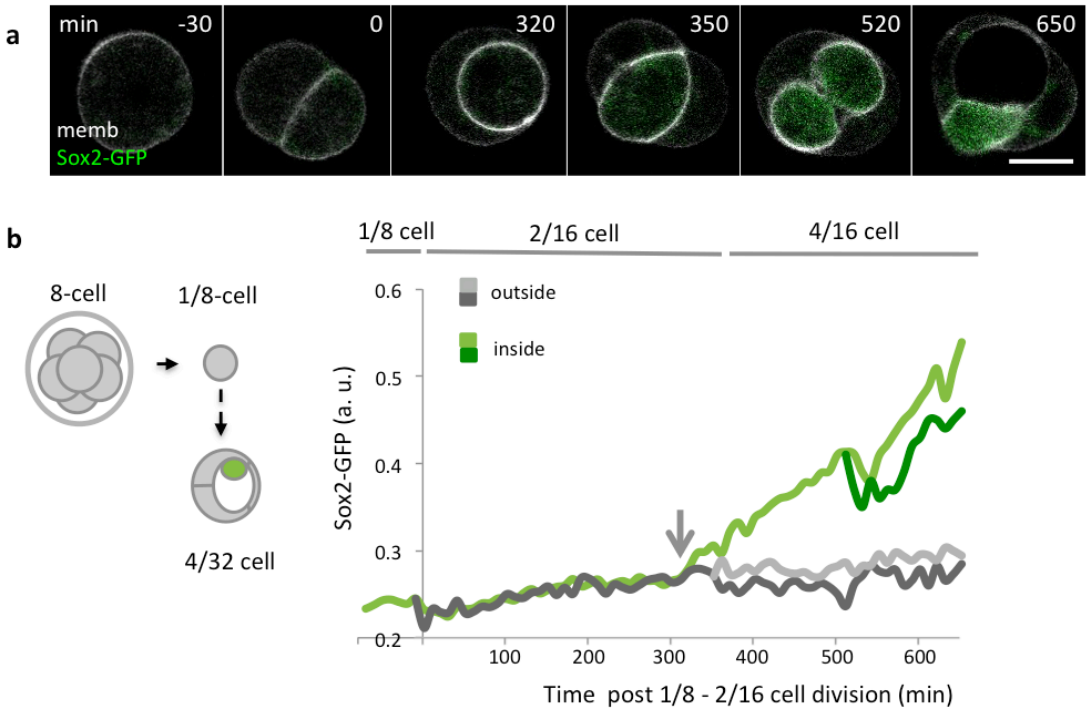

Figure 4.11. Sox2-GFP expression in a reduced system.

a, A single blastomere isolated from an 8-cell embryo expressing membrane market mT and Sox2-GFP dividing two times to give rise to a mini-blastocyst. Shown is representative image for n=6 blastomeres in n=2 experiments. Time shown relative to 1/8- to 2/16-cell division (t=0). **b,** Sox2-GFP expression measured over time in a single 1/8 blastomere and all its descendants. Colours of tracks were set according to final cell position within the mini-blastocyst. Arrow points to the time of envelopment of one sister blastomere by another. Scale bar, 20 µm.

described above (Fig 4.10 a). Sox2 is one of the key transcription factors of transcriptional regulatory network for pluripotency that also includes Oct4 and

Nanog, all of which are so far described as equally important transcription factors (reviewed in Young 2011), yet remarkably, Sox2-GFP expression appears to be clearly segregated between inside and outside populations starting after division to 16-cell stage. This has not been observed for any other ICM markers (Nanog, Oct4, Zfp600^{Gt}, 2610305D13Rik^{Gt}).

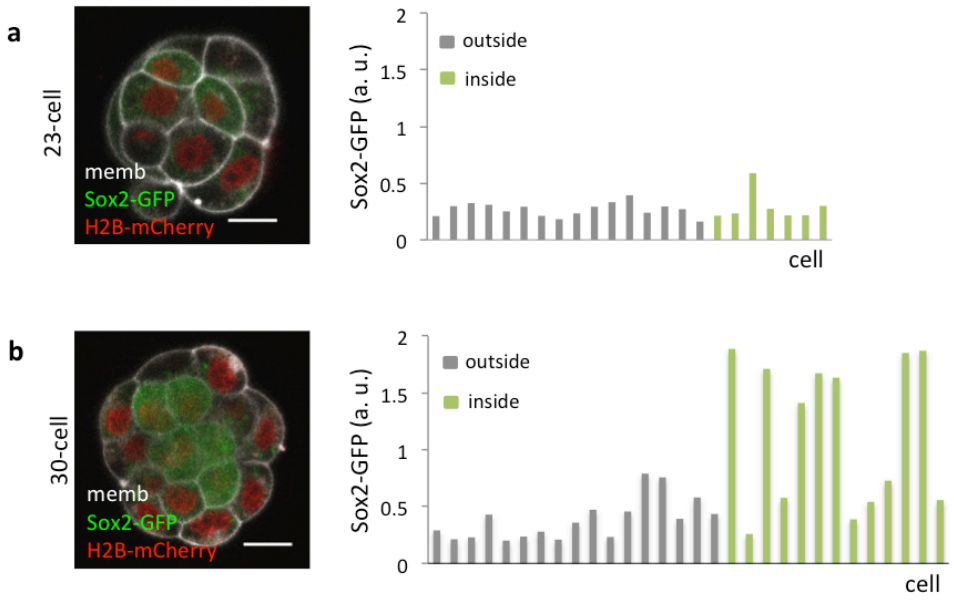

Figure 4.12. Sox2-GFP positive cells in early and late mouse morula.

Representative pictures and Sox2-GFP fluorescence intensity measurements of embryos expressing H2B-mCherry, Sox2-GFP, and an injected cell membrane marker myr-PALM-tdiRFP. **a,** 23-cell embryo, **b,** 30-cell embryo. Scale bars, 20 μm.

Intrigued by the apparent early restriction of Sox2 to the inside cells, we next explored the expression dynamics of Sox2-GFP. First, we wanted to know if Sox2-GFP expression is upregulated after 8-to-16 cell division, or does it rather correlate with cell position inside the embryo. To simplify the complexity of the dynamic embryo, we used a reduced system where a single isolated 1/8-cell stage blastomere is cleaved two more times to produce a 4/32-cell stage mini-blastocyst. As 1/8-cell blastomere divides asymmetrically, one of the daughter blastomeres is enveloped by another, followed by another round of division and start of cavitation (Fig 4.11 a). We observed that expression of Sox2-GFP could first be detected not after 1/8-cell to 2/16-cell division, but only after one of the daughter blastomeres was completely

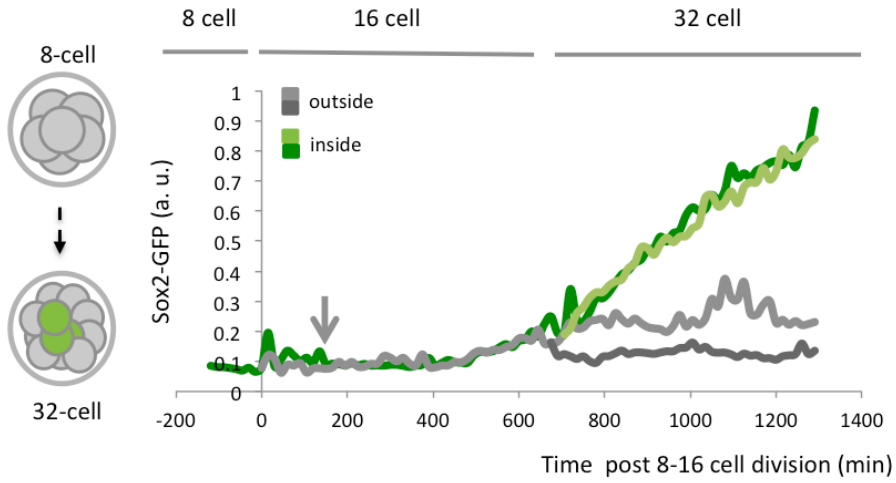

Figure 4.13. Sox2 expression during morula development.

Sox2-GFP expression measured over time in all descendants of one cell in an intact 8-cell embryo expressing H2B-mCherry, Sox2-GFP, and an injected cell membrane marker myr-PALM-tdiRFP. Colours of tracks were set according to final cell position within the embryo. Arrow points to the time when a cell assumed an inner position loosing contact to the outside. Shown is lineage track representative of n=12 cells in n=3 embryos.

enveloped by another (Fig 4.11 b). During 2/16-cell stage, Sox2-GFP expression steadily increased, and after division to 4/32-cell stage, the two daughter blastomeres that were positioned inside the mini-blastocyst displayed a continuous increase in Sox2-GFP expression. In all blastomeres observed that expressed Sox2-GFP (n=6), it took between 360 and 400 min after 1/8- to 2/16-cell division for Sox2-GFP fluorescence intensity to rise above that of background level of the outside cells (Fig 4.11 b). Less than an hour after enveloping has passed before Sox2-GFP expression has risen above the background levels in the inside cell.

The initial observations in a reduced system encouraged us to look back to a complete embryo and ask whether the correlation between inner cell position and Sox2-GFP expression is true in a full system as well. First, we looked at when the first Sox2-GFP expression above the background level could be detected, and where the expressing cell was positioned. We looked at one embryo at the beginning of Sox2-GFP expression until 32-cell stage. At 23-cell stage, the first cell that displayed Sox2-GFP signal slightly above that of other cells and was positioned inside could be observed (Fig 4.12). However, at this time, 7 cells in total were positioned on the

inside of the embryo with no contact to the outside. At 30-cell stage, the background signal had increased and thus the Sox2-GFP fluorescence intensity at which a cell was considered to be above background level was increased accordingly. At this stage, 7 out of 13 inside-positioned cells were expressing Sox2-GFP. These observations were consistent with our finding that asymmetric division does not lead to immediate expression of Sox2, as possibly the cells that are positioned inside the 23-cell morula embryo but do not express Sox2 have been enveloped recently and have not yet upregulated Sox2-GFP at the time of measurement. Since a dynamic cell rearrangement is possible during 16- to 32-cell stage, we stipulated that the same assumption is valid for cells inside 30-cell embryo that did not upregulate Sox2-GFP.

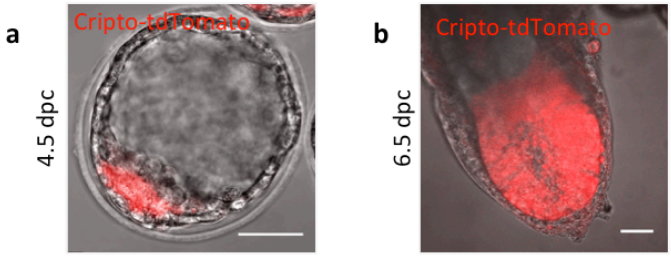

Figure 4.14 Generation of Cripto-tdTomato BAC line.

a, 4.5 dpc blastocyst expressing Cripto-tdTomato restricted to the Epi. **b,** 6.5 dpc embryo expressing Cripto-tdTomato restricted to the Epi. Scale bars, 40 μm.

To understand the relationship between the inner cell position and Sox2-GFP upregulation in an intact embryo, we tracked the lineage of and quantified Sox2-GFP expression over time in one blastomere of an 8-cell embryo that will give rise to the first cell that expresses Sox2-GFP. In the embryo described below, after asymmetric 8- to 16-cell division, the second daughter of this blastomere remained outside and only contributed to TE. As observed in a reduced system, no increase in Sox2-GFP expression was detected immediately after a cell assumed an inside position within the embryo (Fig 4.13). Over 700 min after 8- to 16-cell division, and around 500 min after losing contact to the outside, first increase in Sox2-GFP expression in the inside cell was observed, followed immediately by division of the expressing cell, and further synchronized increase of Sox2-GFP expression in both daughter cells. The cells that remained outside after 8- to 16-cell division did not upregulate Sox2-GFP. Furthermore, similar Sox2-GFP expression upregulation pattern and timing could be

observed in the first Sox2-GFP expressing cells within two more embryos analyzed (total n=12 cells in n=3 embryos).

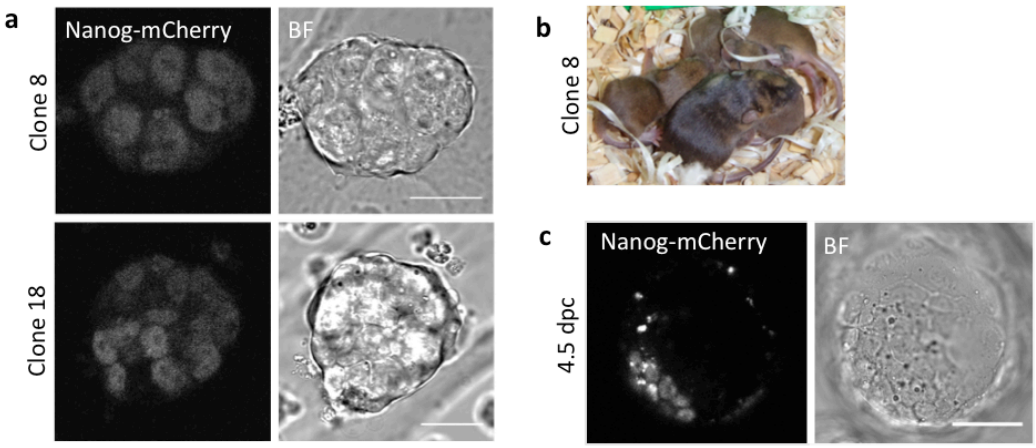

Figure 4.15. Generation of Nanog-mCherry transgenic line.

a, Two comparable ES cell clones expressing Nanog-mCherry reporter. **b,** Chimaeric mouse pups born born from blastocysts injected with clone 8 cells shown in (a). **c,** 4.5 dpc blastocyst expressing Nanog-mCherry reporter restricted to the ICM. Scale bars, a, 20 μm, c, 40 μm.

Even though certain non-heterogeneous patterns can describe Sox2 expression at late morula stage, the first Sox2-GFP expression can be detected only halfway through 16- to 32-cell division, and even at that time a confident lineage prediction can be done only retrospectively from the increase in slope of the fluorescent signal. This does not allow us to predict ICM lineage at the stage when heterogeneity of other ICM markers, such as 2610305D13Rik^{Gt} or Nanog-GFP, is observed. Therefore lastly, to aid further studies that would pursue double lineage reporter imaging, we generated fluorescence reporters targeted for canonical lineage markers. Cripto-tdTomato that marks the epiblast of the late blastocyst and post-implantation epiblast, was generated from BAC construct and can be seen in Fig 4.14. Nanog-mCherry, that displays heterogeneity in the morula, and is restricted to the ICM of the late blastocyst, was generated by injection of ES cells carrying the integration in the endogenous locus and can be seen in Fig 4.15. In the future, these two lineage reporter lines tagged with red-spectrum fluorescent proteins will allow analysis of two lineage-marker heterogeneities in the same embryo, using the framework discussed above.

Emergence of cellular heterogeneity within the blastocyst that forms a basis for body axis specification

I aimed to identify the symmetry breaking within the blastocyst that forms a basis for the embryonic body axis formation, specifically examining the distal visceral endoderm progenitors. To this end, I set out to develop a culture method that would support *in vivo*-like morphogenesis and gene expression change in peri-implantation embryos, and thus allow us to monitor behavior of anterior marker-expressing cells. Next, by observing and manipulating peri-implantation embryos I aimed to understand the mechanism by which DVE progenitors converge onto their final distal position, and how these cells are linked to DVE at 5.5 dpc. Lastly, to elucidate the processes that lead to the emergence of DVE progenitors, I describe the dynamics of DVE-specific gene expression by tracking the corresponding reporters in living embryos.

2D peri-implantation culture supports development of egg cylinder in vitro

We wished to culture the mouse embryo between E4.5 and E6.5 in a way that would be compatible with live imaging.

We first tried culturing embryos as previously described (Bedzhov et al. 2015). We refer to this method as IVC (*in vitro* culture), after the medium used. When using IVC method, many embryos would perish when transferred to IVC1 medium, while most others would form amorphous clumps, as can be seen in Fig 4.16 a. In such clumps, Sox2-positive and Cdx2-positive populations are not segregated, and many cells are expressing either both transcription factors at the same time, or neither. Most of such disorganized structures would continue growing without resembling any embryonic stage. In these conditions, some embryos transferred to IVC would emerge from the amorphous clump stage and start directional elongation. A few of those embryos

would start forming a secondary cavity that is reminiscent of amniotic cavity found within the epiblast population at E5.5 (Fig 4.16 b). The efficiency of forming separate Cdx2-positive and Sox2-positive cell populations and elongation of IVC culture (13.75%; n=28 embryos in n=2 experiments) was lower than described in the published work (average of 20-25%; Bedzhov et al. 2014), possibly due to unintended variations in the protocol between different laboratories.

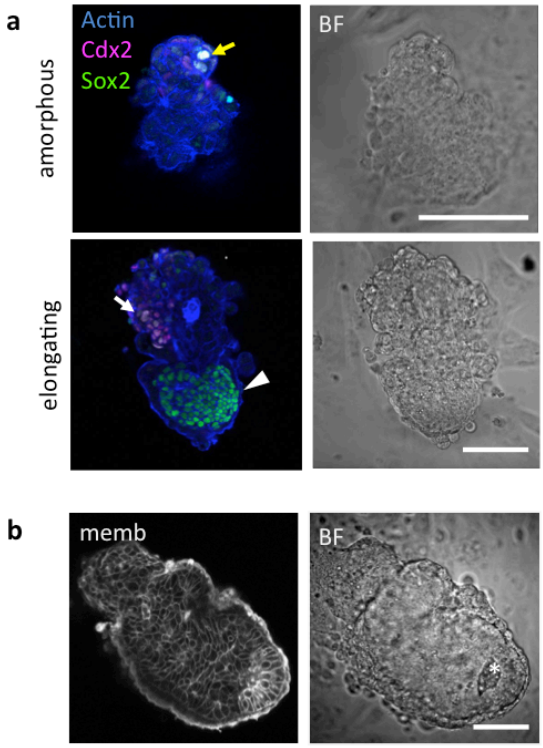

Figure 4.16. Embryos cultured by IVC method.

a, IVC Day 4 embryos stained with antibodies against Cdx2 and Sox2, and actin dye. Yellow arrow, cells positive for both Cdx2 and Sox2; white arrow, Cdx2 population; white arrowhead, Sox2 population; **b,** An example of IVC-cultured embryo expressing membrane marker mT that shows early signs of amniotic cavity marked by an asterisk (*). Scale bars, a, 100µm, b, 50 µm.

Presence of stromal cells does not preserve peri-implantation embryo morphology

Due to the low success rate and the loss of peri-implantation embryo morphology and gene expression when using IVC method for peri-implantation culture, we became interested in exploring alternative culturing methods. We first examined if the uterine environment support is required for proper peri-implantation

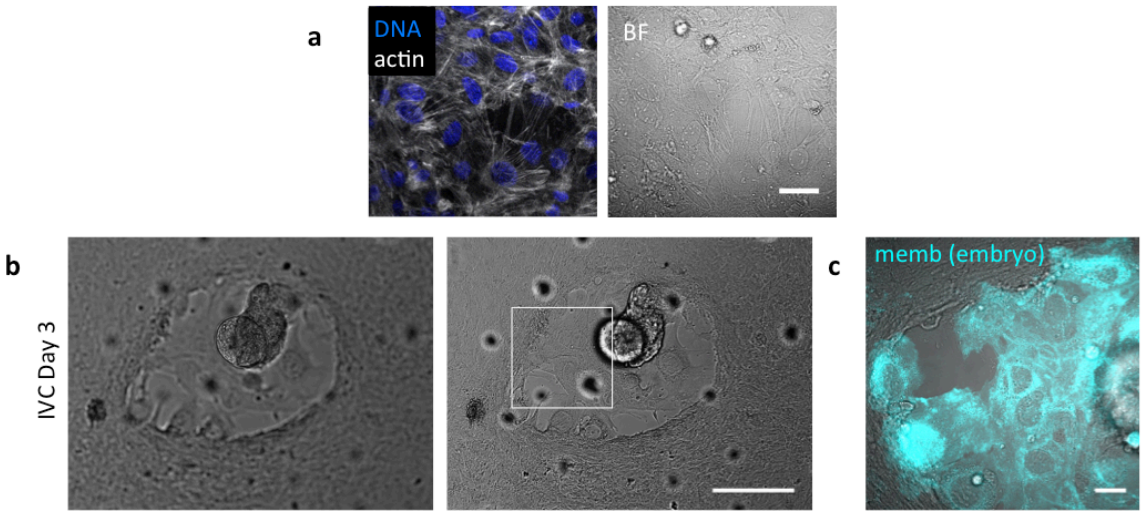

Figure 4.17. Primary uterine cell culture and co-culture with peri-implantation embryos.

a, primary cell culture recovered from the uterus stained with actin and DNA dyes. **b,** Representative brightfield image of an embryo cultured together with primary uterine cells, n=6/30 embryos in n=2 experiments . **c,** a magnified image of picture in (b), showing mT expressing embryo-derived trophoblast cells displacing uterine cells in culture. Scale bars, a and c, 40 µm, b, 200 µm.

development. For this, we have isolated uterine stromal cells and were established a 2D primary endometrial cell culture. When grown on a glass-bottom imaging dish, these cells formed a continuous monolayer (Fig 4.17 a). Next, we added late 4.5 dpc blastocysts on top of this monolayer, and cultured in same conditions as described for IVC method. We observed that at a stage resembling egg cylinder, embryos in such co-culture displaced stromal cells, as indicated by a ring of embryo-derived cells around each embryo that developed to egg-cylinder stage (Fig 4.17 b, c). However, embryos in co-culture attached to the bottom of the dish in the same way as observed in IVC method, and entered a disorganized state as described above. We thus concluded that presence of uterine stromal cells, at least with the methods we have tried so far, does not improve 2D peri-implantation embryo culture, and is not suitable to monitor cell lineage progression during peri-implantation development.

3D culture recapitulates morphogenesis and gene expression dynamics of peri-implantation development

As many embryos remained flattened and disorganized when using IVC and uterine cell co-culture methods, we hypothesized that flattening of the embryo onto a 2D surface mechanically alters peri-implantation embryo morphology and prevents three-dimensional (3D) growth and egg cylinder extension. Therefore we aimed to prevent non-isotropic embryo contact with glass or plastic surfaces by transferring the embryo culture to a 3D environment. We tested embedding in extracellular matrix (ECM) gels composed of different materials. The highest percentage of embryos progressing to egg-cylinder stage was reached when cultured in IVC medium within gels comprised of growth factor-reduced Matrigel and Collagen I. We named this culture '3D-geec', for 3D gel embedded embryo culture (Fig 4.18). Some embryos nevertheless sink to the bottom of the Matrigel-Collagen I drop and attach to the bottom of the dish, resulting in the flattened morphology as in the IVC method, and are thus not used for experiments. Around half (51.85%, n=42/81 embryos in n=4 experiments) the embryos grown in 3D-geec form elongated egg-cylinder like structures with distinct Cdx2-positive and Sox2-positive cell populations (Fig 4.18).

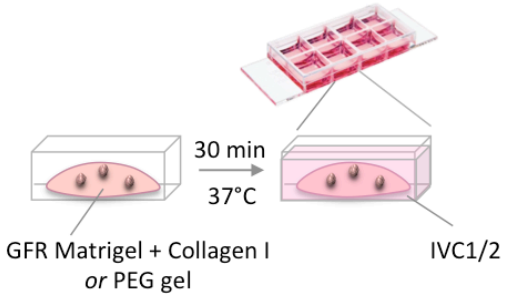

Figure 4.17. Setup of 3D-geec.

Scheme depicting mounting of embryos for 3D-geec. Embryos are suspended within Matrigel-Collagen I mixture or PEG hydrogel, and a drop is made in one well of 8-well imaging-compatible dish. Embryos have no contact with the surface of the dish. The drop is covered with IVC1 or IVC2 medium.

To evaluate the 3D-geec culture conditions, we compared the size distribution of 3D-geec embryos with that of *in vivo* grown embryos. Specifically, we measured the proximal-distal axis of 3D-geec embryos on day 3 of culture (day 0 is the day of

transfer to 3D-geec, 126-130 h post-hCG), when elongation of epiblast covered with visceral endoderm is usually observed, as well as the "short" (future A-P) axis of epiblast in the same embryo. We compared day 3 3D-geec culture embryos (Fig 4.19). When the size (Fig 4.19 a) and the numbers of cells within the Epi and the VE populations (Fig 4.19 b) were compared to *in vivo* grown embryos dissected on 5.5 dpc, many 3D-geec culture embryos were similar to their *in vivo* grown counterparts, although 3D-geec embryos display higher variability. The largest day 3 and day 4 3D-geec embryos resemble 6.5 dpc *in vivo* grown embryos, as can be seen in Fig 4.20. For comparison, the cell number in the epiblast of the largest day 3 3D-geec embryo was around 800 cells, while the same population in 6.5 dpc embryo reportedly consists of around 650 cells (Snow and Bennett, 1978). On day 4 of 3D-geec, embryos that morphologically resemble egg-cylinder stage show separated populations of Sox2-positive and Cdx2-positive cells and an amniotic cavity (Fig 4.18, Fig 4.19 a), retain pluripotent Oct3/4-positive Epi population (Fig 4.20 a), and develop Gata6-positive VE adjacent to the Epi and the extraembryonic ectoderm (Fig 4.19a, Fig 4.20 a).

Most important advantage of 3D-geec for our study is that 3D-embedded embryos do not undergo collapse and do not form amorphous clumps as an intermediate state of *in vitro* development. This is well reflected by maintenance of expression of various lineage markers as described below.

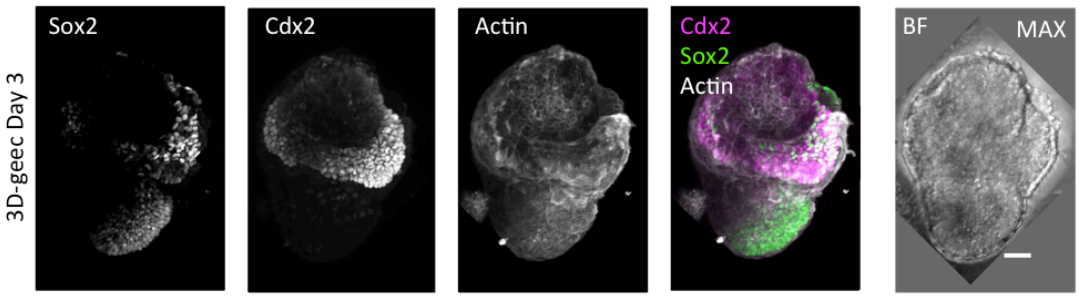

Figure 4.18 3D-geec embryos show lineage-specific marker expression.

3D-geec Day 3 embryo stained with antibodies against Cdx2 and Sox2, and actin dye. 3D-geec embryos form egg-cylinder like structures with segregated Sox2+ and Cdx2+ populations. Maximum intensity projections are shown. Scale bar, 50 μm.

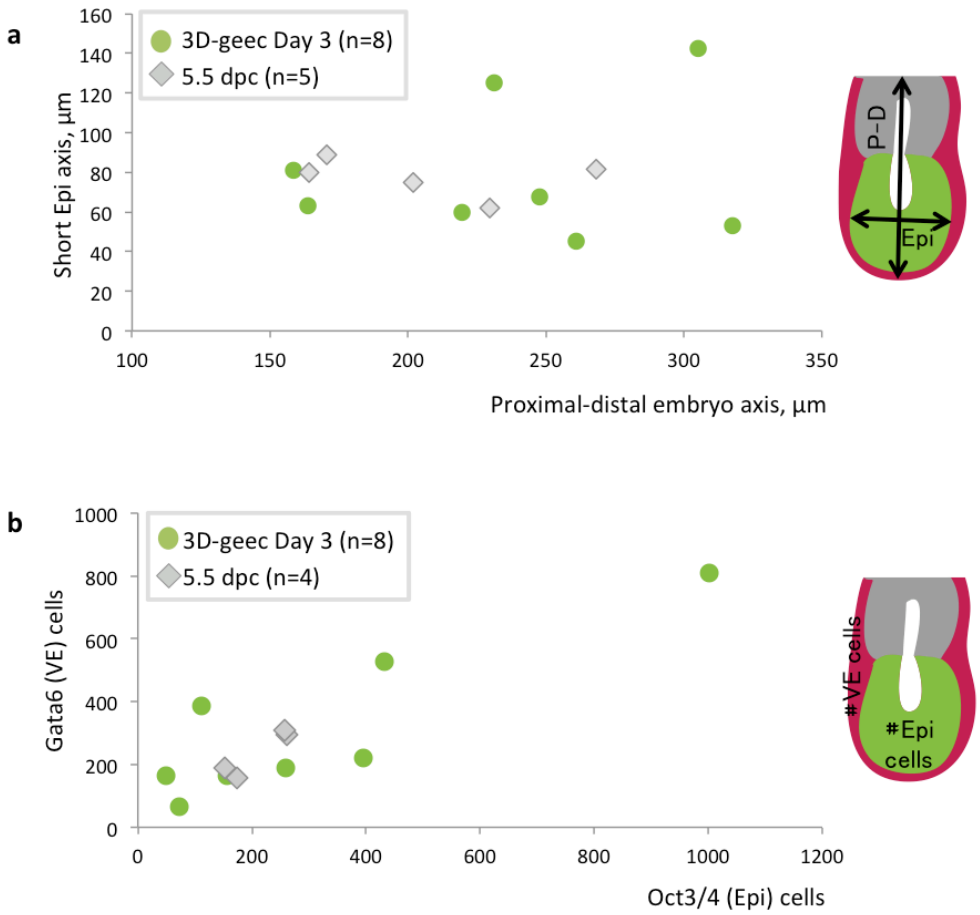

Figure 4.19. Size and cell population distribution of 3D-geec day 3 embryos compared to *in vivo* developed 5.5 dpc embryos.

a, Length measured along P-D axis plotted against length measured along short Epi axis (future A-P axis) in 3D-geec embryos on day 3 and 5.5 dpc *in vivo* grown embryos. **B,** Number of Oct3/4+ cells plotted against Gata6+ positive cells in 3D-geec embryos on day 3, or number of Oct3/4+ cells plotted against VE cells in 5.5 dpc *in vivo* grown embryos. Each dot represents one embryo.

On day 1, after around 16 h of culture, more than a third of the embryos have proceeded further than mature blastocyst stage of the pre-implantation culture (Fig 4.21). In these embryos, Gata4-positive cells of the PrE have proliferated and migrated to give rise to two layers that should develop into VE and parietal endoderm. Enveloped by one layer of Gata4-positive cells, Oct4-positive Epi cells could be seen. Mural and polar trophectoderm cells layers have undergone thickening, but have not made any attachment to the dish surface of any observable contacts with the gel. Less than a third of the embryos on day 1 still had blastocyst morphology, with Gata4-positive PrE cell migration in its early stages. These

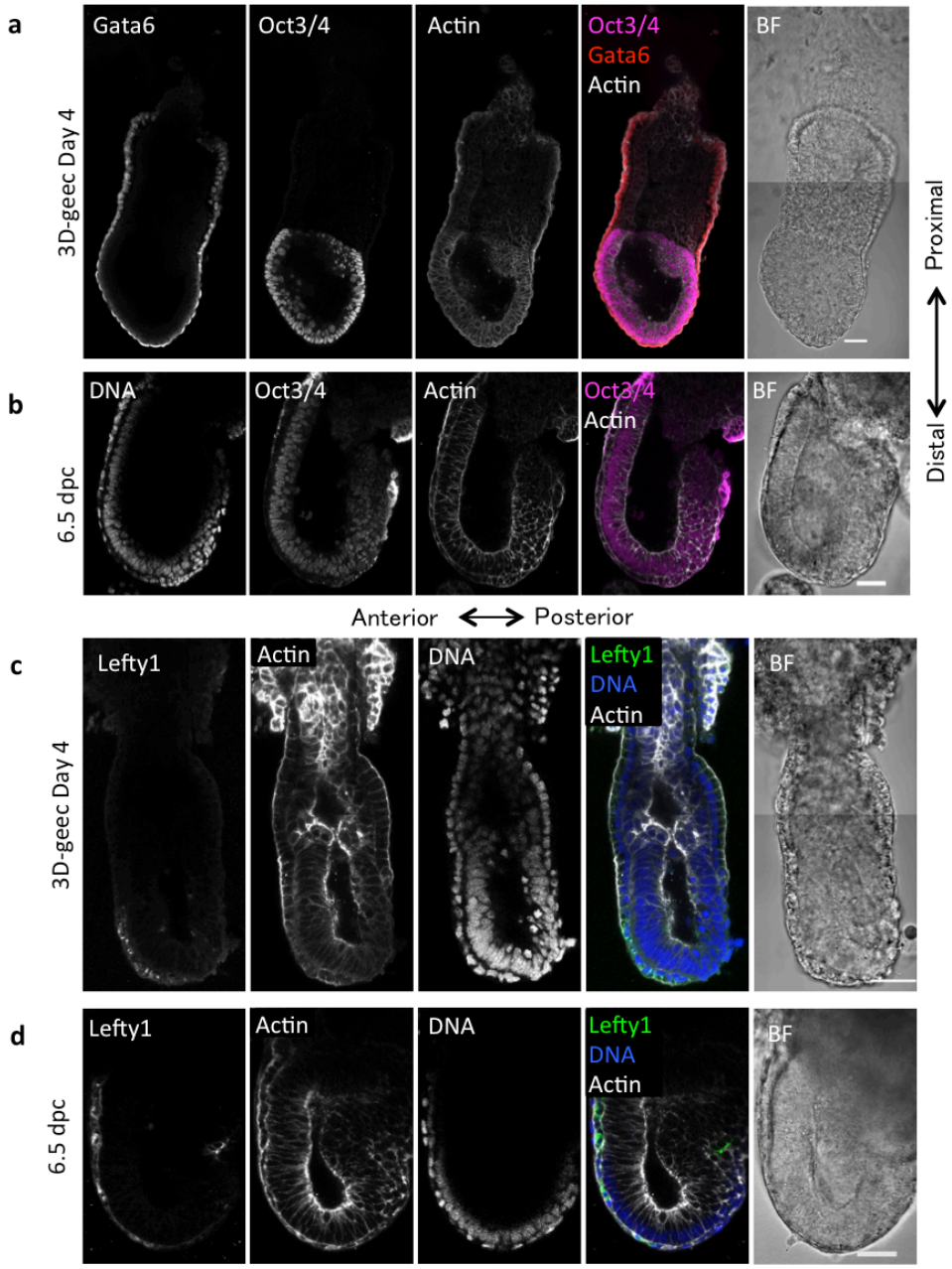

Figure 4.20. Mature 3D-geec embryo morphology and gene expression compared to *in vivo* developed 6.5 dpc embryo.

a, 3D-geec Day 4 embryo stained with actin dye and antibodies against Oct4 and Gata6. **b,** *in vivo* developed 6.5 dpc embryo stained with actin and DNA dyes and antibody against Oct4. **c,** 3D-geec Day 4 embryo; **d,** *in vivo* developed 6.5 dpc embryo stained with actin and DNA dyes and antibody against Lefty1. Scale bars, 50 μm.

embryos could be delayed and some of them could potentially develop further, as evidenced by different developmental timing of day 3 embryos as discussed above. Lastly, in the remaining embryos, no clear morphology could be observed, only a small Oct4-positive and Gata4-positive cell cluster was evident.

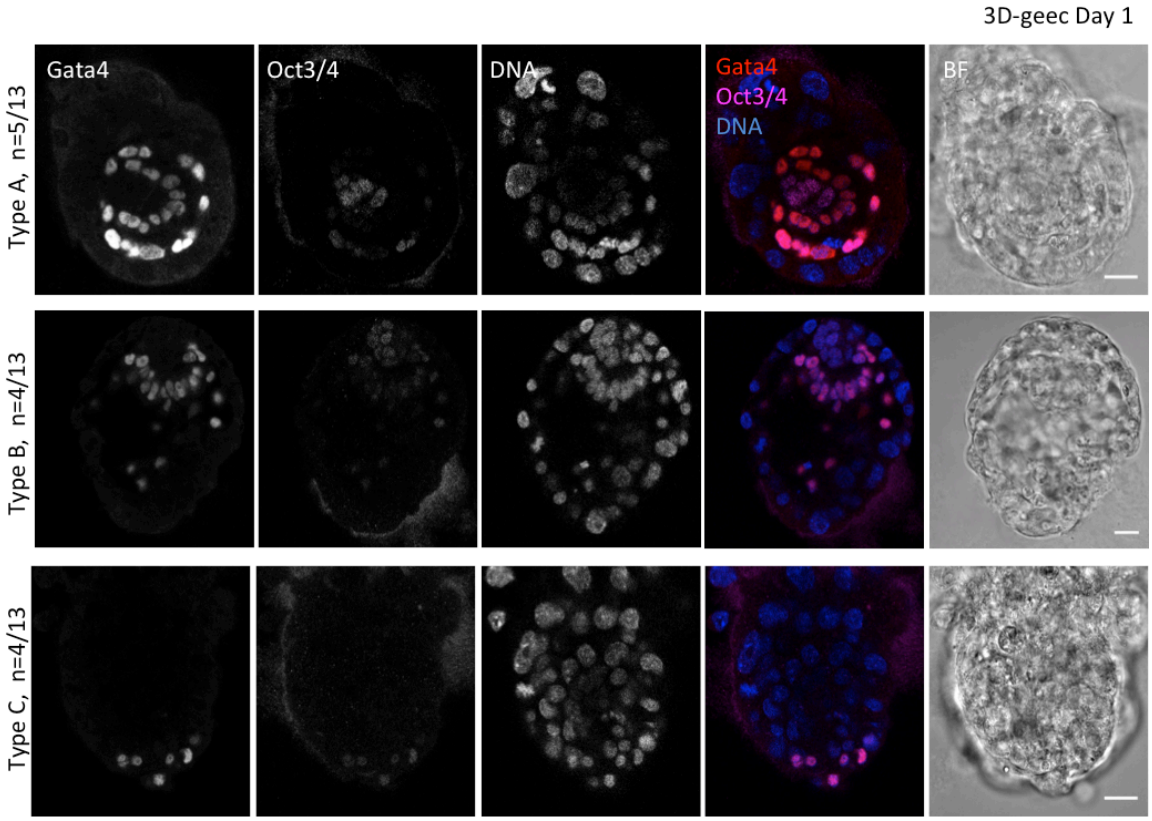

Figure 4.21.. Day 1 of 3D-geec culture.

Embryos cultured in 3D-geec for 1 day and stained with DNA dye and antibodies against Gata4 and Oct3.4. Type A embryos show two layers of Gata4+cells, a single Oct3/4 cell population, and no blastocoelic cavity. Type B embryos show single layer of Gata4+ cells, single Oct3/4 cell population, and blastocoelic cavity. Type C embryos show a mixed Gata4+ and Oct3/4+ population and no blastocoelic cavity. Scale bars, 20 μm. Embryos were collected and images acquired by Anthony Razov.

On day 2 of 3D-geec, some embryos appeared to retain morphology reminiscent of the blastocyst, but two layers of PrE-derived Gata4-positive cells could be seen (Fig 4.22), and Epi and VE were surrounded by apparent TE cells. Mural TE thickening could be observed as well. Around a third of the embryos at this stage formed a single-layer Oct4-positive Epi, with a surrounding Gata4-positive VE, but no surrounding TE. In these embryos, trophectoderm-derived cells were positioned in a clump on one side of the emerging egg-cylinder. Lastly, in accordance with the observations on day 1, a third of the embryos were in a disorganized state, with Gata4-positive and Oct4-positive cell populations positioned on the opposite sides of an amorphous clump.

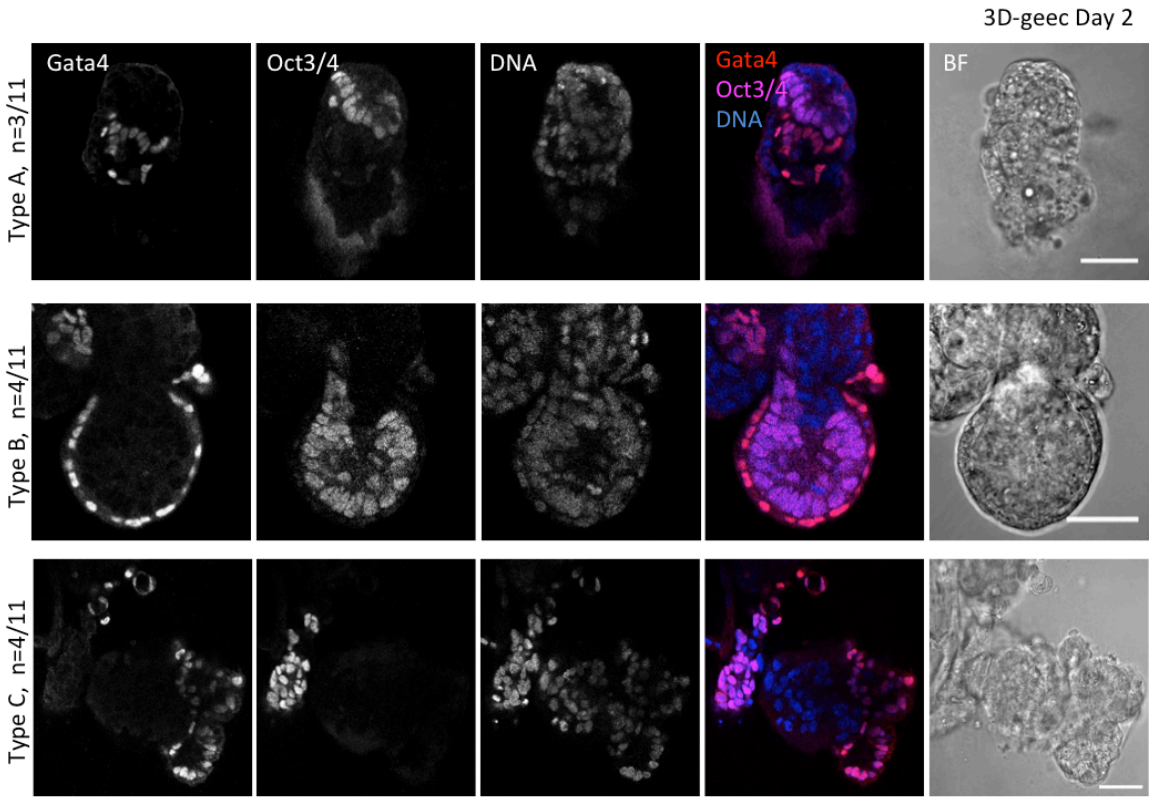

Figure 4.22 Day 2 of 3D-geec culture.

Embryos cultured in 3D-geec for 2 days and stained with DNA dye and antibodies against Gata4 and Oct3.4. Type A embryos show two layers of Gata4+cells, a single Oct3/4 cell population, and a layer of TE-derived cells covering both. Type B embryos show single layer of Gata4+ cells, single Oct3/4 cell population, but no TE-derived cells covering either. Type C embryos show one or multiple Gata4+ or Oct3/4+ populations and clear structure. Scale bars, 20 μm. Embryos were collected and images acquired by Anthony Razov.

Furthermore, some of the egg-cylinder stage embryos on day 3 or 4 of 3D-geec showed asymmetrical positioning of Lefty1 expression domain (Fig 4.20 c), suggesting the anterior-posterior axis specification comparable to 6.5 dpc embryo (Fig 4.20 d). Prolonged 3D-geec culture produced large spherical structures with apparent embryonic structure on top, similar to those previously reported (Hsu 1973). On day 7, somites could be seen under dissecting microscope (Fig 4.23), and contractile activity of 75 contractions per minute was observed. On day 8, it sped up to 150 contractions per minute, consistent with the development of cardiac cells.

Altogether, we have demonstrated that 3D-geec is suitable to study development at 4.5-6.5 dpc, and to monitor morphologenesis and dynamic gene expression changes during peri-implantation development.

Alternative embedding materials for 3D embryo culture

Recent advances in organoid culture have presented a synthetic 3D embedding technique that avoids batch variation of biological gels, is more flexible and easily controllable, and is fully defined and free of biological compounds such as growth factors (Caiazzo et al. 2016). Custom-produced biomimetic hydrogels have been demonstrated to be compatible with organoids and gastruloids (Gjorevski et al. 2016, Ranga et al. 2016, Vannini et al. 2016, M. Lutolf, personal communication).

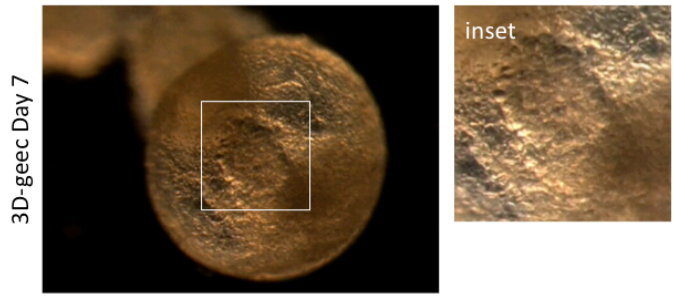

Figure 4.23. Prolonged 3D-geec culture.

Brightfield image of embryo cultured in 3D-geec for 7 days. Inset shows the area where contractile activity was observed. Image acquired with the help of Thomas Chartier.

Wishing to benefit from these advantages, we thus tested 3D-geec with hydrogel as a replacement for Matrigel–Collagen I mixture. While commercial hydrogel-embedded culture performed better than IVC, and fewer embryos failed to exit disorganized state, Matrigel-Collagen I mixture remained the superior embedding technique. Therefore, drawing inspiration from newest developments in hydrogel embedding cultures, we resolved to test embedding within an over-time degradable or non-degradable bio-mimetic hydrogels at different concentrations (Fig 4.24). We observed when using degradable gel that many embryos eventually sank to the bottom of the dish, making contact with and attaching to the dish surface and therefore were not cultured in 3D culture (Fig 4.24 a, b). Several embryos displayed elongated morphology and apparent VE layer (Fig 4.24 a, b). Most, however, formed round small size clumps and did not develop further (Fig 4.24 a, b). Similar morphology was observed when using non-degradable hydrogel (Fig 4.24 c). A third type of Hydrogel that is degradable over time due to exposure to water molecules will be available to us shortly. This type of hydrogel has shown most promise in long-

term organoid and gastruloid 3D culture so far (M. Lutolf, personal communication). Therefore we will work towards fine-tuning this type of degradable gel and developing a synthetic-gel embedded 3D embryo peri-implantation culture.

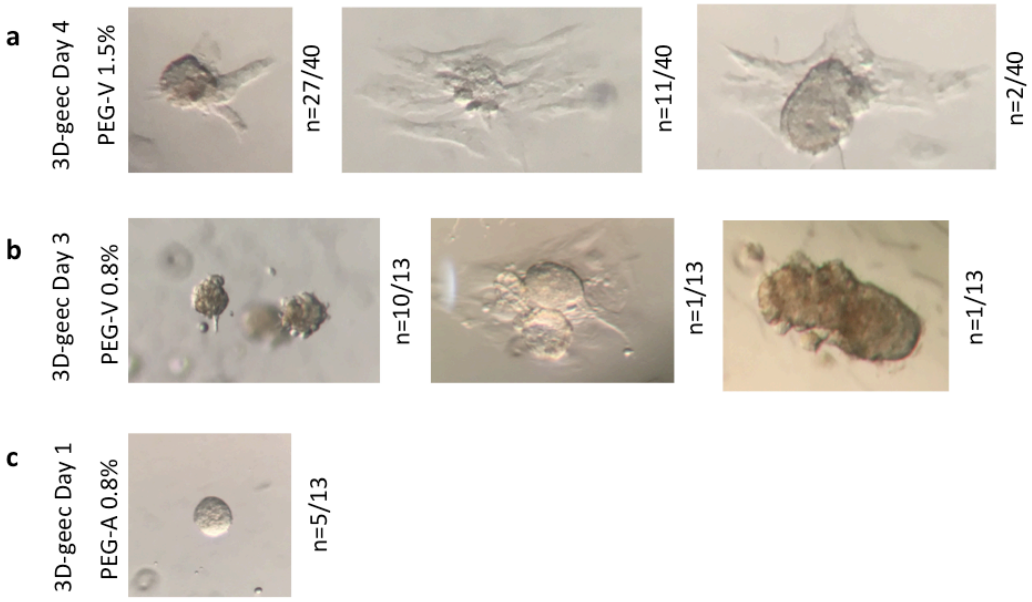

Figure 4.24. 3D-geec using custom-made hydrogel embedding.

Embryos cultured in 3D-geec for 4 days using PEG-V degradable hydrogel (a, b) or PEG-A non-degradable hydrogel (c) as embedding material. **a,** Embedding in 1.5% PEG-V. Many embryos made contact to the bottom of the dish (middle column), while most of the properly embedded embryos did not elongate to form egg cylinder with the exception of two embryos as shown in the right panel. **b,** Embedding in 0.8% PEG-V. Most embryos formed round clumps and did not elongate, with the exception of one embryo shown in the right panel. **c,** Embedding in 0.8% PEG-A. Most embryos perish, while some form smooth edge round clumps.

Imaging peri-implantation development

Most importantly, we wished to image 3D-geec embryos with high time resolution and for extended periods of time. 3D-geec proved not to be compatible with upright setup of confocal laser scanning microscope due to fact that embedding introduces additional distance between the objective and the embryo. In cases when the embryo could be seen, it would be invariably attached to the bottom of the dish and therefore could not be considered to be cultured in 3D-geec.

To overcome this problem, we looked for alternative imaging methods that would allow us to look deeper within the tissue of peri-implantation embryos. Our experience has previously shown that selective plane illumination microscopy, or SPIM (Huisken et al. 2004, Krzic et al. 2012), allows in-depth observation of mouse embryonic tissue at 6.5 dpc. At this stage, we were able to see single nuclei of the egg cylinder, and to resolve membranes between them (Fig 4.25, de Medeiros et al. 2015).

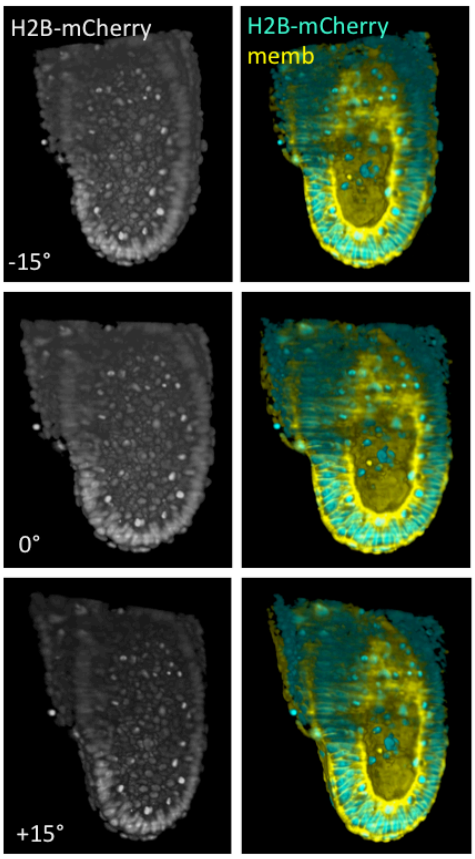

Figure 4.25. Imaging post-implantation mouse embryo in MuVi-SPIM.
3D rendering of transgenic embryo at 6.5 dpc expressing nuclear marker H2B-mCherry and membrane marker mG, imaged with MuVi-SPIM. From top to bottom: rotation of 3D-rendered embryo by 15°. Image was acquired with the help of G. de Medeiros and N. Norlin, and 3D rendering done by M. Albert.

We thus looked for a lightsheet microscope setup that has precise temperature and atmospheric control, and is compatible with 3D-geec mounting. We could achieve high resolution in time and space with Leica DLS SP8. A scheme of mounting for this setup that was adapted to mouse embryo imagining together with Sabine Reither is shown in Fig 4.26 a. With the help of a mold, an elevated agarose column with a

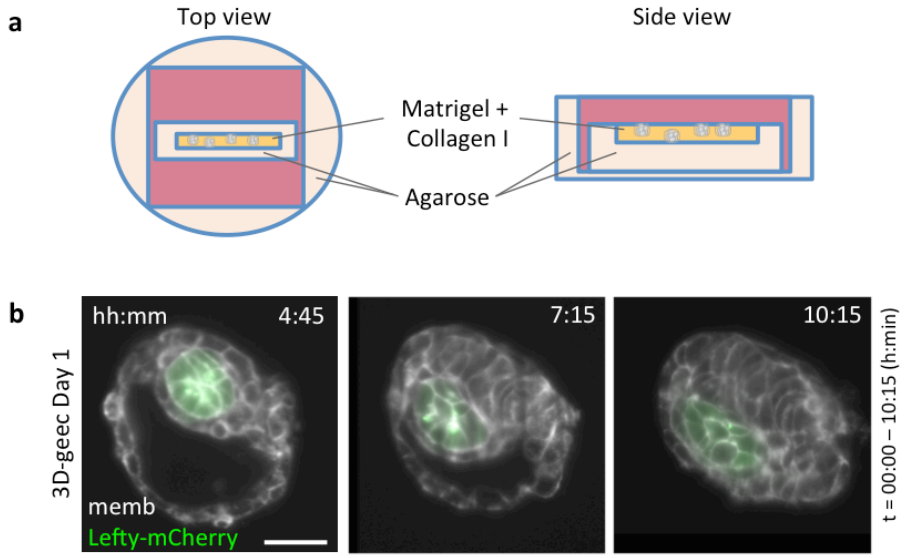

Figure 4.26. Imaging 3D-geec on Leica DLS SP8.

a, schematic illustration of 3D-geec mounting for Leica DLS. Embryos are suspended in Matrigel-Collagen I transferred to the agarose trench. **b,** Time-lapse images of 3D-geec Day 2 of a transgenic embryo expressing Lefty-mCherry and membrane marker mG. The epiblast and PrE move distally into the blastocoel cavity. Time is shown relative to the start of imaging. Scale bar, 50 μm.

trench is produced. Embryos are suspended in Matrigel-Collagen I and gel allowed to solidify inside the agarose trench. The column is then covered with IVC medium. Interestingly, we observed different morphological behaviors during 3D-geec day 2 using this setup. Epi proliferation together with rearrangement and elongation along apicobasal axis of polar TE cells appear to push Epi with the surrounding PrE into blastocoel cavity and towards the distal-most point of mural TE (Fig 4.26 b). In

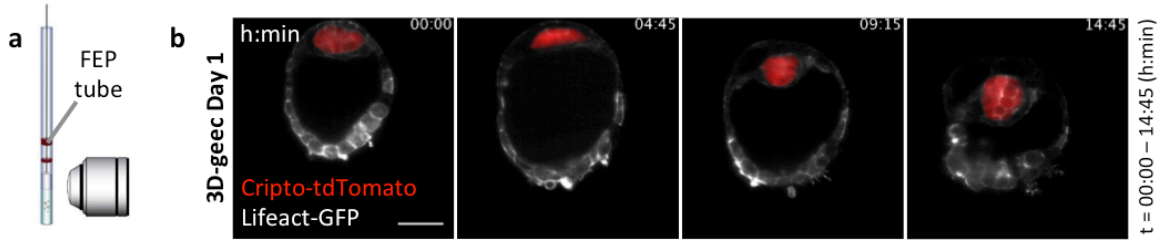

Figure 4.27. Imaging 3D-geec on Zeiss Z1.

a, Mounting of 3D-geec embryos for live imaging. **b,** Time-lapse images of 3D-geec Day 1of a transgenic embryo expressing Cripto-tdTomato and actin marker Lifeact-GFP. Embryo in 3D-geec continues peri-implantation development; the epiblast and PrE move into the blastocoel cavity. Time is shown relative to the start of imaging. Scale bars, 50 μm.

addition, Epi cells appeared to have formed a vertex. However, due to difficulties with sample positioning and atmosphere control, only short-term, single position imaging was possible with Leica DLS, and efficiency of culture was decreased dramatically.

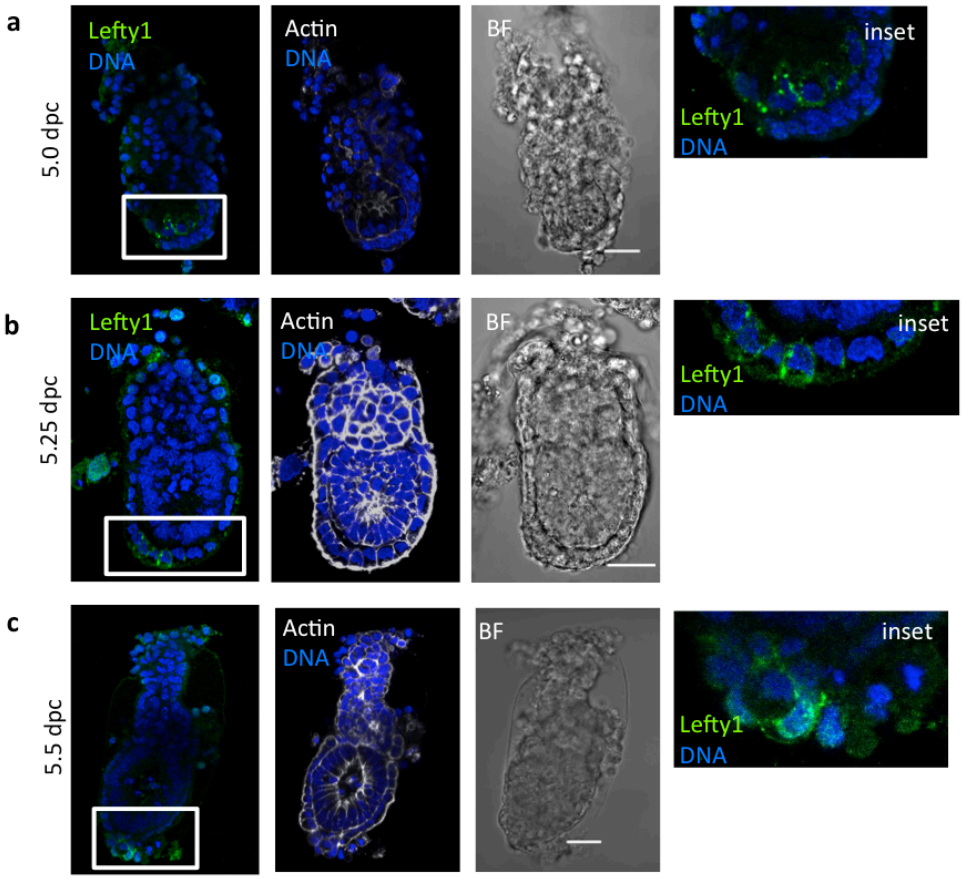

Figure 4.28 Lefty1 in early post-implantation embryos

Embryos dissected from decidua and stained with Actin and DNA stains and Lefty1 antibody. **a,** Embryo at early 5.0 dpc before formation of amniotic cavity showing Lefty1 expression within the epiblast. **b,** Embryo at 5.25 dpc with Lefty1 expressed in distal portion of VE. **c,** Embryo at E5.5 after formation of amniotic cavity with Lefty1 expressed in distal portion of VE. Scale bars, 40 μm.

For longer imaging, we turned to Zeiss Z.1. To image in this setup, the embryos were suspended in Matrigel-Collagen I mixture and were immediately aspirated into a gas-permeable FEP tube, which was in turn suspended in IVC medium (Fig 4.27 a). A representative time-lapse course of an embryo expressing an Epi marker Cripto-tdTomato and an Actin marker Lifeact-GFP can be seen in Fig 4.29 b. Early during 3D-geec, the embryo undergoes expansion and collapse normally observed during late blastocyst stage, followed by combined Epi and PrE movement into the

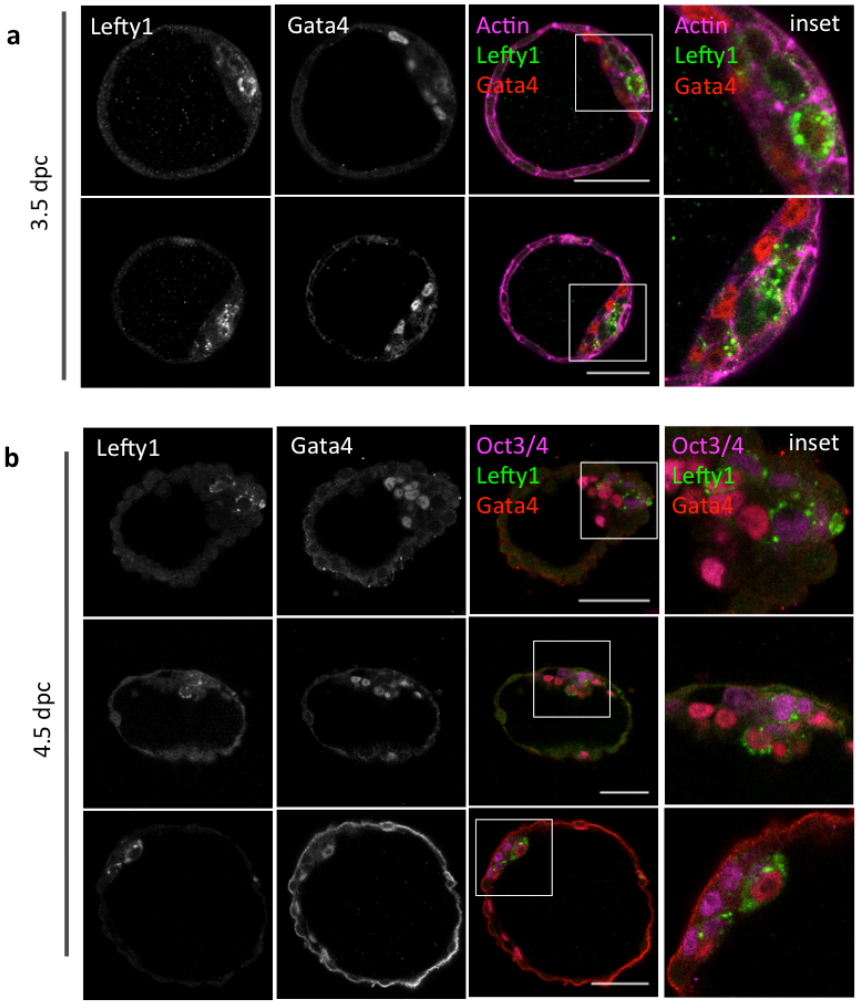

Figure 4.29. Lefty1 expression starts in the blastocyst and gets restricted to PrE.

a, 3.5 dpc embryos stained with antibodies against Gata4 and Lefty1, and actin dye. Lefty1 is located in the ICM. **b,** 4.5 dpc embryos stained with antibodies against Oct2/4, Gata4 and Lefty1. Lefty1 expression is first observed in the Epi and progressively changes to PrE. Scale bars, 50 μm.

blastocoel cavity (Fig 4.27 b), as observed in the initial tests using Leica DLS SP8. To our knowledge, epiblast and primitive endoderm movement into blastocoel cavity has not been previously observed by live imaging.

Anterior marker expression starts in the blastocyst and is maintained during peri-implantation development

Having established tools to bridge the blastocyst and the post-implantation *stages in vitro*, we asked whether the expression of anterior markers persists throughout

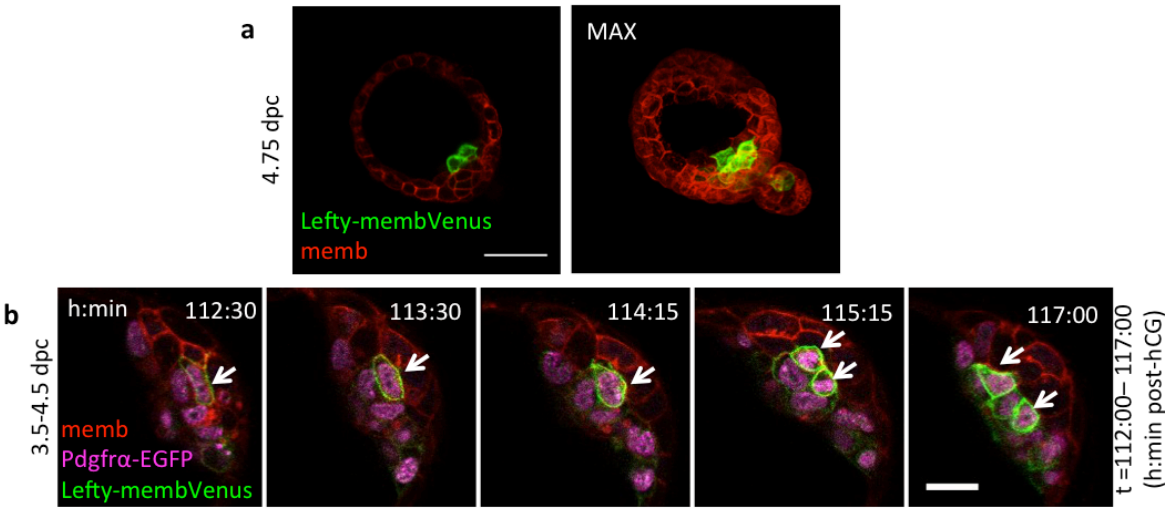

Figure 4.30 Lefty-membVenus expression in pre-implantation embryos.

a, 4.5 dpc embryo expressing Lefty-membVenus reporter and membrane marker mT (center slice and maximum intensity projection). Three Venus$^+$ cells are seen facing the cavity. **b,** Pdgfra-EGFP-positive and Lefty-membVenus-positive cell dividing and moving into a cavity facing position within a 4.5 dpc embryo. Arrows point to the tracked cell and its descendants. Scale bars, a, 50 μm, b, 20 μm.

implantation. To this end, we first performed immunofluorescent staining on early post-implantation stage embryos. Lefty1 protein could be detected at all post-implantation stages examined (Fig 4.28). In embryos dissected very early on 5 dpc, Lefty1-positive cells were found within the epiblast with a Lefty1-negative PrE/VE cell layer surrounding them (Fig 4.28 a). At 5.25 dpc, when the epiblast is elongated but proamniotic cavity has not started to form, Lefty1-positive cells can be seen in the distal tip of VE (Fig 4.28 b). Such expression pattern persists through to E5.5, when amniotic cavity begins to form with the epiblast (Fig 4.28 c). This suggests that Lefty1 expression persists during implantation.

Since AVE/DVE precursors can likely be tracked back to the blastocyst, it is important to discover their origin. Thus we wished to identify the earliest point at which anterior factors are expressed in the mouse embryo. We looked into known anterior markers Lefty1 and Hex in late morula, early and late blastocyst.

We observed the earliest expression of Lefty1 protein in mid-to-late blastocyst (Fig 4.29.a). As the blastocyst matures, the Lefty1-positive cell population grows, and

finally shifts from the epiblast to the PrE (Fig 4.29 b). First Lefty1-positive cells appear in the ICM before Epi and PrE sorting is finished. By the time that a cavity-facing Gata4-positive PrE population is established, many cells within Epi are expressing Lefty1. Importantly, expression of Lefty1 and Gata4 do not initially overlap. Fist Gata4-positive /Lefty1-positive cells can be observed in the PrE at 4.5 dpc.

We next asked when and how does the "switch" of Lefty1 expression between Epi and PrE/VE occur. As observed by immunofluorescent staining of dissected post-implantation embryos, this possibly occurs at around 5 dpc *in vivo* (Fig 4.28). However, we observe that Lefty-membVenus blastocysts cultured *in vitro* lose Lefty expression in the Epi at 4.75 dpc, when the only Lefty-membVenus-positive cells can be seen in the PrE (Fig 4.30 a). Similar timing is observed in fixed embryos

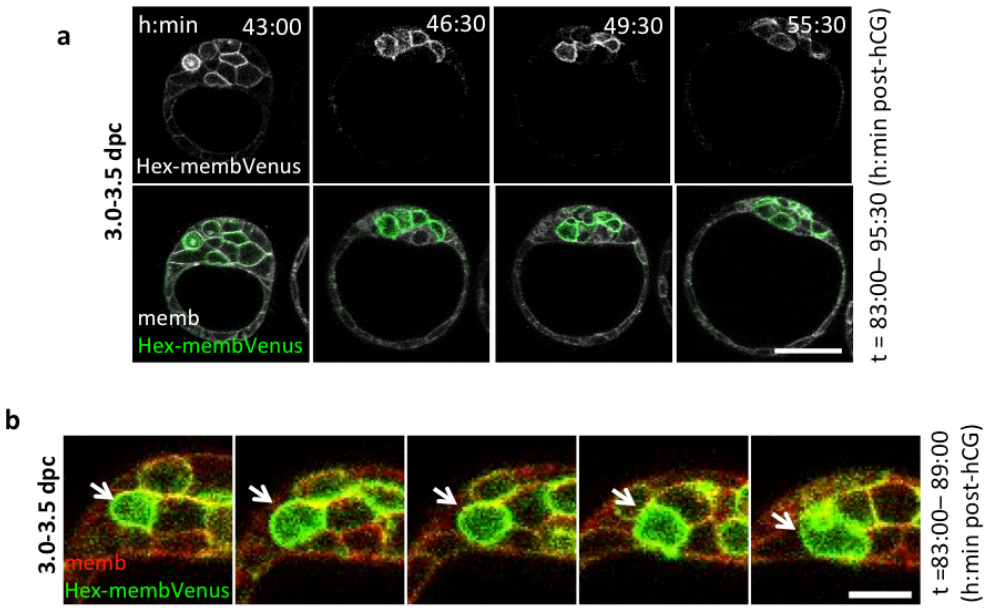

Figure 4.31. Hex-membVenus expression in pre-implantation embryos.

a, Time-lapse of E3.0-E4.5 embryo expressing Hex-membVenus and membrane marker mT. Hex-membVenus expression starts in the ICM and progressively moves to PrE. **b,** Time-lapse of E3.0 embryo expressing Hex-membVenus and mT. The arrows point to Hex-membVenus expressing cell moving from inner position in ICM to cavity-facing position in future PrE. Scale bars, a, 50 µm, b, 20 µm.

Immunofluorescently stained with Lefty1 antibody (Fig 4.29 b). *In vitro*-cultured blastocysts at this stage do not undergo Epi elongation. This contradiction can be explained by the unsuitability of pre-implantation embryo culturing media and culturing protocols for late blastocysts, which could delay morphological development without delaying gene expression.

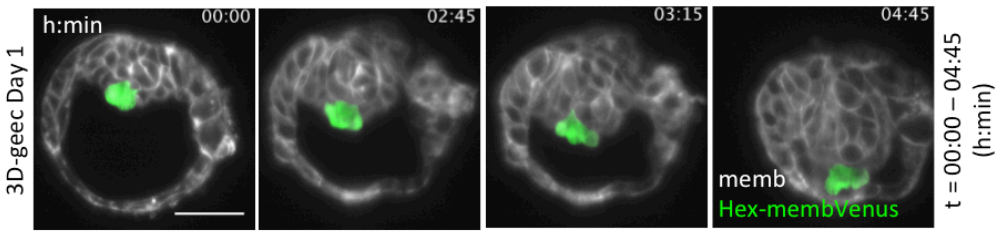

Figure 4.32. DVE/AVE progenitors maintain Hex expression during peri-implantation development.
3D-geec embryo on day 1 of culture expressing Hex-membVenus and membrane marker mT. Hex-membVenus is continuously expressed during implantation. Epi and PrE move into the blastocoel cavity. Time is shown relative to the start of imaging. Scale bars, 50 μm.

To capture the transition of the first Lefty-membVenus cells to cavity-facing position, we turned to live imaging and cell tracking. Interestingly, when observing the expression of PrE reporter Pdgfrα-EGFP simultaneously with Lefty-membVenus marker in the same embryo, we have noticed that the first cells that express Lefty-membVenus late on 3.5 dpc are Pdgfrα-EGFP-positive (Fig 4.30 b). Such cells then move to the cavity facing position during blastocyst maturation. On the other hand, Hex-membVenus expression can be detected in early 3.5 dpc blastocysts, around 12 hours earlier than Lefty-membVenus (Fig 4.31 a). Similar to Lefty, several of Epi cells are expressing Hex–membVenus at 3.5 dpc, but first Hex-membVenus-positive cells appear in future PrE earlier, namely at 3.5 dpc, by movement from inner position within ICM to a cavity-facing position (Fig 4.31 b).

3D-geec allows preserving the correct morphological development of late blastocysts. Being able to image peri-implantation development, we were in a unique position to track Lefty-membVenus or Hex-membVenus expressing cells from the moment they appear in PrE to their final position in the distal tip of VE. For this, we tracked the expression of Lefty-membVenus and Hex-membVenus reporters in embryos during 3D-geec (Fig 4.32). We observed that the expression of Hex-

membVenus reporter persists in PrE cells in 3D-geec embryos, and that Hex-membVenus is restricted to the distal tip of the PrE during implantation.

Altogether, the expression of Lefty-membVenus reporter and Lefty1 protein in the blastocyst and at early post-implantation stages, and persistence of Hex expression during implantation suggests that DVE/AVE precursors originate from the blastocyst population of Lefty1-positive (and/or Hex-positive) cells, contrary to the previous suggestion that anterior marker expression arises de novo during post-implantation development.

Mechanisms underlying the generation and maintenance of DVE/AVE precursors

Having observed Lefty-membVenus and Hex-membVenus expression dynamics, we were further intrigued by mechanisms that generate these progenitors and restrict Lefty1 and Hex to a defined population of cells within the PrE/VE.

First, to know if the early setting aside of the AVE/DVE is a robust process, we asked whether the PrE population of anterior marker-positive cells can be replenished if lost. We chose to eliminate Hex-membVenus-positive or Lefty-membVenus-positive cells by laser ablation, and observe further development in 3D-geec. We are currently setting up laser ablation for late pre-implantation culture and for 3D-geec. First, we targeted the center areas of three cavity-facing cells within the blastocyst (Fig 4.33 a). After laser ablation with two-photon laser, we observed expansion and consecutive collapse and rupture of all three cells targeted. To avoid severe damage that would lead to release of cell contents to the cavity, the experiment will be adjusted further. Next, we tested ablating Lefty-membVenus-positive cells in 3D-geec day 0 embryos immediately after embedding, using MuVi-SPIM Mikan laser (Fig 4.33 b). We observed initial formation of fluorescent granules within the cell indicative of protein damage response, and subsequent membrane expansion of the cell targeted for ablation.

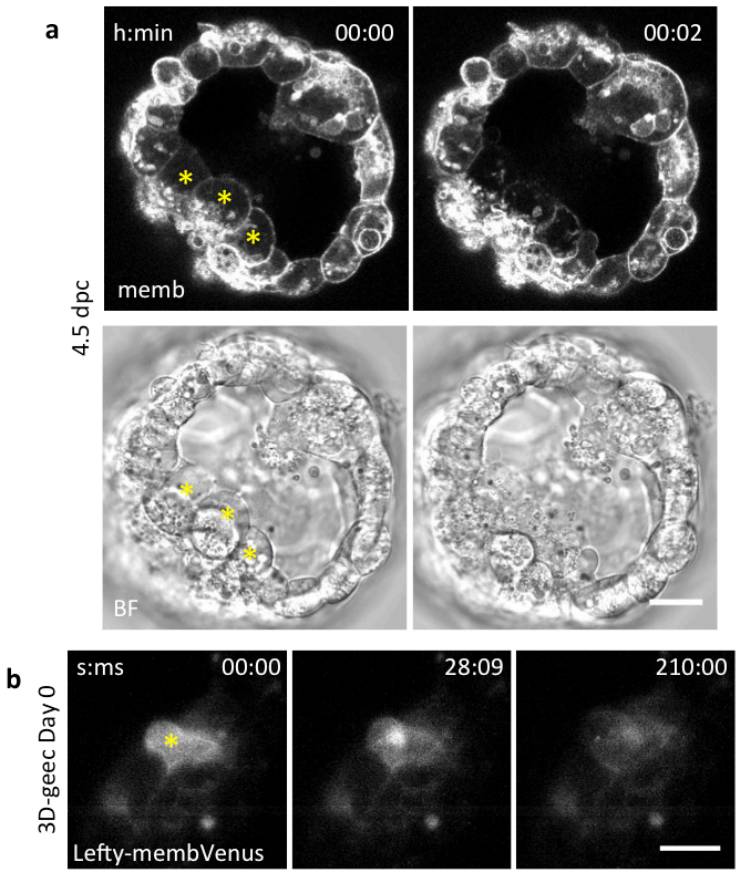

Figure 4.33. Laser ablation of cavity-facing or Lefty-membVenus expressing cells in 4.5 dpc embryo.

a, An embryo expressing membrane marker mT before and after ablation with two-photon laser. **b,** a cell expressing Lefty-membVenus within 4.5 dpc embryo before and after ablation with Mikan laser. Asterisks (*) mark cells to be ablated. Scale bars, a, 50 µm, b, 20 µm. Ablation in (b) was performed with the help of G. de Medeiros.

Initial tests with mature blastocysts in pre-implantation culture and in 3D-geec proved that we can specifically target single PrE /VE cells for ablation, and induce cell damage that could lead to elimination of these cells. In the next steps, we will aim to fine-tune laser ablation and follow up with live imaging and cell tracking to determine whether the eliminated cells will be replaced by new Hex-expressing or Lefty1-expressing cells in the PrE/VE of peri-implantation embryo.

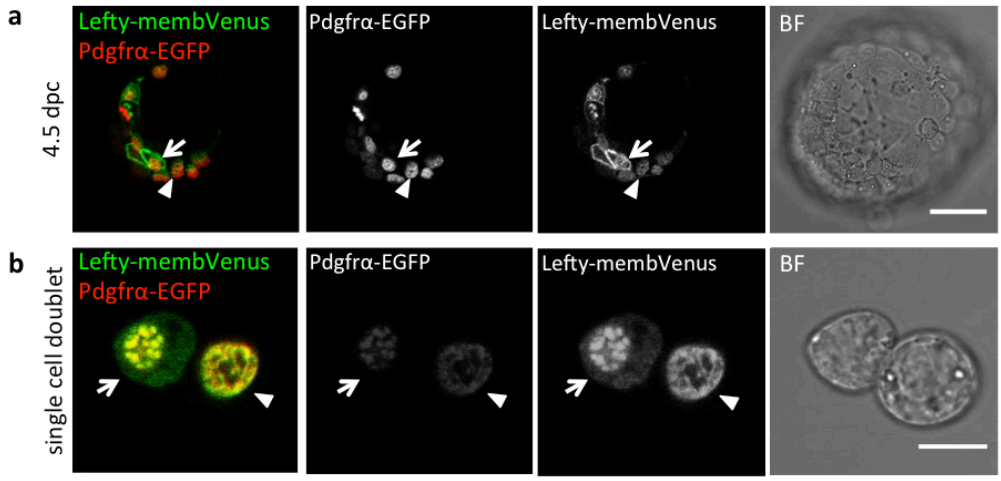

Figure 4.34. Cell isolation from the blastocyst for single-cell RNA-seq.

a, 4.5 dpc embryo expressing Lefty-membVenus and PrE reporter Pdgfrα-EGFP before single-cell isolation. **b,** a doublet of cells isolated from embryo shown in (a). Arrow, a cell positive for both reporters, arrowhead, a cell positive for Pdgfrα-EGFP only. Scale bars, a, 40 μm, b, 10 μm.

Establishment of DVE/AVE marker expression domain in late PrE

Having observed the distinct morphology and behavior of DVE/AVE progenitors., we wanted to know how do these cells differ from other PrE cells in the late 4.5 dpc blastocyst, and later during peri-implantation development. To answer this question, we aimed to probe the transcriptional character of each cell type. We established a protocol to isolate single cells from mature blastocysts expressing Lefty-membVenus and Pdgfrα-EGFP. Lefty-membVenus is restricted to a few cells in the PrE at this stage and Pdgfrα-EGFP marks all PrE cells (Fig 4.34 a). After isolating single cells, we were able to determine their previous position within the blastocyst and their identity by recording nuclear or membrane fluorescence under confocal microscope (Fig 4.34 b). Collaboration with Tang laboratory (Beijing University, China) to perform single cell RNA-seq on these cells is ongoing. We will ask whether all DVE/AVE precursors co-express Lefty1, Cerl and Hex, and how transcriptionally different are these precursors from their neighbors in PrE.

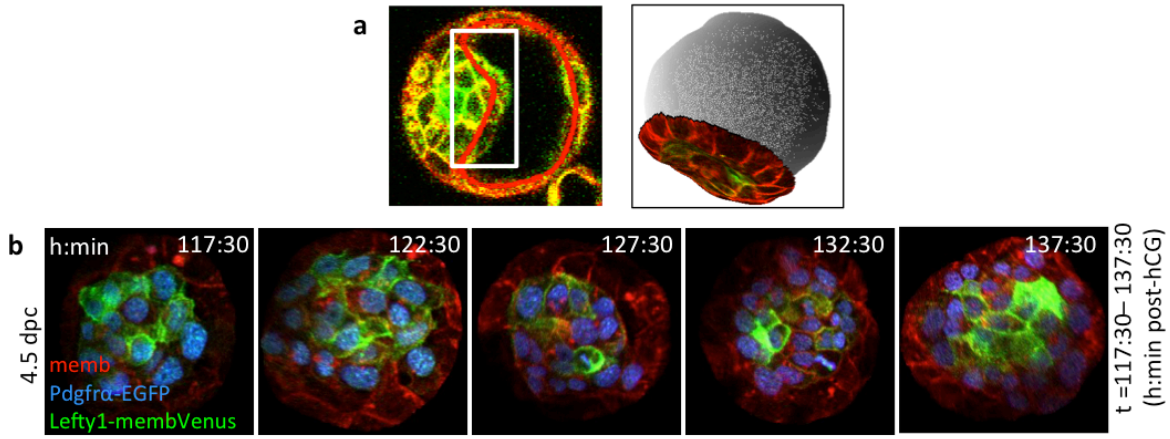

Figure 4.35. Planned analysis of DVE/AVE domain establishment.

4.5 dpc embryo expressing Lefty-membVenus, Pdgfrα-EGFP and membrane marker mT. **a,** Left: area selected for 2D unfolding analysis. Right: Segmented cavity with overlaying PrE layer in 3D. **b,** consecutive time points of 2D-unfolded PrE layer with Lefty-membVenus-positive cells close to the center of Pdgfrα-EGFP-positive PrE layer.

To understand cell behavior that leads to a single Lefty1-positive or Hex-positive domain establishment within PrE, we wished to follow these cells as they take up a cavity-facing position, divide further, and converge onto the center of PrE. For analysis of cell lineage, movement and gene expression pattern, as well as for visualization, we deemed it useful to mathematically unfold the PrE layer from 3D time-lapse images into a 2-dimensional sheet as previously described (Heemskerk and Streichan, 2015). An example of such image transformation is shown in Fig 4.35. We are now able to track the emergence, position and lineage of Hex- membVenus and Lefty-membVenus expressing cells in the PrE of the blastocyst and PrE/VE of the peri-implantation embryos cultured in 3D-geec.

5. DISCUSSION

Resolution of gene expression heterogeneity in the blastocyst

As a self-organizing system, the early mouse embryo is capable of forming first lineages within initially equivalent cells that exhibit gene expression heterogeneity. Our findings suggest that there are distinct mechanisms for specification of the TE and ICM cell fate. While both TE and ICM-specific markers show initial expression heterogeneity, asymmetric division drives the upregulation of trophectoderm-specific gene expression. Importantly, this is not the case for ICM-specific genes. ICM-specific markers are restricted to ICM (ICM-specific gene network established) only at 64-cell stage (Fig 5.1).

We found that currently available ICM-markers do not allow predicting ICM fate by the onset of its expression as a single gene. An exciting question remains whether the onset of a yet-unknown gene, or combination of two or more genes, confers lineage-predictive power. Ultimately, it will be interesting to ask what role (if any) the gene-expression heterogeneity, or the earlier onset of the ICM lineage marker expression in a few cells, plays in specifying the ICM cell fate. It is as well possible that an unknown lineage determinant may drive and be required for the initiation of the ICM differentiation, placing it on top of the hierarchy of other stochastically expressed pluripotency genes.

A recent study has shed light on heterogeneous expression of TE-specific genes. The heterogeneity in this case can be explained by the fact that after asymmetric division, initially apolar cells can be positioned outside repolarized and change their fate accordingly when they do not fit inside the embryo. In this way, the onset of TE-specific gene can be delayed in certain number of outside cells (Korotkevich et al. 2017).

The ICM cell population, on the other hand, exhibits higher gene expression heterogeneity that may be induced by stochastic mechanisms (Dietrich and Hiiragi 2007). What drives this heterogeneity, and what reinforces the ICM fate? Mechanical properties such as contractility have been shown to direct cell position within the early morula (Maitre et al. 2016). The time during which ICM cells are enclosed by

other cells may influence gene expression, as evidenced by correlation of prolonged inside position with upregulation of pluripotency network TF, Sox2. However, even during blastocyst stage, ICM is heterogeneous in its gene expression pattern (Ohnishi et al. 2014). Ultimately, feedback loops between a combination of factors such as cell position, cell-cell contact, mechanical properties and activity of specific transcriptional regulatory networks act to guide cells towards and refine their lineage decisions.

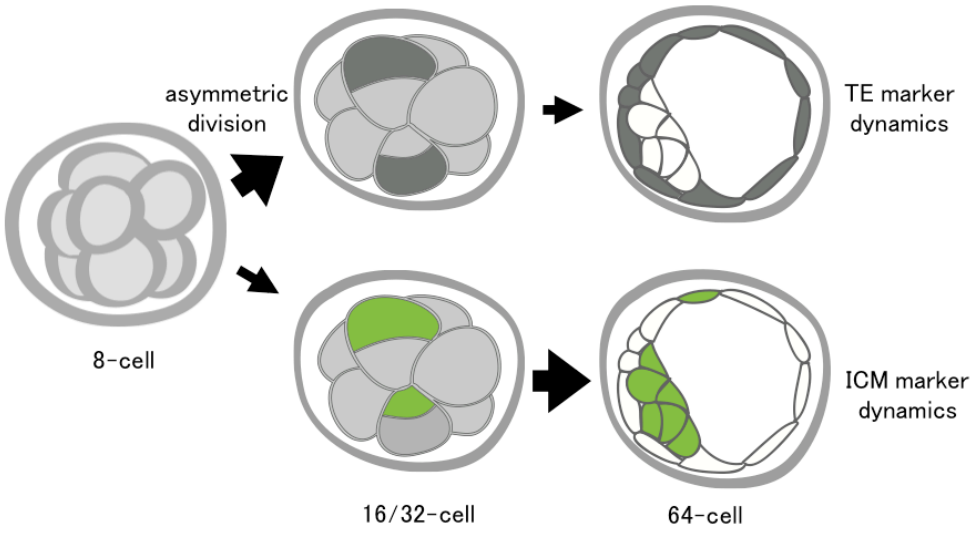

Figure 5. 1. Distinct mechanisms for the acquisition of the TE or ICM molecular identity.

TE or ICM molecular identity is acquired in a non-binary fashion and at different developmental times. The specific expression of a TE fate marker (grey) is established through asymmetric divisions from 8- to 16-cell and 16- to 32-cell stage, as quantified by our reporter mice. The ICM-specific gene (green) expression is non-reciprocal to the TE marker and only becomes ICM-specific at the late 64-cell stage.

It would be most interesting to investigate whether gene expression heterogeneity has a function in lineage segregation and embryonic axis establishment. A key experiment to address this question would be to try diminishing gene expression heterogeneity by using genetic knock-out of heterogeneously expressed genes and reintroducing the missing gene product at equal level amongst all cells. For example, in $Fgf4^{-/-}$ embryos, ICM was shown to be normal in size, but it had a reduced number of Gata6-positive cells in the ICM, and did not form any PrE (Kang et al. 2013). When those embryos were cultured in the medium supplemented with Fgf2/4, all ICM cells were converted to Gata6-positive PrE or Nanog-positive Epi, depending on the

concentration. This strongly suggests that the local heterogeneity in Fgf4 is important to produce salt-and-pepper distribution of cells committed to PrE or to Epi. In a similar way we can ask how heterogeneity of other factors will be important early in development, when TE and ICM lineages are established, or later, when body axes start to emerge.

Emergence of heterogeneity within the blastocyst that marks future body axis

During my PhD study I discovered that within the population of cells that had been considered as homogeneous, a few cells exhibit heterogeneous gene expression that could be employed for lineage specification or body patterning in the next stage. Specifically, Lefty1 and Hex- positive cells emerge from within ICM population during blastocyst maturation. The key remaining question is how Lefty1 and Hex expression is restricted into a few cells within the ICM.

In the case of Lefty, its asymmetrical expression at 5.5 dpc requires activity of a Nodal-dependent enhancer (Norris et al. 2002, Takaoka et al. 2006). However, while asymmetric inheritance of unevenly distributed axis determinants has been demonstrated in other organisms (Gore et al. 2005), Nodal and members of Nodal signaling pathway, such as Cripto shown above, are expressed evenly throughout ICM or Epi cells. Alternatively, a mechanism called self-enhancement lateral inhibition (SELI) has been proposed to restrict Lefty1 to a small subset of cells in the blastocyst (Nakamura et al. 2006, Takaoka et al. 2007). In such scenario, a small difference in expression is autonomously converted into a robust asymmetry, as cells that express Lefty1 at a slightly higher level will maintain its expression while suppressing and ultimately eliminating Lefty1 expression in cells with initially low level expression of this gene. It is apparent that heterogeneity of anterior-marker gene expression is a prerequisite for SELI model to function.

It is important to note that at this stage of development, ICM undergoes active sorting of PrE and Epi precursors from initial salt-and pepper distribution. Therefore we may also ask if there is a possible interplay between tissue flow and signaling center rearrangement.

Is expression induced in a single PrE domain, or do cells arrive there from another place within the embryo? Consistent with the dynamic features of Lefty1 or Hex-expressing cells during A-P axis specification at 6.5 dpc, it is possible that these cells have a particular property to be able to actively move. Thus tissue mechanics could be implicated in single DVE/AVE precursor domain establishment in PrE of the late blastocyst. Both Lefty-membVenus- and Hex-membVenus-positive cells were shown in this work to move to cavity-facing position. Whether this movement is active could be tested by determining apical-basal polarity of these cells. Alternatively, Lefty-membVenus- or Hex-membVenus-positive cells arrive at PrE due to a sorting mechanism that is already acting on PrE precursors. Gata4-positive PrE layer is established before first Lefty1-expressing cells are seen in PrE, yet Hex-membVenus-expressing cells appear to move to their final position earlier.

How is the "center" position of PrE, around which Hex or Lefty1 expression domain is established, defined? If a blastocyst is confined by the uterine crypt, this can lead to elongation of embryonic-abembryonic axis, and the resulting shape of ICM can change the distance of a point within it from a signaling center within Epi, polar TE or distal point of mural TE. However, this proposition is challenged by the fact that Lefty-membVenus-positive cells in the center of PrE are also observed in round *in vitro* cultured 4.5 dpc blastocysts.

A question to be addressed in parallel to understand the establishment of a single DVE/AVE precursor domain is the involvement of signaling in early specification of these precursors and in maintaining their precise position within the embryo.

Role of signaling pathways in the early embryo

At post-implantation stage, signaling activities that specify or maintain distal visceral endoderm (DVE) cells are relatively well characterized. On the other hand, how signaling in the pre-implantation embryo could contribute to body plan establishment is not comprehensively understood. What signaling can produce

heterogeneity? Is there any signaling pattern existing within the blastocyst that would asymmetrically affect ICM/Epi?

A number of signaling pathways important for embryo patterning are active in the blastocyst and during early post-implantation development. A member of the transforming growth factor beta (TGF-β) family of growth factors, Nodal is a secreted factor that is known for its role in cell-fate specification during post-implantation development and in embryonic axis establishment (Shen, 2007). Nodal and the key components of the Activin/Nodal signaling pathway are expressed as early as E3.5 in the mouse embryo, and Nodal has an earlier role in maintaining the undifferentiated status of the epiblast. Embryos lacking Nodal downregulate pluripotency markers and undergo premature anterior neuralization of the epiblast population (James et al. 2005, Camus et al. 2006, Mesnard et al. 2006). In addition, Nodal mutant embryos display VE effects and lack DVE cells (Mesnard et al. 2006, Brennan et al. 2001).

Moreover, the molecular players that establish the embryonic axes in vertebrates and in sea urchin have been demonstrated to act downstream of Wnt/β-catenin signaling pathway (Agius et al. 2000, Range et al. 2007, Schier 2001, Stern 2006). This includes Nodal homologues. In the mouse embryo, a Nodal regulatory element active in pre-implantation epiblast and responsive to Wnt/β-catenin signaling has been identified (Granier et al. 2011). In addition, zygotic β-catenin knock-out has no Hex and mislocalized Cerl (Huelsken et al. 2000, Arnold et al. 2000, Haegel et al. 1995, De Vries et al. 2004). Taken together, these findings suggest that Wnt is a likely candidate to act on DVE/AVE precursors in the blastocyst as well.

Furthermore, components of Notch signaling pathway were found expressed in the blastocyst (Cormier et al. 2004, Wang et al. 2004). Specifically, Notch pathway has been demonstrated to regulate trophectoderm-specific expression of Cdx2 (Rayon et al. 2014). It is so far unclear whether Notch is required for pre-implantation and early post-implantation embryo development. Maternal-zygotic abrogation of crucial components of canonical Notch signaling lead to normal early development, with embryonic defects observed after gastrulation (Souilhol et al. 2006, Shi et al. 2005). Interestingly, Notch signaling has previously been shown to be able to generate heterogeneity in a homogenous cell population (Artavanis-Tsakonas et al. 1999).

Finally, maturation of ICM and generation of AVE/DVE could be under control by several signaling pathways. Which of these signaling pathways has an effect on Lefty1 or Hex expression, and thus a direct impact on the establishment of DVE/AVE precursors in the blastocyst remains to be elucidated using pharmacological inhibitors and genetic knock-outs.

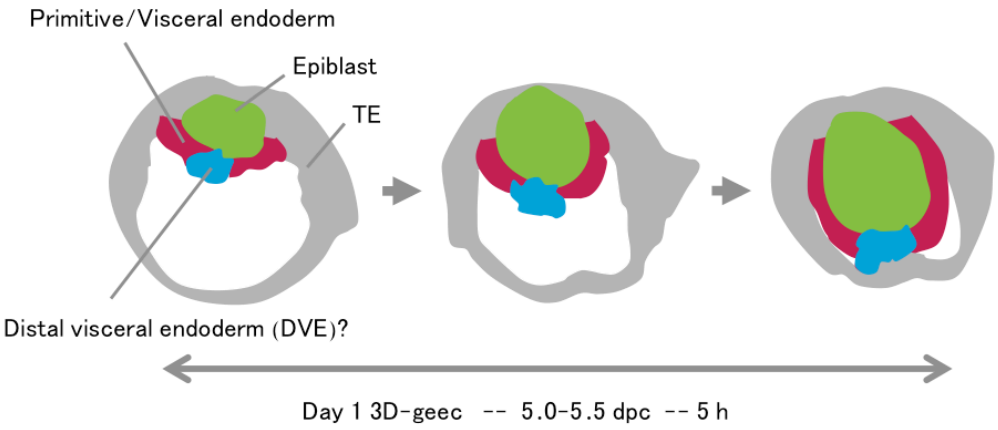

Figure 5.2. Morphological changes and cell populations in peri-implantation embryo.

At the moment when a mature blastocyst is transferred into 3D peri-implantation culture, it contains a small population of PrE/VE (red) cells that express anterior markers (blue). This population is maintained throughout Epi(green)/VE elongation, likely forming DVE. If the blastocyst morphology is preserved by culturing in 3D during peri-implantation, elongation of Epi and VE towards the distal point of mural TE (grey) can be observed.

Formation of the cup-shaped epiblast

The inward movement of ICM may be a unique feature of rodents, possibly influenced by spatial restrictions imposed by a particular shape of the rodent uterine crypts. The embryo could have thus evolved to elongate along mesometrial – anti-mesometrial axis. Indeed in 3D culture, we found a strong inward elongation/movement of PrE and Epi. Understanding the mechanism for this morphological change would be the key to understand why only rodents form the cup-shaped epiblast. It is possible that this mechanism is physical in nature, and thus certain constriction could be sufficient to induce cup-shaped epiblast in embryos of other species. Another possibility is that a specific gene, or specific transcriptional program, is responsible for the distinctive morphology of rodent post-implantation

embryo. It is therefore interesting to ask whether forced expression of such genes or activation of certain transcriptional programs would induce cup-shaped epiblast in other mammalian, e.g. in rabbit, embryos.

What is driving the change in morphology during peri-implantation (Fig 5.2)? Increased cell growth or division rate in Epi cells is unlikely, since the inward movement occurs over a short 5 h period. Active cell migration would produce morphology different from what was observed, though intercalation, apical constriction and lateral elongation could all contribute to the shape changes of the Epi. Individual cell shape changes can arise from local contractility in the epithelium. This can be tested by determining cell mechanical properties by micropipette aspiration, quantifying myosin II localization by immunofluorescence and live reporter imaging, laser ablation to determine the magnitude and directionality of tension, i.e. the distribution of forces in the moving ICM cells, or by chemical contractility inhibition followed by observing changes in morphology and tissue dynamics.

Does the uterus provide essential cue for establishing embryonic axes?

Why is 3D peri-implantation culture superior to 2D alternative when it comes to preserving embryo morphology and gene expression? Potentially, very early during implantation only a limited contact to the uterine wall is made by the embryo, the opposite of a robust attachment. If in *in vitro* culture the blastocysts are allowed to settle on the bottom of the dish, their trophoblasts attach strongly to the dish surface, and this affects further development. Thus the biggest advantage of 3D culture might be that it helps avoid attachment of the embryo to the surface of the dish. This method of culturing embryos without uterine attachments could well recapitulate the early post-implantation development.

It is noteworthy that even after a long phase of disorganization, the embryo is capable to re-organize as an emerging egg cylinder. Interestingly, other species of mammals have been shown to develop A-P axis prior to implantation (Eakin and Behringer, 2004). Marsupial embryos, for example, form A-P axis and gastrulate

prior to hatching from zona pellucida, and even some eutherian mammals can proceed as far as limb bud formation stage without interactions with the mother's uterus. It is therefore clear that in principle the embryo is capable to form axis autonomously, without instructions, guidance or feedback from the uterus. We therefore believe that 3D-geec mimics in utero conditions during peri-implantation and early axis-establishment stages by preventing trophoblast attachment.

6. PERSPECTIVES

Studying cellular heterogeneity

In recent years, there has been an increasing interest in gene expression heterogeneities and their potential role in stem cell systems. It is well established that ES cells in culture as well as pluripotent cells within the epiblast of the embryo exist in one of two states of pluripotency: either ground (naïve) state, or primed state (reviewed in Silva and Smith 2008, Nichols and Smith 2009). In ground state, the cells are unrestricted in their developmental potential, while primed state represents cells that are primed for lineage specification and commitment. Several studies have implicated gene expression heterogeneity as a prerequisite for pluripotent cells to be able to explore the variety of primed states and developmental outcomes, as illustrated by the example of TF Nanog (Kalmar et al. 2009, Canham et al. 2010, Abranches et al. 2014). Furthermore, addressing heterogeneity and presence of cancer stem cells in tumors will be crucial to address variable response to cancer therapy and relapse after treatment (reviewed in Beck and Blanpain, 2013).

In all cases it will be important to investigate the possible role of heterogeneity. To begin with, we will have to evaluate, i.e. quantitatively measure, the degree of cellular heterogeneities, in terms of gene expression, cell geometry, and other parameters. To gain functional insights, we will need tools to manipulate the degree of cellular heterogeneities, i.e. to increase, decrease, or dampen them. For such approaches, early mouse embryos would be one of the best-suited systems to study the role of cellular heterogeneity.

Studying mouse peri- and post-implantation development

The key problem in the current research of mammalian peri- and post-implantation development, including my own studies, is the lack of verification: it is not possible to verify the viability (full-term developmental potential) of the embryos as a result of *in vitro* culture. This problem could be in principle solved in one of two ways: to develop methods to implant the embryos back to the uterus after *in vitro* culture, or to monitor the embryo development *in utero* without disruption.

The former has been demonstrated to be feasible when egg cylinder stage embryos were transferred from deciduae of one pregnant female to those of another female from which embryos were previously removed (Beddington 1985). This study reported placentation and normal development of such transferred embryos for another 6-8 days, though at a low rate of success.

The latter may be more amenable at present, given the remarkable advance in intra-vital imaging. Specifically, we would need to image *in vivo* intact peri- and post-implantation embryos through uterine wall *in situ*. First we could aim to image the whole intact uteri in culture (Grant 1973 (1) and (2)) using multi-photon microscopy. This system, while certainly a bigger challenge for live imaging, would enable us to image mouse embryo development in an *in vivo*-like condition. When successful in imaging embryos through isolated uterus, it would be possible to proceed further to a completely *in vivo* system using abdominal imaging window, as reported for multiple organ long-term imaging in living mice (Ritsma et al. 2012, Ritsma et al. 2013).

Furthermore, using newest developments in hydrogel technology would allow increasing the efficiency of 3D culture, increasing reproducibility and avoiding variability between experiments. This will ultimately allow controlling the 3D environment in space and time to understand the specific conditions required and sufficient for pre and post implantation embryo development. Specifically, we should be able to modify hydrogel chemical and mechanical properties, by addition of small peptides, local embedding of light-releasable caged molecules, use of gradually softening degradable gels, and light-inducible gel softening of stiffening at defined areas.

To investigate the embryo-uterus interaction ex utero, it will be interesting to further explore the 3D-matrix-embedded uterine stromal cell based peri-implantation culture. Therefore the next step would be to transfer primary endometrial cell culture to 3D by embedding uterine cells in Matrigel-Collagen I mixture or synthetic hydrogels.

Altogether, further developments in *in vitro* peri-implantation culture and live in-utero imaging will be crucial for studying questions pertaining to peri-implantation and early post-implantation embryo development.

REFERENCES

Abranches E, Guedes AM, Moravec M, Maamar H, Svoboda P, Raj A, Henrique D (2014). Stochastic NANOG fluctuations allow mouse embryonic stem cells to explore pluripotency. Development 141(14):2770-9.

Agius E, Oelgeschlager M, Wessely O, Kemp C, De Robertis EM (2000). Endodermal Nodal-related signals and mesoderm induction in Xenopus. Development 127, 1173–1183.

Arnold K, Sarkar A, Yram MA, Polo JM, Bronson R, Sengupta S, Seandel M, Geijsen N, Hochedlinger K (2011). Sox2(+) adult stem and progenitor cells are important for tissue regeneration and survival of mice. Cell Stem Cell 9, 317–329.

Arnold SJ, Robertson EJ. (2009) Making a commitment: cell lineage allocation and axis patterning in the early mouse embryo. Nat Rev Mol Cell Biol 10(2):91-103.

Arnold, S.J., Stappert, J., Bauer, A., Kispert, A., Herrmann, B.G., Kemler, R., 2000. Brachyury is a target gene of the Wnt/beta-catenin signaling pathway. Mech. Dev. 91, 249–258.

Artavanis-Tsakonas S, Rand MD, Lake RJ (1999). Notch signaling: cell fate control and signal integration in development. Science 284, 770–776.

Barbera JPM, Clements M, Thomas P, Rodriguez T, Meloy D, Kioussis D, Beddington RS: (2000). The homeobox gene Hex is required in definitive endodermal tissues for normal forebrain, liver and thyroid formation. Development 127:2433-2445.

Beck B, Blanpain C (2013). Unravelling cancer stem cell potential. Nature Reviews Cancer 13, 727–738.

Beddington RS (1985). The development of 12th to 14th day foetuses following reimplantation of pre- and early-primitive-streak-stage mouse embryos. J Embryol Exp Morphol 88:281-91.

Beddington RS, Robertson EJ (1999) Axis development and early asymmetry in mammals. Cell 96(2):195-209.

Bedzhov I, Bialecka M, Zielinska A, Kosalka J, Antonica F, Thompson AJ, Franze K, Zernicka-Goetz M (2015). Development of the anterior-posterior axis is a self-

organizing process in the absence of maternal cues in the mouse embryo. Cell Res 25(12):1368-71.

Bedzhov I, Leung CY, Bialecka M, Zernicka-Goetz M (2014). *In vitro* culture of mouse blastocysts beyond the implantation stages. Nat Protoc. 9(12):2732-9.

Behringer RR, Eakin GS, Renfree MB (2006). Mammalian diversity: gametes, embryos and reproduction. Reprod Fertil Dev 18(1-2):99-107.

Beier HM, Mootz U, Fischer B, Ströbele-Müller R (1983). Fertilization of the Human Egg In Vitro, chapter Growth and Differentiation of Rabbit Blastocysts in Defined Culture Media. p371-386. Springer press.

Belo JA, Bouwmeester T, Leyns L, Kertesz N, Gallo M, et al. (1997) Cerberus- like is a secreted factor with neutralizing activity expressed in the anterior primitive endoderm of the mouse gastrula. Mech Dev 68: 45–57.

Berg DK, Smith CS, Pearton DJ, Wells DN, Broadhurst R, Donnison M, Pfeffer PL (2011). Trophectoderm lineage determination in cattle. Dev Cell. 20(2):244-55.

Biggers JD, McGinnis LK, Raffin M (2000). Amino acids and preimplantation development of the mouse in protein-free potassium simplex optimized medium. Biol Reprod 63(1):281-93.

Bray SJ (2006). Notch signalling: a simple pathway becomes complex. Nat Rev Mol Cell Biol 7(9):678-89.

Brennan J, Lu CC, Norris DP, Rodriguez TA, Beddington RS, Robertson EJ (2001). Nodal signalling in the epiblast patterns the early mouse embryo. Nature 411, 965 – 969.

Caiazzo M, Okawa Y, Ranga A, Piersigilli A, Tabata Y, Lutolf MP (2016). Defined three-dimensional microenvironments boost induction of pluripotency. Nat Mater 15(3):344-52.

Camus A, Perea-Gomez A, Moreau, A, Collignon, J (2006). Absence of Nodal signaling promotes precocious neural differentiation in the mouse embryo. Dev. Biol. 295, 743–755.

Canham MA, Sharov AA, Ko MS, Brickman JM (2010). Functional heterogeneity of embryonic stem cells revealed through translational amplification of an early endodermal transcript. PLoS Biol 8(5):e1000379.

Carson DD1 Bagchi I, Dey SK, Enders AC, Fazleabas AT, Lessey BA, Yoshinaga K (2000). Embryo implantation. Dev Biol 223(2):217-37.

Chazaud, C., Yamanaka, Y., Pawson, T. & Rossant, J. (2006). Early lineage segregation between epiblast and primitive endoderm in mouse blastocysts through the Grb2-MAPK pathway. Dev. Cell 10, 615–624

Cormier S, Vandormael-Pournin S, Babinet C, Cohen-Tannoudji M (2004). Developmental expression of the Notch signaling pathway genes during mouse preimplantation development. Gene Expr. Patterns 4, 713–717.

Dasen JS, Liu JP, Jessell TM (2003). Motor neuron columnar fate imposed by sequential phases of Hox-c activity. Nature 425(6961):926-33.

de Medeiros G, Norlin N, Gunther 1, Albert M, Panavaite L, Fiuza UM, Peri F, Hiiragi T, Krzic U, Hufnagel L (2015). Confocal multiview light-sheet microscopy. Nat Commun. 6:8881

Deglincerti A, Croft GF, Pietila LN, Zernicka-Goetz M, Siggia ED, Brivanlou AH (2016). Self-organization of the *in vitro* attached human embryo. Nature 533(7602):251-4.

Dey SK, Lim H, Das SK, Reese J, Paria BC, Daikoku T, Wang H (2004). Molecular cues to implantation. Endocr Rev 25(3):341-73.

Dietrich JE, Panavaite L, Gunther S, Wennekamp S, Groner AC, Pigge A, Salvenmoser S, Trono D, Hufnagel L, Hiiragi T (2015). Venus trap in the mouse embryo reveals distinct molecular dynamics underlying specification of first embryonic lineages. EMBO Rep 16(8):1005-21.

Dietrich, J. E. and Hiiragi T. (2007). Stochastic patterning in the mouse pre-implantation embryo. Development 134, 4219-31.

Ding J, Yang L, Yan YT, Chen A, Desai N, et al. (1998) Cripto is required for correct orientation of the anterior-posterior axis in the mouse embryo. Nature 395: 702–707.

Eakin GS, Behringer RR (2004). Diversity of germ layer and axis formation among mammals. Semin Cell Dev Biol 15:619-629.

Filipczyk, A, Gkatzis K. Fu J, Hoppe PS, Lickert H, Anastassiadis K, Schroeder T (2013). Biallelic expression of Nanog protein in mouse embryonic stem cells. Cell Stem Cell 13, 12–13.

Gefen O, Balaban NQ (2009). The importance of being persistent: heterogeneity of bacterial populations under antibiotic stress. FEMS Microbiol Rev 33(4):704-17

Genbacev OD, Prakobphol A, Foulk RA, Krtolica AR, Ilic D, Singer MS, Yang ZQ, Kiessling LL, Rosen SD, Fisher SJ (2003). Trophoblast L-selectin-mediated adhesion at the maternal-fetal interface. Science 299(5605):405-8.

Gjorevski N, Sachs N, Manfrin A, Giger S, Bragina ME, Ordóñez-Morán P, Clevers H, Lutolf MP (2016). Designer matrices for intestinal stem cell and organoid culture. Nature 539(7630):560-564.

Golding MC, Snyder M, Williamson GL, Veazey KJ, Peoples M, Pryor JH, Westhusin ME, Long CR (2015). Histone-lysine N-methyltransferase SETDB1 is required for development of the bovine blastocyst. Theriogenology 84(8):1411-22.

Gore A, Maegawa S, Cheong A, Gilligan PC, Weinberg ES, ? Sampath K: The zebrafish dorsal axis is apparent at the four-cell stage. Nature 2005, 438:1030-1035.

Grabarek, J. B. et al. (2012). Differential plasticity of epiblast and primitive endoderm precursors within the ICM of the early mouse embryo. Development 139, 129–139

Granier C, Gurchenkov V, Perea-Gomez A, Camus A, Ott S, Papanayotou C, Iranzo J et al. (2011). Nodal cis-regulatory elements reveal epiblast and primitive endoderm heterogeneity in the peri-implantation mouse embryo. Dev. Biol. 349, 350 – 362.

Grant PS (1973 (1)). The effect of progesterone and oestradiol on immature mouse uteri maintained as organ cultures. J Endocrinol. 57(1):171-4.

Grant PS (1973 (2)). The effect of progesterone and oestradiol on blastocysts cultured within the lumina of immature mouse uteri. J Embryol Exp Morphol. 29(3):617-38.

Greenwald I (1998). LIN-12/Notch signaling: lessons from worms and flies. Genes Dev 12(12):1751-62.

Haegel, H., Larue, L., Ohsugi, M., Fedorov, L., Herrenknecht, K., Kemler, R., 1995. Lack of beta-catenin affects mouse development at gastrulation. Development 121, 3529–3537.

Heemskerk I and Streichan SJ (2015). Tissue cartography: compressing bio-image data by dimensional reduction. Nat Methods 12(12):1139-42.

Helmbacher F, Dessaud E, Arber S, deLapeyrière O, Henderson CE, Klein R, Maina F (2003). Met signaling is required for recruitment of motor neurons to PEA3-positive motor pools. Neuron 39(5):767-77.

Hiramatsu R, Matsuoka T, Kimura-Yoshida C, Han SW, Mochida K, Adachi T, Takayama S, Matsuo I (2013). External mechanical cues trigger the establishment of the anterior-posterior axis in early mouse embryos. Dev Cell 27:131-144.

Hoshino H, Shioi G, Aizawa S. (2015). AVE protein expression and visceral endoderm cell behavior during anterior-posterior axis formation in mouse embryos: Asymmetry in OTX2 and DKK1 expression. Dev Biol. 402(2):175-91.

Hsu Y.C. (1972). Differentiation *in vitro* of mouse embryos beyond the implantation stage. Nature. 239(5369):200-2.

Hsu Y.C. (1973). Differentiation *in vitro* of mouse embryos to the stage of early somite. Dev Biol. 33(2):403-11.

Huelsken, J., Vogel, R., Brinkmann, V., Erdmann, B., Birchmeier, C., Birchmeier, W., 2000. Requirement for beta-catenin in anterior-posterior axis formation in mice. J. Cell Biol. 148, 567–578.

Huisken J, Swoger J, Bene FD, Wittbrodt J, Stelzer EHK (2004). Optical sectioning deep inside live embryos by selective plane illumination microscopy. Science 305, 1007–1009.

James D, Levine AJ, Besser D, Hemmati-Brivanlou, A (2005). TGF-β/activin/nodal signaling is necessary for the maintenance of pluripotency in human embryonic stem cells. Development 132, 1273–1282.

Johnson MH (2009). From mouse egg to mouse embryo: Polarities, axes and tissues. Seminars in Cell & Developmental Biology 15(5), 583-597.

Johnson, M. H. and Ziomek, C. A. (1981). The foundation of two distinct cell lineages within the mouse morula. Cell 24, 71-80.

Johnston RJ, Desplan C (2010). Stochastic Mechanisms of Cell Fate Specification that Yield Random or Robust Outcomes. Annu Rev Cell Dev Biol 26: 689–719.

Kalmar T, Lim C, Hayward P, Muñoz-Descalzo S, Nichols J, Garcia-Ojalvo J, Martinez Arias A (2009). Regulated fluctuations in nanog expression mediate cell fate decisions in embryonic stem cells. PLoS Biol 7(7):e1000149.

Kang M, Piliszek A, Artus J, Hadjantonakis AK (2013). FGF4 is required for lineage restriction and salt-and-pepper distribution of primitive endoderm factors but not their initial expression in the mouse. Development 140(2):267-79.

Karsenti E (2008). Self-organization in cell biology: a brief history. Nat Rev Mol Cell Biol 9(3):255-62.

Kaufman MH (1999). The atlas of mouse development. Academic Press, 1st edition, p22-23.

Korotkevich E, Niwayama R, Courtois A, Friese S, Berger N, Buchholz F, Hiiragi T (2017). The Apical Domain Is Required and Sufficient for the First Lineage Segregation in the Mouse Embryo. Dev Cell 40(3):235-247.e7.

Krzic U, Gunther S, Saunders TE, Streichan SJ, Hufnagel L (2012). Multiview light-sheet microscope for rapid in toto imaging. Nat. Methods 9, 730–733.

Kuijk EW, Du Puy L, Van Tol HT, Oei CH, Haagsman HP, Colenbrander B, Roelen BA (2008). Differences in early lineage segregation between mammals. Dev Dyn 237(4):918-27.

Li Y, Sun X, Dey SK (2015). Entosis allows timely elimination of the luminal epithelial barrier for embryo implantation. Cell Rep 11(3):358-65.

Livet J, Sigrist M, Stroebel S, De Paola V, Price SR, Henderson CE, Jessell TM, Arber S (2002). ETS gene Pea3 controls the central position and terminal arborization of specific motor neuron pools. Neuron 35(5):877-92.

Lu CC, Brennan J, Robertson EJ (2001). From fertilization to gastrulation: axis formation in the mouse embryo. Curr. Opin. Genet. Dev. 11, 384–392.

Maître JL, Turlier H, Illukkumbura R, Eismann B, Niwayama R, Nédélec F, Hiiragi T (2016). Asymmetric division of contractile domains couples cell positioning and fate specification. Nature 536(7616):344-8.

Mesnard D, Guzman-Ayala M, Constam DB (2006). Nodal specifies embryonic visceral endoderm and sustains pluripotent cells in the epiblast before overt axial patterning. Development 133, 2497–2505.

Morris SA, Grewal S, Barrios F, Patankar SN, Strauss B, Buttery L, Alexander M, Shakesheff KM, Zernicka-Goetz M (2012). Dynamics of anterior-posterior axis formation in the developing mouse embryo. Nat Commun 3:673.

mouse development. Development 139, 3711–3721.

Nagy A, Gertsenstein M, Vintersten K, Behringer R (2003). Manipulating the Mouse Embryo: A Labortory manual, 3rd edition. Cold Spring Harbour Laboratory Press.

Nakamura T, Mine N, Nakaguchi E, Mochizuki A, Yamamoto M, Yashiro K, Meno C, Hamada H (2006). Generation of robust left-right asymmetry in the mouse embryo requires a self-enhancement lateral inhibition system. Dev Cell 11:495-504.

Nakamura T, Okamoto I, Sasaki K, Yabuta Y, Iwatani C, Tsuchiya H, Seita Y, Nakamura S, Yamamoto T, Saitou M (2016). A developmental coordinate of pluripotency among mice, monkeys and humans. Nature 537(7618):57-62.

Niakan KK, Eggan K (2013).Analysis of human embryos from zygote to blastocyst reveals distinct gene expression patterns relative to the mouse. Dev Biol. 375(1):54-64.

Nichols J, Smith A (2009). Naive and primed pluripotent states. Cell Stem Cell 4(6):487-92.

Niwa H, Toyooka Y, Shimosato D, Strumpf D, Takahashi K, Yagi R, Rossant J. (2005). Interaction between Oct3/4 and Cdx2 determines trophectoderm differentiation. Cell 123(5):917-29.

Nonaka S, Tanaka Y, Okada Y, Takeda S, Harada A, Kanai Y, Kido M, Hirokawa N (1998). Randomization of left-right asymmetry due to loss of nodal cilia generating leftward flow of extraembryonic fluid in mice lacking KIF3B motor protein. Cell 95(6):829-37. Erratum in: Cell 1999 Oct 1;99(1):117.

Nonaka S, Yoshiba S, Watanabe D, Ikeuchi S, Goto T, Marshall WF, Hamada H (2005). De novo formation of left-right asymmetry by posterior tilt of nodal cilia. PLoS Biol 3(8):e268.

Norris DP, Brennan J, Bikoff EK, Robertson EJ (2002) The Foxh1-dependent autoregulatory enhancer controls the level of Nodal signals in the mouse embryo. Development 129: 3455–3468.

O'Sullivan CM, Rancourt SL, Liu SY, Rancourt DE (2001). A novel murine tryptase involved in blastocyst hatching and outgrowth. Reproduction 122(1):61-71.

Ohnishi Y, Huber W, Tsumura A, Kang M, Xenopoulos P, Kurimoto K, Oleś AK, Araúzo-Bravo MJ, Saitou M, Hadjantonakis AK, Hiiragi T (2014). Cell-to-cell expression variability followed by signal reinforcement progressively segregates early mouse lineages. Nat Cell Biol 16(1):27-37.

Okada Y, Takeda S, Tanaka Y, Izpisúa Belmonte JC, Hirokawa N (2005). Mechanism of nodal flow: a conserved symmetry breaking event in left-right axis determination. Cell 121(4):633-44.

Papanayotou C, Collignon J (2014). Activin/Nodal signalling before implantation: setting the stage for embryo patterning. Phil. Trans. R. Soc. B 369: 20130539.

Paria BC, Reese J, Das SK, Dey SK (2002). Deciphering the cross-talk of implantation: advances and challenges. Science 296(5576):2185-8.

Parr EL, Tung HN, Parr MB (1987). Apoptosis as the mode of uterine epithelial cell death during embryo implantation in mice and rats. Biol Reprod 36(1):211-25.

Perona RM, Wassarman PM (1986). Mouse blastocysts hatch *in vitro* by using a trypsin-like proteinase associated with cells of mural trophectoderm. Dev Biol. 114(1):42-52.

Plusa, B., Piliszek, A., Frankenberg, S., Artus, J. & Hadjantonakis, A. K. (2008).Distinct sequential cell behaviours direct primitive endoderm formation in the mouse blastocyst. Development 135, 3081–3091.

Price SR, De Marco Garcia NV, Ranscht B, Jessell TM (2002). Regulation of motor neuron pool sorting by differential expression of type II cadherins. Cell 109(2):205-16.

Ralston A, Rossant J (2008). Cdx2 acts downstream of cell polarization to cell-autonomously promote trophectoderm fate in the early mouse embryo. Dev Bio 313, 614–629.

Ranga A, Girgin M, Meinhardt A, Eberle D, Caiazzo M, Tanaka EM, Lutolf MP (2016). Neural tube morphogenesis in synthetic 3D microenvironments. Proc Natl Acad Sci U S A 113(44):E6831-E6839.

Range R, Lapraz F, Quirin M, Marro S, Besnardeau L, Lepage T (2007). Cis-regulatory analysis of nodal and maternal control of dorsal-ventral axis formation by Univin, a TGF-beta related to Vg1. Development 134, 3649–3664.

Rayon T, Menchero S, Nieto A, Xenopoulos P, Crespo M, Cockburn K, et al. (2014) Notch and hippo converge on Cdx2 to specify the trophectoderm lineage in the mouse blastocyst. Dev Cell 30:410–22.

Riedl J, Flynn KC, Raducanu A, Gärtner F, Beck G, Bösl M, Bradke F, Massberg S, Aszodi A, Sixt M, Wedlich-Söldner R (1010). Lifeact mice for studying F-actin dynamics. Nat Methods 7(3):168-9.

Rit**sma** L, Steller EJ, Beerling E, Loomans CJ, Zomer A, Gerlach C, Vrisekoop N, Seinstra D, van Gurp L, Schäfer R, Raats DA, de Graaff A, Schumacher TN, de Koning EJ, Rinkes IH, Kranenburg O, van Rheenen J (2012). Intravital microscopy through an abdominal imaging window reveals a pre-micrometastasis stage during liver metastasis. Sci Transl Med 4(158):158ra145.

Ritsma L, Steller EJ, Ellenbroek SI, Kranenburg O, Borel Rinkes IH, van Rheenen J. (2013). Surgical implantation of an abdominal imaging window for intravital microscopy. Nat Protoc. 8(3):583-94.

Rivera-Pérez JA, Mager J, Magnuson T (2003) Dynamic morphogenetic events characterize the mouse visceral endoderm. Dev. Biol. 261, 470–487.

Rossant J, Tam PP (2009). Blastocyst lineage formation, early embryonic asymmetries and axis patterning in the mouse. Development 136, 701-13.

Rudloff, S., Kemler, R., 2012. Differential requirements for beta-catenin during

Saetzler K, Sonnenschein C, Soto AM (2011). Systems biology beyond networks: generating order from disorder through self-organization. Semin Cancer Biol. 21(3):165-74.

Salomon DS, Sherman MI (1975). Implantation and invasiveness of mouse blastocysts on uterine monolayers. Exp Cell Res 90(2):261-8.

Sasai Y (2013). Cytosystems dynamics in self-organization of tissue architecture. Nature. 493(7432):318-26.

Sasaki K, Nakamura T, Okamoto I, Yabuta Y, Iwatani C, Tsuchiya H, Seita Y, Nakamura S, Shiraki N, Takakuwa T, Yamamoto T, Saitou M (2016). The Germ Cell Fate of Cynomolgus Monkeys Is Specified in the Nascent Amnion. Dev Cell 39(2):169-185.

Schier AF (2001). Axis formation and patterning in zebrafish. Curr Opin Genet Dev 11, 393–404.

Schrode, N. et al. (2013).Anatomy of a blastocyst: cell behaviors driving cell fate choice and morphogenesis in the early mouse embryo. Genesis 51, 219–233

Shahbazi MN, Jedrusik A, Vuoristo S, Recher G, Hupalowska A, Bolton V, Fogarty NM, Campbell A, Devito LG, Ilic D, Khalaf Y, Niakan KK, Fishel S, Zernicka-Goetz M (2016). Self-organization of the human embryo in the absence of maternal tissues. Nat Cell Biol 18(6):700-8.

Shen MM (2007). Nodal signaling: developmental roles and regulation. Development 134, 1023–1034.

Shi S, Stahl M, Lu L, Stanley P (2005). Canonical Notch signaling is dispensable for early cell fate specifications in mammals. Mol Cell Biol 25(21):9503-8.

Shinohara K, Kawasumi A, Takamatsu A, Yoshiba S, Botilde Y, Motoyama N, Reith W, Durand B, Shiratori H, Hamada H (2012). Two rotating cilia in the node cavity are sufficient to break left-right symmetry in the mouse embryo. Nat Commun 3:622.

Silva J, Smith A (2008). Capturing pluripotency. Cell 132(4):532-6.

Simons BD, Clevers H (2011). Strategies for homeostatic stem cell self-renewal in adult tissues. Cell 145(6):851-62.

Snow MH, Bennett D (1978). Gastrulation in the mouse: assessment of cell populations in the epiblast of tw18/tw18 embryos. J Embryol Exp Morphol. Oct;47:39-52.

Souilhol C, Cormier S, Tanigaki K, Babinet C, Cohen-Tannoudji M (2006). RBP-Jkappa-dependent notch signaling is dispensable for mouse early embryonic development. Mol Cell Biol 26(13):4769-74.

Srinivas S (2006). The anterior visceral endoderm-turning heads. Genesis 44(11):565-72.

Srinivas S, Rodriguez T, Clements M, Smith JC, Beddington RS (2004) Active cell migration drives the unilateral movements of the anterior visceral endoderm. Development 131: 1157–1164.

Stern CD (2006) Evolution of the mechanisms that establish the embryonic axes. Curr. Opin. Genet. Dev. 16, 413–418.

Takaoka K, Hamada H (2012). Cell fate decisions and axis determination in the early mouse embryo. Development 139(1):3-14.

Takaoka K, Yamamoto M, Hamada H (2007). Origin of body axes in the mouse embryo. Curr Opin Genet Dev 17(4):344-50.

Takaoka K, Yamamoto M, Shiratori H, Meno C, Rossant J, Saijoh Y, Hamada H (2006). The Mouse Embryo Autonomously Acquires Anterior-Posterior Polarity at Implantation. Dev Cell 10, 451–459.

Takaoka K, Yamamoto M., Hamada H (2011). Origin and role of distal visceral endoderm, a group of cells that determines anterior–posterior polarity of the mouse embryo. Nat Cell Biol 13, 743-752.

Tarkowski, A. K. and Wroblewska, J. (1967). Development of blastomeres of mouse eggs isolated at the 4- and 8-cell stage. J Embryol Exp Morphol 18, 155-80.

Thomas P, Beddington R (1996). Anterior primitive endoderm may be responsible for patterning the anterior neural plate in the mouse embryo. Curr Biol. 6(11):1487-96.

Thomas PQ, Brown A, Beddington RS (1998). Hex: a homeobox gene revealing peri-implantation asymmetry in the mouse embryo and an early transient marker of endothelial cell precursors. Development 125, 85-94

Torres-Padilla ME, Richardson L, Kolasinska P, Meilhac SM, Luetke-Eversloh MV, Zernicka-Goetz M (2007). The anterior visceral endoderm of the mouse embryo is

established from both preimplantation precursor cells and by de novo gene expression after implantation. Dev. Biol. 309, 97-112.

Trimarchi JM, Stadler MB, Cepko CL (2008). Individual retinal progenitor cells display extensive heterogeneity of gene expression. PLoS One 3(2):e1588

Vannini N, Girotra M, Naveiras O, Nikitin G, Campos V, Giger S, Roch A, Auwerx J, Lutolf MP (2016). Specification of haematopoietic stem cell fate via modulation of mitochondrial activity. Nat Commun 7:13125.

Veening JW, Smits WK, Kuipers OP (2008). Bistability, epigenetics, and bet-hedging in bacteria. Annu Rev Microbiol. 62:193-210.

Voas MG, Rebay I (2004). Signal integration during development: insights from the Drosophila eye. Dev Dyn 229(1):162-75.

Wang H, Dey SK. (2006). Roadmap to embryo implantation: clues from mouse models. Nat Rev Genet. 7(3):185-99.

Wang QT, Piotrowska K, Ciemerych MA, Milenkovic L, Scott MP, Davis RW, Zernicka-Goetz M (2004). A genome-wide study of gene activity reveals developmental signaling pathways in the preimplantation mouse embryo. Dev. Cell 6, 133–144.

Welsh AO, Enders AC (1993). Chorioallantoic placenta formation in the rat. III. Granulated cells invade the uterine luminal epithelium at the time of epithelial cell death. Biol Reprod 49(1):38-57.

Wennekamp S (2013). Molecular heterogeneity and lineage segregation in the early mouse embryo. PhD Thesis, University of Aachen.

Wennekamp S, Mesecke S, Nedelec F, Hiiragi T (2013). A self-organization framework for symmetry breaking in the mammalian embryo. Nat. Rev. Mol. Cell Biol. 14, 454–461.

Wolpert L, Tickle C, Martinez Arias A (2014). Oxford Principles of development, 5th ed. Chapter Vertebrate development, p122. Oxford press.

Wu TC, Wan YJ, Damjanov I (1981). Positioning of inner cell mass determines the development of mouse blastocysts *in vitro*. J Embryol Exp Morphol 65:105-17.

Xue B, Li Y, He Y, Wei R, Sun R, Yin Z, Bou G, Liu Z (2016). Porcine Pluripotent Stem Cells Derived from IVF Embryos Contribute to Chimeric Development In Vivo. PLoS One 11(3):e0151737.

Yamamoto, M., Saijoh, Y., Perea-Gomez, A., Shawlot, W., Behringer, R. R., Ang, S. L., Hamada, H. and Meno, C. (2004). Nodal antagonists regulate formation of the anteroposterior axis of the mouse embryo. Nature 428, 387- 392.

Yamanaka Y, Lanner F, Rossant J (2010). FGF signal-dependent segregation of primitive endoderm and epiblast in the mouse blastocyst. Development 137, 715–724.

Young RA (2011). Control of the embryonic stem cell state. Cell 144, 940-954.

Zhang P, Zucchelli M, Bruce S, Hambiliki F, Stavreus-Evers A, Levkov L, Skottman H, Kerkelä E, Kere J, Hovatta O (2009). Transcriptome profiling of human pre-implantation development. PLoS One 4(11):e7844.

ACKNOWLEDGEMENTS

As I am at the end of my PhD studies, I am amazed by what a long and exciting adventure has it been. On one hand, time has passed by like it does when you are working against a fast-approaching deadline, and many things have been left on the sidelines because of the sharp focus necessary to make it. On the other hand, as I realized when writing down the names of all the people who have been with me throughout this journey, I have learned so much, done so much, and met so many like-minded souls that it might as well have been a hundred years since I started. I must only say that this was the exact right thing for me to do, and that I will be always grateful to people who got me started in biology years ago, and to those who helped me all throughout the amazing years of my PhD.

First of all, I would like to thank my supervisor Takashi Hiiragi, for inviting me to join his lab, for the opportunity to work on some of the most exciting problems in biology, and for guiding me throughout my PhD.

I would like to give my thanks to my thesis advisor committee – Alexander Aulehla, Nicholas Foulkes and Peter Lenart – for their kindness and indispensible advice

Every scientific result is produced by a joint effort of the lab. Thus I would like to thank all the people in our lab, as well as all the alumni that I had the pleasure to work with and to learn from. I thank Jens, Sebastian and Stefan for their work on gene-trap projects that built basis for this work. I thank Aurelien and Yusuke for getting me started in the lab. I thank Jean-Leon and Ritsuya for all their truly valuable feedback on my projects, and for being good friends and a positive presence throughout my time here. I send many many thanks to Steffi, Ramona, Ivica and Katja for all their help with everything in the lab. The list of things they helped me with would be longer than this thesis. I thank Allyson, Esther, Dimitri, Joe, Ulla and Judith for being great labmates, sharing their thoughts on my work, for their good ideas and their friendship. I thank Wibke for the feedback on this thesis, and for helping me start as a scientist in the first place. I also thank Anthony for his company and for sharing the 3D-geec adventure with me.

Extra thanks goes to all the people who have helped me with my project. I would like to thank Henning for all the time he invested in helping me image my beloved peri-

implantation stage. I thank Balint and Gustavo for excellent collaborations as well as fun (and sometimes scientific) discussions. I also thank Sabine and Stefan for their help at the ALMF. And another big thanks goes to EMBL animal and transgenic facilities, especially Yvonne, Alessandro, Andrea and David – without their daily effort no experiments would have been possible.

I would like to say an big thank you to all the lovely people I have met throughout my PhD that made these the best years of my life. I thank Rukshala and Ivica for helping me out in the lab, but most importantly for their friendship. I thank Thomas, Paul, Hannah, Martina and Chris for helping me feel like EMBL is my home from the first week of the predoc course. I thank Serge for always listening to me, and Kostek for giving me someone to listen to. A big thanks goes to Silvia and Andreas, for being there when I needed the most and ever since. And last, but not the least, I not only want, but really have to thank Katya. I thank her for all she taught me in the lab, from experimental techniques to PhD coping and survival skills.

While experiments, presentations and papers are the concern of the scientist, the scientist's survival is the concern of their family. Therefore I know that this last group of people have contributed to this work as much as I did by always keeping me going.

Joran – I cannot imagine a better friend, and I cannot imagine how I would have made it through all the ups and downs of my PhD, and like a million parties, if I did not have you.

Fabian – thank you for being my biggest fan and supporter, who always tells me I can do it. I can, because I have you.

Ieva – thank you for always watching over me and for helping me follow my dreams from the start.

Finally, I want to say the biggest thanks of all to my parents Milda and Arūnas. Everything that I am and that I have achieved I owe to you, and every day in my life is made better by your continuous love and support.

Many many thanks to every one of you for making all of this possible!